

IMPACT OF PAVEMENTS ON THE URBAN HEAT ISLAND

FINAL PROJECT REPORT

by

Jeffery Roesler

Sushobhan Sen

University of Illinois at Urbana-Champaign

for

Center for Highway Pavement Preservation

(CHPP)



In cooperation with US Department of Transportation-Research and Innovative Technology
Administration (RITA)

October, 2016

Disclaimer

The contents of this report reflect the views of the authors, who are responsible for the facts and the accuracy of the information presented herein. This document is disseminated under the sponsorship of the U.S. Department of Transportation's University Transportation Centers Program, in the interest of information exchange. The Center for Highway Pavement Preservation (CHPP), the U.S. Government and matching sponsor assume no liability for the contents or use thereof.

| Technical Report Documentation Page | | | |
|---------------------------------------------------------------------------------------------------------------------------------------------------------------------------------------------------------------------------------------------------------------------------------------------------------------------------------------------------------------------------------------------------------------------------------------------------------------------------------------------------------------------------------------------------------------------------------------------------------------------------------------------------------------------------------------------------------------------------------------------------------------------------------------------------------------------------------------------------------------------------------------------------------------------------------------------------------------------------------------------------------------------------------------------------------------------------------------------------------------------------------------------------------|-------------------------------------------------------------|-------------------------------------------------------|-----------------|
| 1. Report No. ICT-16-025 | 2. Government Accession No. | 3. Recipient's Catalog No. | |
| 4. Title and Subtitle IMPACT OF PAVEMENTS ON THE URBAN HEAT ISLAND | | 5. Report Date October, 2016 | |
| | | 6. Performing Organization Code UILU-ENG-2016-2025 | |
| 7. Author(s) Jeffery Roelser; Sushobhan Sen | | 8. Performing Organization Report No. | |
| 9. Performing Organization Name and Address CHPP Center for Highway Pavement Preservation, Tier 1 University Transportation Center Michigan State University, 2857 Jolly Road, Okemos, MI 48864 | | 10. Work Unit No. (TRAIS) | |
| | | 11. Contract or Grant No. | |
| 12. Sponsoring Organization Name and Address United States of America Department of Transportation Research and Innovative Technology Administration | | 13. Type of Report and Period Covered | |
| | | 14. Sponsoring Agency Code | |
| 15. Supplementary Notes Report uploaded at http://www.chpp.egr.msu.edu/ | | | |
| 16. Abstract Increasing urbanization has led to the development of Urban Heat Islands (UHIs), with serious implications for the environment. Pavements play a role in this by absorbing and storing more heat than the natural surfaces that they replace. To quantify this effect, a method based on radiation view factors was developed to measure the surface albedo of pavement mixes. Furthermore, the aging behavior of both asphalt and concrete was also investigated. These inputs were then used in a 1D pavement thermal model, ILLI-THERM, and several criteria were developed to study the UHI impact of the pavement. The radiative forcing (RF) metric showed that albedo was the most significant thermal property affecting pavement UHI. However, considering the energetics through the pavement during an average seasonal day revealed that RF does not take into account lags in the temperature field that have the potential to mitigate UHI during certain hours of the day. Finally, a demonstration of how concrete inlays may be used to mitigate UHI through multi-functional materials and mix designs was conducted. | | | |
| 17. Key Words | | 18. Distribution Statement No restrictions. | |
| 19. Security Classification (of this report) Unclassified. | 20. Security Classification (of this page) Unclassified. | 21. No. of Pages 99 pages | 22. Price NA |

Table of Contents

| | |
|---------------------------------------------------------------------------------------------|----|
| CHAPTER 1: INTRODUCTION | 1 |
| 1.1 Motivation | 1 |
| 1.2 Goals and Methodology | 5 |
| CHAPTER 2: ASSESSMENT OF CONCRETE PAVEMENT STRUCTURE ON URBAN HEAT ISLAND | 6 |
| 2.1 Introduction | 6 |
| 2.2 Materials and Methodology | 7 |
| 2.3 EICM Results | 10 |
| 2.4 Discussion | 10 |
| 2.5 Alternative Concrete Pavement System for Balancing Surface Temperature Difference | 11 |
| 2.6 Conclusion..... | 14 |
| CHAPTER 3: A HEAT FLUX-BASED APPROACH TO URBAN HEAT ISLANDS IN CONCRETE PAVEMENTS | 17 |
| 3.1 Introduction | 17 |
| 3.2 Materials and Methodology | 18 |
| 3.3 Results and Discussion | 24 |
| 3.4 Conclusion..... | 31 |
| CHAPTER 4: ENVIRONMENTAL BENEFITS OF MULTI-FUNCTIONAL CONCRETE INLAYS | 33 |
| 4.1 Introduction | 33 |
| 4.2 Materials and Methodology | 34 |
| 4.3 Results and Discussion | 37 |
| 4.4 Conclusion..... | 39 |
| CHAPTER 5: AGING ALBEDO MODEL FOR ASPHALT PAVEMENT SURFACES ... | 42 |
| 5.1 Introduction | 42 |
| 5.2 Materials and Methodology | 43 |
| 5.3 Results and Discussion | 47 |
| 5.4 Conclusion..... | 55 |
| CHAPTER 6: CONCRETE ALBEDO MEASUREMENT FOR FINITE SIZED SPECIMENS | 57 |
| 6.1 Introduction | 57 |
| 6.2 Methodology | 59 |
| 6.3 Results and Discussion: Stage I..... | 69 |
| 6.4 Results and Discussion: Stage II | 81 |
| 6.5 Conclusion..... | 86 |
| CHAPTER 7: CONCLUSIONS AND RECOMMENDATIONS..... | 88 |
| 7.1 Findings..... | 88 |
| 7.2 Recommendations for Future Work | 90 |
| REFERENCES | 92 |

List of Figures

| | |
|----------------------------------------------------------------------------------------------------------------------------------------------------------------------------------------------------------------------------------------------------------------------------------------------------------------------------------------------------------------------------|----|
| FIGURE 1: PHASES OF A PAVEMENT LIFE CYCLE ASSESSMENT..... | 2 |
| FIGURE 2: THERMAL PROCESSES INVOLVED INSIDE A PAVEMENT..... | 4 |
| FIGURE 3: CONCRETE PAVEMENT SYSTEM DEFINED AS THE CONTROL CASE P 8 | |
| FIGURE 4: FREQUENCY DISTRIBUTION FOR SURFACE TEMPERATURE DIFFERENCES (°F) IN CHICAGO..... | 12 |
| FIGURE 5: FREQUENCY DISTRIBUTION FOR SURFACE TEMPERATURE DIFFERENCES (°F) IN AUSTIN..... | 13 |
| FIGURE 6: FREQUENCY DISTRIBUTIONS OF SURFACE TEMPERATURE DIFFERENCES (°F) FOR THE CASE P-PF..... | 15 |
| FIGURE 7: HYPOTHETICAL RIGID PAVEMENT CROSS SECTIONS | 19 |
| FIGURE 8: SCHEMATIC OF (A) NODAL ELEMENTS USED TO CALCULATE HEAT STORED; AND (B) LAYERS THROUGH WHICH HEAT CONDUCTION IS CALCULATED (DIRECTION OF ARROWS DOES NOT NECESSARILY INDICATE DIRECTION OF HEAT FLOW. THICKNESS IN BRACKETS | 23 |
| FIGURE 9: RF AND GWP OF ANALYZED PAVEMENT OPTIONS FOR A FIVE-YEAR ANALYSIS PERIOD..... | 25 |
| FIGURE 10: NET SURFACE HEAT FLUX (IN W/M ²) FOR EACH PAVEMENT CASE IN (A) THE WARM SEASON AND (B) THE COLD SEASON. TIMES OF SUNRISE AND SUNSET ARE ONLY INDICATIVE | 27 |
| FIGURE 11: HEAT CONDUCTED (IN W) THROUGH EACH LAYER IN AN AVERAGE SEASONAL DAY IN (A) WARM SEASON AND (B) COLD SEASON. SOLID LINES REPRESENT SURFACE COURSE WHILE CROSSED LINES REPRESENT CTB). THE SURFACE COURSE IS 100 MM THICK, WHILE THE CTB IS 150 MM THICK. TIMES OF SUNRISE AND SUNSET ARE ONLY INDICATIVE | 28 |
| FIGURE 12: HEAT STORED (IN KJ) IN SPECIFIED NODAL ELEMENTS IN AN AVERAGE SEASONAL DAY IN (A) WARM SEASON AND (B) COLD SEASON. SOLID LINES REPRESENT SURFACE NODAL ELEMENTS, CROSSED LINES SURFACE-BASE INTERFACE NODAL ELEMENTS AND DASHED LINES LAST NODAL ELEMENTS IN THE CTB, WHEREVER APPLICABLE. TIMES OF SUNRISE AND SUNSET ARE ONLY INDICATIVE | 29 |
| FIGURE 13: REFLECTED AND INCIDENT SOLAR RADIATION (A) BEING MEASURED USING A CMA 6 ALBEDOMETER OVER (B) THE THREE AREAS OF THE SMOOTH SURFACE OF THE BEAM | 35 |
| FIGURE 14: PAVEMENT STRUCTURES FOR SURFACE TEMPERATURE ANALYSES | 36 |
| FIGURE 15: FIVE POINT SUMMARY STATISTICS FOR THE ALBEDO OF FFC BEAM SURFACES..... | 37 |
| FIGURE 16: FREQUENCY DISTRIBUTION OF SURFACE TEMPERATURE DIFFERENCES OVER (A) THE ENTIRE ANALYSIS PERIOD (B) DAYTIME HOURS (C) NIGHTTIME HOURS..... | 40 |
| FIGURE 17: GOOGLE EARTH™ SCREENSHOT OF THE ATLAS FACILITY WITH THE FIVE SECTIONS UNDER STUDY LABELED AC 1-3 AND PCC 1-2..... | 43 |
| FIGURE 18: TOP VIEW OF PCC1 WITH POLYMER FIBERS ON THE SURFACE..... | 44 |
| FIGURE 19: HYPOTHETICAL PAVEMENT SECTION | 47 |
| FIGURE 20: ALBEDO OF SUBSECTIONS OF AC1 | 50 |
| FIGURE 21: ALBEDO OF SUBSECTIONS OF AC2 | 50 |
| FIGURE 22: ALBEDO OF SUBSECTIONS OF AC3 | 51 |
| FIGURE 23: ALBEDO OF SUBSECTIONS OF PCC1 | 51 |

| | |
|----------------------------------------------------------------------------------------------------------------------------------------------------------------------------------------------------------------------------------------------------|----|
| FIGURE 24: ALBEDO OF SUBSECTIONS OF PCC2 | 52 |
| FIGURE 25: AGING ALBEDO MODEL | 53 |
| FIGURE 26: RF AND GWP OF ALBEDO CASES | 54 |
| FIGURE 27: SMOOTHED SPECTRAL REFLECTANCE OF POLYMER MACROFIBER. STANDARD AM 1.5G SOLAR SPECTRUM IS ALSO SHOWN ON THE SECONDARY AXIS | 55 |
| FIGURE 28: TIO ₂ CONCRETE SLAB ON THE SITE FOR STAGE I TESTING | 60 |
| FIGURE 29: TIO ₂ CONCRETE SLAB ON THE SITE FOR STAGE II TESTING..... | 61 |
| FIGURE 30: TEST SITE FOR (A) STAGE I TESTING IN URBANA, ILLINOIS AND (B) STAGE II TESTING IN RANTOUL, ILLINOIS. PICTURES ARE TAKEN FROM GOOGLE EARTH™. THE SIZE OF THE CONCRETE SLAB IS NOT TO SCALE. 61 | |
| FIGURE 31: SCHEMATIC DIAGRAM OF THE CONCRETE SLAB IN STAGE I AND ITS ADJACENT SURFACES – A RAMP AND GRASS THAT TOGETHER FORM A COMPOSITE ‘INFINITE BACKGROUND’ AND BLACK PAPER THAT FORMS A ‘FINITE BACKGROUND’. FIGURE NOT TO SCALE..... | 62 |
| FIGURE 32: ALBEDO BEING MEASURED AT A HEIGHT OF 0.50 M WHEN THE EXPOSED SLAB SIZE IS 0.0 M I.E., WHEN IT IS FULLY COVERED IN THE ‘FINITE BACKGROUND’ (BLACK PAPER) | 63 |
| FIGURE 33: SLAB COVERED WITH THE ‘FINITE BACKGROUND’ (BLACK PAPER) WITH AN EXPOSED SIZE OF 0.6 M | 64 |
| FIGURE 34: MEASUREMENT OF ALBEDO OVER (A) GRASS SURFACE AND (B) CONCRETE RAMP SURFACE. AN AVERAGE OF THESE TWO IS CALLED A COMPOSITE ‘INFINITE’ BACKGROUND ALBEDO | 64 |
| FIGURE 35: STAGE II MEASUREMENT OF ALBEDO OVER THE TIO ₂ CONCRETE SLAB WITH ASPHALT PAVEMENT BACKGROUND SURFACE | 65 |
| FIGURE 36: GRAPHICAL REPRESENTATION OF EQUATION 4 TO CALCULATE THE VIEW FACTOR OF THE FINITE BACKGROUND | 66 |
| FIGURE 37: SPECTRAL REFLECTANCE OF VARIOUS MATERIALS FROM THE CARY 5G SPECTROPHOTOMETER WITH AM 1.5 G SPECTRUM ON THE SECONDARY AXIS | 70 |
| FIGURE 38: SPECTRAL REFLECTANCE OF BLACK PAPER AND LIMESTONE AGGREGATE CHIP FROM THE CARY 5000 SPECTROPHOTOMETER WITH AM 1.5 G SPECTRUM ON THE SECONDARY AXIS | 70 |
| FIGURE 39: CALCULATED ALBEDO OF TIO ₂ WHITE CEMENT, SAND, LIMESTONE AGGREGATE AND THE BLACK PAPER (AVERAGE OF TWO SIDES) | 71 |
| FIGURE 40: BOX AND WHISKER PLOTS OF THE MEASURED ALBEDO OF (A)-(E) THE SLAB WITH VARIOUS EXPOSED SIZES (F) THE SLAB FULLY COVERED IN THE FINITE BACKGROUND AND (G)-(H) THE COMPONENTS OF THE INFINITE BACKGROUND | 73 |
| FIGURE 41: VARIATION OF MEAN ALBEDO WITH HEIGHT OF ALBEDOMETER AND EXPOSED SLAB SIZE | 77 |
| FIGURE 42: VIEW FACTORS FOR EACH CASE FOR (A) TIO ₂ CONCRETE SLAB (B) FINITE BACKGROUND AND (C) INFINITE BACKGROUND | 78 |
| FIGURE 43: SPECTRAL REFLECTANCE OF CUBES MADE OF TIO ₂ CONCRETE WITH AM 1.5 G SPECTRUM ON THE SECONDARY AXIS | 81 |
| FIGURE 44: BOX AND WHISKER PLOTS OF THE MEASURED ALBEDO OF (A) TIO ₂ CONCRETE SLAB AFTER WEATHERING AND (B) THE INFINITE BACKGROUND | 83 |
| FIGURE 45: VARIATION OF MEAN ALBEDO WITH HEIGHT OF ALBEDOMETER ABOVE SLAB SURFACE | 84 |

FIGURE 46: SPATIALLY-DISTRIBUTED CORES FROM THE SLAB SURFACE
OBTAINED BY WET CORING 86

FIGURE 47: SPECTRAL REFLECTANCE OF CORES AND AM 1.5G STANDARD
SOLAR SPECTRUM WITH AM 1.5 G SPECTRUM ON THE SECONDARY AXIS 86

List of Tables

| | |
|--------------------------------------------------------------------------------------------------------------------------------------------------------------------------------------------------------------------------------------------------------------------------------------------------------------------------------------------------------------------------------------------------------|----|
| TABLE 1: THERMAL AND PHYSICAL PROPERTIES OF PAVING MATERIALS ASSUMED FOR THIS STUDY | 9 |
| TABLE 2: RESULTS OF CONCRETE PAVEMENT SURFACE TEMPERATURE DIFFERENCES (°F) IN CHICAGO..... | 12 |
| TABLE 3: RESULTS OF CONCRETE PAVEMENT SURFACE TEMPERATURE DIFFERENCES (°F) IN AUSTIN | 13 |
| TABLE 4: RESULTS OF A STATISTICAL ANALYSIS OF TEMPERATURE DIFFERENCES (°F) FOR THE CASE P-PF..... | 15 |
| TABLE 5: THERMAL PROPERTIES OF PAVING MATERIALS..... | 21 |
| TABLE 6: STATISTICS OF THE SURFACE TEMPERATURE DIFFERENCES (IN °C) RELATIVE TO THE CONTROL CASE P FOR AUSTIN, TX IN THE WARM SEASON; SPLIT FOR DAYTIME AND NIGHTTIME CONDITIONS | 30 |
| TABLE 7: STATISTICS OF THE SURFACE TEMPERATURE DIFFERENCES (IN °C) OF ANALYZED PAVEMENT SYSTEMS RELATIVE TO THE CONTROL CASE P FOR AUSTIN, TX IN THE COLD SEASON; SPLIT FOR DAYTIME AND NIGHTTIME CONDITIONS..... | 31 |
| TABLE 8: TIO ₂ FFC MIX DESIGNS | 34 |
| TABLE 9: WEATHER DATA FOR SEPTEMBER 3, 2014 AT WILLARD AIRPORT, CHAMPAIGN STATION (SOURCE: [91])..... | 35 |
| TABLE 10: THERMAL PROPERTIES OF LAYER MATERIALS ARE THE MEPDG LEVEL 3 DEFAULT VALUES UNLESS OTHERWISE NOTED | 36 |
| TABLE 11: STATISTICS OF ALBEDO MEASUREMENTS | 37 |
| TABLE 12: STATISTICS FOR HOURLY SURFACE TEMPERATURE DIFFERENCES BETWEEN CASE 1 AND CASE 2 (IN °C) OVER THE PERIOD OF STUDY (CUMULATIVE) AS WELL AS BETWEEN DAYTIME AND NIGHTTIME HOURS. POSITIVE INDICATES THAT THE EXISTING AC PAVEMENT HAD A HIGHER TEMPERATURE THAN THE INLAY, NEGATIVE THAT IT HAD A LOWER TEMPERATURE AND ZERO THAT IT HAD THE SAME TEMPERATURE TO THE FOURTH DECIMAL PLACE | 38 |
| TABLE 13: YEAR OF CONSTRUCTION AND OTHER DETAILS OF THE TEST SECTIONS..... | 44 |
| TABLE 14: REPRESENTATIVE WEATHER DATA FOR THE PERIOD OF MEASUREMENT FOR RANTOUL, IL [108] | 49 |
| TABLE 15: MEAN ALBEDO OF THE ATLAS TEST SECTIONS | 52 |
| TABLE 16: AGE AND ALBEDO DATA FOR AGING ALBEDO MODEL CALIBRATION | 53 |
| TABLE 17: CONCRETE MIX DESIGN | 60 |
| TABLE 18: WEATHER DATA FOR STAGE I FIELD MEASUREMENTS FROM [125] AT CHAMPAIGN WILLARD AIRPORT | 72 |
| TABLE 19: SUMMARY OF ALBEDO CALCULATION FOR VARYING NUMBER OF UNKNOWN FOR STAGE I..... | 80 |
| TABLE 20: WEATHER DATA FOR STAGE II FIELD MEASUREMENTS FROM (NATIONAL CLIMATIC DATA CENTER 2015) AT RANTOUL ELLIOT FIELD NATIONAL AVIATION CENTER..... | 81 |
| TABLE 21: SUMMARY OF ALBEDO CALCULATION FOR VARYING NUMBER OF UNKNOWN FOR STAGE II..... | 85 |

List of Abbreviations

AC: Asphalt Concrete
AM: Air Mass
BLUHI: Boundary Layer Urban Heat Island
CHPP: Center of Highway Pavement Preservation
CLUHI: Canopy Layer Urban Heat Island
CTB: Cement Treated Base
EICM: Enhanced Integrated Climatic Model
FFC: Flowable Fibrous Concrete
FHWA: Federal Highway Administration
FRC: Fiber Reinforced Concrete
GWP: Global Warming Potential
ILLITHERM: Illinois Thermal Analysis Program
LCA: Life Cycle Assessment
MEPDG: Mechanistic Empirical Pavement Design Guide
NCDC: National Climatic Data Center
NIR: Near Infrared
NOAA: National Oceanic and Atmospheric Administration
NOx: Nitrogen Oxides
PCC: Portland Cement Concrete
RF: Radiative Forcing
RMSE: Root Mean Squared Error
SCC: Self-Consolidating Concrete
SUHI: Surface Urban Heat Island
SWCC: Soil-Water Characteristic Curve
UHI: Urban Heat Island
UV: Ultraviolet
Vis: Visible

Acknowledgments

The authors are thankful to Daniel King for his extensive assistance in the concrete laboratory as part of our joint project on Multi-Functional Concrete Inlays, Armen Amirkhanian for his insights on modeling and programming, Alexander Brand for his insights on materials characterization, James Meister for his assistance at the Illinois Center for Transportation, and Prof. Barry Dempsey and Greg Larson for their assistance in the development of the ILLITHERM program.

Part of the work for this thesis was performed at the Frederick Seitz Materials Research Lab Central Facilities at the University of Illinois.

Executive Summary

Globally, the rapid pace of urbanization has led to several environmental challenges since the time of the Industrial Revolution. Recently however, unhindered use and modification of natural materials and ecosystems and the resulting consequences have led to a renewed focus on sustainability. Among the challenges faced, the Urban Heat Island (UHI) is caused by the replacement of natural materials with man-made ones such as concrete and asphalt, among other factors. UHIs can be studied at three elevations – surface, canopy layer and boundary layer – with Canopy Layer UHIs (CLUHIs) being the most significant as most human activity takes place in this layer. CLUHIs are pronounced during nighttime and smaller during daytime. In the study of sustainable pavements, UHIs are studied under the use phase of a pavement Life Cycle Assessment (LCA) to quantify the impact of the pavement on the local heat budget and microclimate.

To study UHI within a pavement LCA framework, two challenges were tackled. The first was to develop suitable models and metrics to characterize UHI. A thermal analysis program that uses weather data to model and analyze a pavement including its sub-surface layers, called the Illinois Thermal Analysis Program (ILLI-THERM), was developed and applied to a variety of pavement sections in Chicago, IL and Austin, TX to represent two different climatic conditions. A new method to calculate the Radiative Forcing (RF) and the corresponding Global Warming Potential (GWP) over the analysis period was proposed. The RF of a pavement was found to be most strongly affected by its surface albedo, with only small variations caused by changing other layer properties such as density, thermal conductivity and heat capacity of the pavement layers.

While RF is a measure of the overall environmental impact of a pavement, it fails to take account of diurnal and seasonal variations in heat flux due to differences in thermal properties of the pavement structure. These variations are the key to managing UHI at critical times of the day. The Average Seasonal Day metric was developed to obtain a snapshot of these variations over a given season for the analysis period. Two strategies were developed to mitigate UHI in concrete pavements: using a cement-treated base as a thermal storage layer to induce a thermal delay in the pavement and thus mitigate the nighttime CLUHI by passing on a part of the burden to the less-pronounced daytime CLUHI; and using Lightweight Aggregates (LWAs) in the surface course to quickly emit absorbed heat and thus reduce the amount of time during which CLUHI is prominent. Finally, the percentage of effectiveness metric was developed as a quick method to compare different pavement options by considering the relative difference in their hourly surface temperatures over the analysis period.

As albedo has the most significant impact on RF of a pavement, the second challenge was in determining the albedo of paving materials and incorporating it into the thermal analysis program, ILLI-THERM. For this study, a relatively new material, cement with titanium dioxide nanoparticles, was selected and a 1 m x 1 m concrete slab cast with it. An albedometer was used to measure the composite albedo of the slab and background surfaces. Geometric analysis to determine the relative contribution of each surface (called the view factor of the surface with respect to the albedometer) together with a least square regression analysis to take care of surfaces that were not explicitly considered. This new method estimated the albedo of the 1 m² concrete slab to be 0.54 with the background albedo found to be 0.21. After being allowed to weather over one winter cycle, the albedo was found to decrease to 0.50. However, this decrease was determined to be on account of dust and dirt accumulating on the slab and could be restored to its original value by washing thoroughly, as was determined by taking cores and testing them on a UV-Vis-NIR spectrophotometer.

The albedo of several existing asphalt and concrete test sections of various ages was also determined using an albedometer. The results from the asphalt sections were used to calibrate an aging albedo model. Most of the aging due to environmental weathering in asphalt was found to take place within the first two years, with very little change thereafter. This model was implemented in a pavement LCA using ILLI-THERM and compared to the existing practice of using a static albedo over the analysis period. Over a five-year analysis period, the static models were found to overestimate the GWP of a hypothetical pavement section in Austin, TX by 25% as compared to a more realistic case with an aging albedo.

In addition, the albedo of one of the concrete sections made of Flowable Fibrous Concrete was measured. Fibers that were visible on the surface were covered by the cement paste and not expected to change the overall albedo of the section. However, if they became exposed on account of abrasion, their albedo would have an impact. Therefore, the albedo the fiber was determined using a spectrophotometer as 0.07, which would have an impact on the overall albedo depending on the surface area exposed.

CHAPTER 1-INTRODUCTION

1.1 MOTIVATION

1.1.1 Defining Urban Heat Island

As human population continues to expand and move into urban areas around the world, the effects of human intervention in the natural environment are becoming increasingly important. In general, human activities tend to modify the natural ecosystem by changing materials and energy cycles on a large scale. For example, forests and grasslands are usually replaced by paving and roofing materials such as asphalt and concrete. Thus, permeable materials with latent heat are replaced by generally impermeable materials having no latent heat but high specific heat capacity (Oke, 1982). In cities, this building process leads to an increase in average annual air temperature by 1 to 3°C (Wong, Akbari, Bell, & Cole, 2011), an effect that is called the Urban Heat Island (UHI).

UHI has been observed in a variety of geographies around the world and is characterized a marked difference between the temperature in an urban area and in adjacent rural areas. This difference is called the UHI intensity, ΔT_{u-r} . This difference can be observed at three levels and thus, there are three types of UHIs that are studied – Surface UHI (SUHI) that is studied at the surface of an urban area, Canopy Layer UHI (CLUHI) that is studied at a height of 2 m above the surface, often called the Canopy Layer, and Boundary Layer UHI (BLUHI) at a height of about 2 km at the atmospheric boundary layer, where large-scale effects come to fore. Of these, CLUHIs are the most significant because a majority of human activity takes place in the Canopy Layer and this has a direct impact on most human activity. Previously, satellite observations have been used to observe CLUHIs (Pichierri, Bonafoni, & Biondi, 2012; Wong & Chaudhry, 2012; Liu & Zhang, 2011; Tran, Uchihama, Ochi, & Yasuoka, 2006; Fabrizi, Biondi, & Biondi, 2010; Keeler & Kristovich, 2012; Mackey, Lee, & Smith, 2012; Golden & Kaloush, 2006) and has been correlated to growth in urban sprawl (Mingshi, Du, & Shen, 2012; Bacci & Maugeri, 1992), with a nighttime intensity of 3-4°C or higher (even as high as 12°C) on average, depending on the local climate.

UHI has several effects on human activities and well-being. Previous studies (Guhathakurta & Gober, 2007; Aggarwal, Guhathakurta, Grossman-Clarke, & Lathey, 2012; Chow, Brennan, & Brazel, 2012) in the city of Phoenix, AZ, which has a strong UHI effect, have shown that an increase in nighttime UHI intensity by 1°F (1.8°C) leads to an increase in average household water usage by 1.4-1.8%. Other studies have shown that UHI leads to an increase in building cooling loads (Taha, Akbari, Rosenfeld, & Huang, 1988) and that implementing cool roof, green roof and cool pavement technologies can reduce those loads and provide energy savings to consumers (Akbari & Konopacki, 2005; Akbari & Konopacki, 2004; Carnielo & Zinzi, 2013; Kolokotronia, Gowreesunker, & Giridharan, 2013; Kolokotsa, Santamouris, & Zerefos, 95; Simpson & McPherson, 1997).

There are several factors that cause UHI, such as the large-scale use of energy in urban systems to maintain human lifestyle, the elimination of natural water reservoirs, the extensive use of paving and roofing materials etc. (Kleerekopera, van Esch, & Salcedo, 2012), and each of these factors can be studied separately while keeping in mind that they are related to each other. The effect of roofing materials in UHI has been extensively studied (Santamouris, 2014; Santamouris, Synnefa, & Karlessi, 2011; Kolokotsa, Santamouris, & Zerefos, 95; Bretz, Akbari, & Rosenfeld, 1998) and several cool roof and green roof mitigation strategies are now commercially applied (Kleerekopera, van Esch, & Salcedo, 2012). Cool pavements

(Santamouris, 2013) are currently under active study under the larger framework of pavement sustainability.

Recently, the Federal Highway Administration (FHWA) released a reference document (FHWA, 2015), in which sustainability is defined as “development that meets the needs of the present without compromising the ability of future generations to meet their own needs”. It takes a systems approach to sustainability, in which the entire life cycle of a pavement is divided into five phases (Santero, Masanet, & Horvath, 2011a; Santero, Masanet, & Horvath, 2011b), as shown in Figure 1-1. The analysis of the environmental impact of a pavement under these five phases is called Pavement Life Cycle Assessment (LCA).



Figure 1-1 Phases of a pavement life cycle assessment

In the study of UHI caused by pavements, the Use Phase is the most relevant phase. This phase also includes the study of carbonation, air emissions, lighting, rolling resistance and leachate. It covers the environmental impact over the design life of the pavement, which typically extends from 10-30 years and even longer in some cases. Therefore, any Use Phase Pavement LCA must have a temporal component associated with it.

Most UHI studies to date have relied on a top-down approach, such as remote sensing and atmospheric modeling. While useful from the perspective of a city-planner or government policymaker, such methods generalize between pavements, buildings, lawns, water bodies and other types of urban surfaces and thus distort a Pavement LCA, which is strictly limited to the pavement itself. A major goal of this study is to develop a ‘bottom-up’ approach to UHI that can assess pavements alone without distortion of results from adjacent surfaces. This is of immense use to agencies that would like to incorporate sustainable practices in road construction as well as sustainable cities.

1.1.2 Energetics of Urban Heat Island

From a thermodynamic systems perspective, UHI is studied as an imposed change in the surface energy budget of the earth. From the First Law of Thermodynamics, the earth’s surface energy budget can be expressed as shown in Equation 1.1 (Rizwan, Dennis, & Liu, 2008; Mirzaei & Haghighat, 2010).

$$Q^* + Q_F = Q_H + Q_E + \Delta Q_S + \Delta Q_A \quad (1.1)$$

Where,

Q^* = Net incoming radiation after passing the atmosphere and other barriers which attenuate short-wave radiation

Q_F = Anthropological heat generated within the control volume

Q_H = Energy flux of sensible heat

Q_E = Energy flux of latent heat

ΔQ_S = Heat stored by all energy storage mechanisms in the control volume, including man-made surfaces and natural objects

ΔQ_A = Net advective flux through the control volume, which is an error caused due to spatial gradient in temperature, humidity and wind. It can be ignored if care is taken in deciding the measurement height

The left side of Equation 1.1 is simply all the heat sources and the right side heat sinks. In particular for Pavement LCA, ΔQ_A , Q_E and Q_F can be taken as zero, so that the net heat stored is simply the algebraic sum of the incoming solar radiation and the outgoing sensible heat flux, which is called the net ground heat flux. Therefore, as compared to a natural system in which Q_E is substantial as compared to Q_H , a pavement has very little latent heat but much higher sensible heat flux, which leads to higher temperatures.

Moreover, in addition to the sensible heat flux, man-made materials tend to absorb and store more heat than natural ones. This is described in terms of the average solar reflectance or albedo of the surface, which is one minus the absorption. Typically, dark colored surfaces have a lower albedo (and hence, higher absorptivity), although this is not necessary for selectively reflective surfaces. The study of cool pavements looks at ways to increase the albedo of pavements so that they absorb less heat and thus maintain lower temperatures (Bretz, Akbari, & Rosenfeld, 1998; Li H. , Harvey, Holland, & Kayhanian, 2013; Santamouris, Synnefa, & Karlessi, 2011). Alternative methods include using permeable pavements to artificially induce latent heat through stored water (Li H. , Harvey, Holland, & Kayhanian, 2013; Stempihar, Pourshams-Manzouri, Kaloush, & Rodezno, 2012; Novo, Bayon, Castro-Fresno, & Rodriguez-Hernandez, 2012; Haselbach, Boyer, Kevern, & Schaefer, 2011), Phase Change Materials (PCMs), which induce latent heat through other materials such as wax (Sharma, Tyagi, Chen, & Buddhi, 2009; Tung-Chai & Poon, 2013; Guan, Ma, & Qin, 2011; Bentz & Turpin, 2007; Dehdezi P. K., Hall, Dawson, & Casey, 2013; Hunger, Entrop, Mandilaras, Brouwers, & Founti, 2009), and hydronic pavement systems that extract the stored heat in pavements (Pan, Wu, Xiao, & Liu, 2015; Dawson, Dehdezi, Hall, Wang, & Isola, 2012; Chiasson, Spilter, Rees, & Smith, 2000; Gary, 2007; Guangxi & Yu, 2012).

1.1.3 Urban Heat Island Caused by Pavements

The surface energetic basis of pavements-induced UHI was described in the previous section. The incoming solar radiation Q^* is partly absorbed by the pavement and partly reflected, depending on the albedo of the pavement. The reflected radiation is short-wave and given by Equation 1.2.

$$Q_{reflected} = aQ^* \quad (1.2)$$

Where, a is the albedo of the pavement surface.

In addition, the pavement also emits long-wave radiation following the Stefan-Boltzmann Equation, as shown in Equation 1.3, and loses heat to the air through convection, following Newton's Law of Cooling, as shown in Equation 1.4.

$$Q_{emitted} = \epsilon\sigma(T^4 - T_a^4) \quad (1.3)$$

Where, ϵ is the emissivity of the pavement surface material, T is its temperature, T_a is the air temperature and σ is the Stefan-Boltzmann constant, $5.670 \times 10^{-8} W/m^2K^4$.

$$Q_{convection} = h(T - T_a) \quad (1.4)$$

Where, h is the convection coefficient.

The net heat entering the pavement is the difference between $(Q^* - Q_{reflected})$ and $(Q_{emitted} + Q_{convection})$. This heat can then be modeled using Fourier's Law for the surface course and sub-surface stabilized layers. A notable difference between pavements and roofs is the extensive use of unbound aggregate layers in the former, which cannot be modeled using Fourier's Law due to their porous nature that creates suction, which eventually changes the moisture content of the layer from the natural water table. These layers are then modeled using the Philip-de Vries coupled heat and moisture flow equations (Philip & de Vries, 1957). Figure illustrates these processes in a pavement, which take place continuously over time.

The principle of reflective pavements to mitigate UHI is to increase the albedo and thus decrease the amount of heat stored by the pavement (Santamouris, Using cool pavements as a mitigation strategy to fight urban heat island—a review of the actual developments, 2013). While this has been shown to be effective in reducing the surface temperature of the pavement and thus the pavement-induced UHI, it has been shown to have certain negative consequences on the rest of the urban environment, most prominently changes in the local climate and increased cooling loads in buildings as a result of short-wave radiation reflected by the pavement into buildings (Qin, 2015; Jiachuan, Wang, & Kaloush, 2015). Therefore, while extremely useful, high albedo should not be seen as a panacea to UHI.

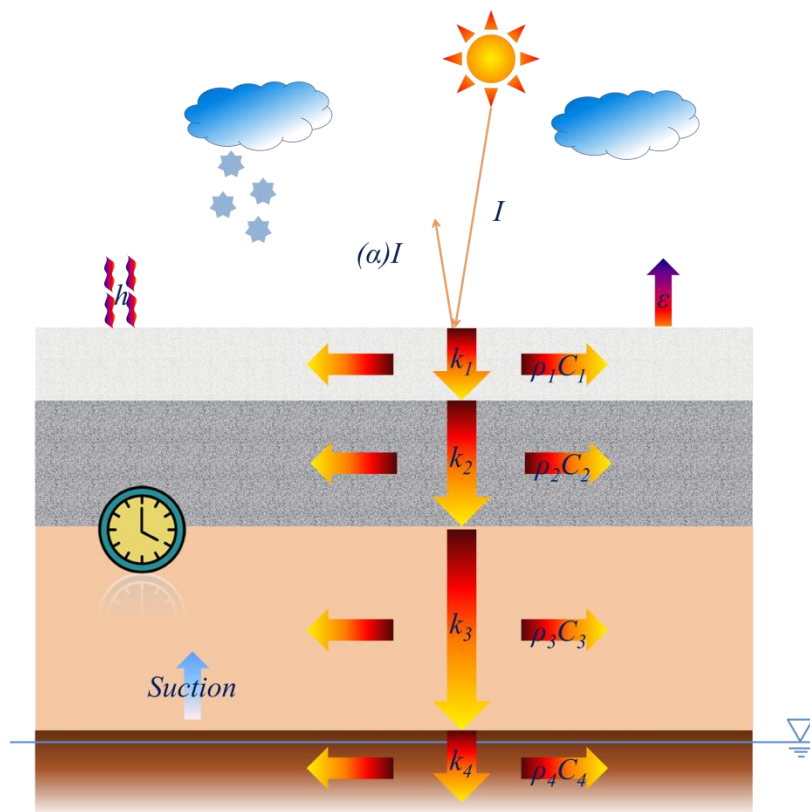


Figure 1-2 Thermal processes involved inside a pavement

1.2 GOALS AND METHODOLOGY

The two goals of this study are as follows:

- (a) To thermally model pavement layers over their design life and assess the results using suitable metrics to quantify their impact on UHI at various timescales and geographies. This goal also includes the development of alternative pavement designs to mitigate UHI without necessarily changing the surface albedo alone; and
- (b) To estimate the albedo of concrete and asphalt surfaces over time using various experimental methods and implement them in the previously developed models. In the long run, all thermal properties need to be quantified, but for this study, only albedo is quantified while values of other properties are taken from literature.

In addition to these goals, this study also considers a relatively new material, white cement incorporated with titanium dioxide (TiO₂) nanoparticles, that has a number of structural and environmental benefits (Cackler, Alleman, Kevern, & Sikkema, 2012; Bo Yeon, 2012; Wei & He, 2013). This study focuses on the UHI related benefits of the material as applied to pavements, particularly concrete pavements.

Goal (a) is discussed in Chapters 2-4. Chapter 2 demonstrates how variations to the thermal properties of pavements layers change the surface temperature of the pavement. A new metric, called the percentage of effectiveness, is introduced to compare different pavement options in terms of their relative effectiveness over time in mitigating surface UHI. Chapter 3 then introduces a heat flux-based approach to the problem of UHI to understand how pavement structure can provide mitigation solutions. This chapter includes a new metric called the average seasonal day and introduces a new method to quantify the overall environmental impact of a pavement in terms of its Radiative Forcing (RF) and Global Warming Potential (GWP). Finally, Chapter 4 demonstrates how TiO₂ concrete can be used in inlays to effectively mitigate UHI.

Goal (b) is then taken up in Chapters 5 and 6. Chapter 5 presents albedo measurements from several asphalt and concrete test sections. The measurements from the asphalt sections are used to calibrate an aging albedo model, which is then implemented into the Use Phase of a Pavement LCA. This model shows how the current state of practice in Pavement UHI studies can be improved with better experimental data. This chapter also includes the albedo of a section made of Flowable Fibrous Concrete and is also believed to be the first study to discuss the impact of using fibers in concrete pavements on albedo. Finally, Chapter 6 introduces a new method to evaluate the albedo of concrete samples of any geometric size and simple statistical analyses. This method takes into account various unknown variables involved in measuring the albedo of surfaces of limited area. This is applied to a sample of TiO₂ concrete to evaluate its albedo both before and after one winter cycle of weathering, adding to the very limited literature on the subject.

Chapter 6 is followed by a short conclusion and a discussion of future work.

CHAPTER 2-ASSESSMENT OF CONCRETE PAVEMENT STRUCTURE ON URBAN HEAT ISLAND¹

2.1 INTRODUCTION

The Urban Heat Island (UHI) effect is a phenomenon observed in built-up urban environments, where the average temperature of cities is higher than that of surrounding rural areas. One of the factors that leads to the development of a UHI is the higher thermal energy storage of building and paving materials (Kleerekopera, van Esch, & Salcedo, 2012), which subsequently increases near surface temperatures because of their increased thermal energy content. This increased energy content is later emitted back to the atmosphere, heating up the surrounding urban environment, which can increase water consumption (Aggarwal, Guhathakurta, Grossman-Clarke, & Lathey, 2012; Guhathakurta & Gober, 2007) and energy loads (Taha, Akbari, Rosenfeld, & Huang, 1988), especially in summer.

Understanding UHIs is a part of the larger Pavement Lifecycle Assessment (LCA), which seeks to understand the impact of pavements on the environment through materials, construction, use, maintenance and end-of-life phases (Santero, Masanet, & Horvath, 2011a). UHIs constitute one of those impacts and can be assessed in the use phase of an LCA. Several studies have shown that the albedo of roofs and pavements has a significant impact on UHI mitigation (Bretz, Akbari, & Rosenfeld, 1998; Santamouris, 2013). One main shortcoming of these studies is that they report the maximum decrease in surface temperature as compared to conventional pavements without examining how it varies over days, seasons, or alternative climates. Reporting the maximum peak surface temperature alone gives an incomplete view of the effect of the modification.

Limited studies have been undertaken to quantify the impact of changes to albedo on LCA (Munoz, Campra, & Fernandez-Alba, 2010; Yu & Lu, 2014; Susca, 2012), which show that a higher albedo is beneficial to the urban environment. However, studies such as (Yang, Wang, & Kaloush, 2013; Yang, Wang, & Kaloush, 2015) contest these findings and contend that higher pavement albedo leads to higher potential heating penalty in buildings in winter while also raising cooling loads in summer because of the reflected shortwave solar radiation from pavements. Therefore, there is an ongoing debate on the true benefits of modifying albedo to mitigate the UHI.

All the thermal properties of a pavement system – albedo, thermal conductivity, heat capacity, dry density and emissivity – have an impact on UHI and hence on pavement LCA. The impact of these properties on surface temperature was studied parametrically in (Gui, Phelan, Kaloush, & Golden, 2007) but only over three days without going into their seasonal and climatic spatial variations. Furthermore, only minimum and maximum surface temperatures were studied without analyzing the temporal variation of surface temperatures. Finally, only the properties of the surface course were varied, leaving out the impact of other support layers, which form an integral part of the pavement system. Thus, such an analysis

¹ Adapted from:

Sen, S, and Roesler, J (2014). *Assessment of concrete pavement structure on urban heat island*. Papers from the International Symposium on Pavement Life Cycle Assessment – Harvey, Jullien and Jones (Eds), Davis, CA, pp. 191-200.

only provides a partial understanding of the impact of the pavement system's thermal properties on Pavement LCA and at best captures an instantaneous view. The objective of this chapter is to move to a more comprehensive analysis and suggest the inclusion of the thermal properties of all the pavement layers in a lifecycle assessment.

2.2 Materials and Methodology

2.2.1 Pavement Cases

To assess the impact of changes to various thermal properties of the surface course as well as the base course, a control case was established. As shown in Figure 2-1, the control case is a hypothetical concrete pavement with a 4 in (100 mm) Portland Cement Concrete (PCC) surface course, a 6 in (150 mm) granular base of type A-2-4, a 12 in (300 mm) granular subbase of type A-3 and an A-6 subgrade. The control case was designated as P.

Three independent modifications were made to the control case to study changes in thermal and physical properties without changing the thicknesses of the pavement layers. To lower the thermal conductivity, lower density concrete was selected, which was designated PL. In another case, cement containing titanium dioxide (TiO₂) was used, which modified the surface albedo, and was labeled as PT. Finally, the base layer was changed from granular to a cement treated base (CTB). The base layer change modifies its thermal conductivity as well as heat capacity while maintaining the concrete surface layer. This case was designated PC.

To determine the surface temperature for each case, the Enhanced Integrated Climatic Model (EICM) embedded in the Mechanistic Empirical Pavement Design Guide (MEPDG) version 1.100 was used. The model uses hourly weather data to calculate the hourly temperature at various nodes of the pavement system. The data was analyzed from 1996 to 2005. For this preliminary study, only the surface temperatures were reported. The program outputs the surface temperature to the first decimal place.

In order to quantify the seasonal variation of surface temperatures, the study was divided into two periods: a warm season from April 2003 to September 2003 and a cold season from October 2002 to March 2003. Although these periods do not strictly represent summer and winter respectively, they do correspond to periods when temperatures are relatively warmer and cooler respectively. Thus, one full year of hourly data, totaling over 8000 hours, was obtained for each case. A similar analysis was done for a longer period from 1999 to 2004 but did not change the conclusions derived from the one-year analysis. Therefore, only results from the one-year analysis are discussed in this paper.

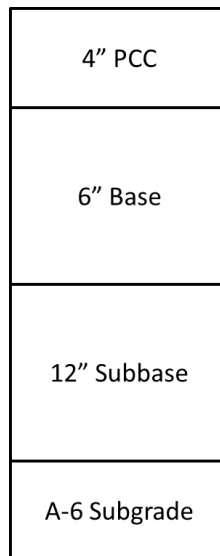


Figure 2-1 Concrete pavement system defined as the control case P

Finally, to observe climatic variation of the surface temperature, the models were analyzed in two different cities – Chicago, IL (O’Hare International Airport) and Austin, TX (Bergstrom International Airport). The former is in the northern US and experiences more severe winters but still hot summers, while the latter is in the southern US and experiences high summer temperatures and mild winter temperatures above freezing. Both are major metropolitan areas with built-up urban environments conducive to UHI formation. While neither of the two are coastal cities, Chicago is adjacent to Lake Michigan, which has an effect on its weather.

The predicted surface temperatures of the three modified cases (PL, PT and PC) are then subtracted from the corresponding surface temperature of the control case (P) at every hour of the analysis to measure the impact of the modification on surface temperature. These hourly temperature differences are designated (P-PL), (P-PT) and (P-PC) respectively for the three modified cases and are reported separately for each city and season.

2.2.2 Material Properties

Although the thermal properties of materials have a significant impact on the surface temperature of pavements and hence pavement performance, they have been sparingly measured without any single, comprehensive study. The frequency distribution of the surface temperature differences (P-PL), (P-PT) and (P-PC) are shown for Chicago in Figure 2-2 and Austin in Figure 2-3 with the statistical analysis of the results presented in Table 2-2 and Table 2-3, respectively. Table 2-1 summarizes the thermal properties of paving materials taken from the literature and assumed for this study.

Table 2-1 Thermal and physical properties of paving materials assumed for this study

| Material | Absorptivity | Thermal Conductivity (BTU/hr-ft-°F) | Heat Capacity (BTU/lb-°F) | Dry Unit Weight (pcf) |
|-----------------------------------------|---------------------|--------------------------------------------|----------------------------------|------------------------------|
| PCC (JPCP) | 0.70 | 1.25 | 0.28 | 150 |
| A-2-4 (Base) | - | Internally calculated | Internally calculated | 121.9 |
| A-3 (Subbase) | - | Internally calculated | Internally calculated | 120 |
| A-6 (Subgrade) | - | Internally calculated | Internally calculated | 100.8 |
| Low-Density Concrete | 0.70 | 0.35 | 0.25 | 86 |
| Cement-Treated Base | - | 1.25 | 0.28 | 150 |
| TiO ₂ -incorporated concrete | 0.65 | 1.25 | 0.28 | 150 |

In Table 2-1, the first input property is the absorptivity, which is simply one minus albedo. In general, darker materials have a lower albedo than lighter materials. Albedo varies with the time of day and even spatially over surfaces (Li, Harvey, & Kendall, 2013) and only a representative value can be assigned with the understanding that it is not necessarily constant. For concrete surfaces, 0.30 is such a representative value (Li, Harvey, & Kendall, 2013) with a corresponding absorptivity of 0.70, although it can range from 0.65 to 0.85. For the case of titanium dioxide cement (PT), albedo studies are still ongoing but (National Concrete Pavement Technology Center, 2012) suggests that 0.33 is a reasonable value. Since no statistical analysis of the variation of the albedo was provided, a slightly higher value of 0.35 (absorptivity of 0.65) was adopted for this study.

The thermal conductivity of conventional PCC was taken as the MEPDG default value (National Cooperative Highway Research Program Report 1-37A, 2004) of 1.25 BTU/hr-ft-°F (2.2 W/mK) with the same value applied for the CTB and TiO₂-incorporated concrete. The MEPDG internally calculates thermal conductivity for unbound materials. For casting lower density concrete, a variety of options are available, such as permeable concrete or lightweight aggregate concrete. For this study, the concrete contained 100% coarse and 50% fines from lightweight aggregates (expanded shale), which had a concrete compressive strength of 5200 psi (35.8 MPa), as measured in reference (Nguyen, Beaucour, Ortola, & Noumowé, 2014). The thermal conductivity was 0.35 BTU/hr-ft-°F (0.61 W/mK) at a density of 86 pcf (1380 kg/m³).

For heat capacity, the MEPDG default value for PCC and CTB is 0.28 BTU/lb-°F (1.2 kJ/kgK) and again is internally calculated for unbound materials. Since heat capacity is primarily dependent on the morphology of the aggregates, the same value is adopted for TiO₂-incorporated concrete. For the lower density concrete, a value of 0.25 BTU/lb-°F (1.06 kJ/kgK) was selected to correspond to the thermal conductivity from reference (Nguyen, Beaucour, Ortola, & Noumowé, 2014).

The default unbound aggregate gradations and Soil-Water Characteristic Curve (SWCC) parameters were assumed for the EICM runs.

2.3 EICM Results

The frequency distribution of the surface temperature differences (P-PL), (P-PT) and (P-PC) are shown for Chicago in Figure 2-2 and Austin in Figure 2-3 with the statistical analysis of the results presented in Table 2-2 and Table 2-3, respectively. In the statistical analysis, the percentage of hours for which the deviations are positive (the control pavement has a higher surface temperature), negative (modified pavement has a higher surface temperature) and zero (the modification does not cause any difference in surface temperature to the first decimal) are also listed in Table 2-2 and Table 2-3. This percentage, called the percentage of effectiveness, provides insights into how effective any given pavement option is in mitigating UHI as compared to the control.

2.4 Discussion

For the case of pavement system PL in the cold season, the modified pavement tends to be cooler than the control case in both cities. In the warm season though, the modification has a mixed impact with equal distribution of warmer and cooler surface differences (P-PL) in Chicago while in Austin, the same pavement system (PL) is cooler a higher percentage of the time. It is inferred that the lower thermal mass in pavement system PL leads to less heat storage. The behavior in the warm season in Chicago can be explained by the relatively milder season as compared to Austin. Notice also the high magnitude of the minimum and maximum differences, which shows that the change in thermal mass has a significant impact on the surface temperature.

For the case of titanium dioxide cement, PT, there is always a decrease in surface temperature over the control concrete pavement, i.e., a more positive surface temperature difference. Moreover, the surface temperature difference (P-PT) is higher in Austin relative to Chicago because of the greater incoming solar radiation for both warmer and colder seasons. The other significant observation for pavement system PT is the cooler surface temperatures it produces during the cold season, which may be detrimental in terms of energy impact in the city.

For the case of pavement system PC, a complete inversion takes place in the surface temperature difference between warm and cold seasons. The replacement of the aggregate base by a CTB leads to warmer surface temperatures in the cold season and cooler surface temperatures in the warm season for both cities. This is explained by the fact that, by increasing the thermal conductivity and heat capacity of the base layer, a CTB creates a pavement system with a higher thermal mass (Gui, Phelan, Kaloush, & Golden, 2007).

To understand these predicted results from an LCA perspective, there is no consensus on the metric to be used to relate surface temperatures to environmental impact, with energy consumption and CO₂-equivalent both being used (Santero, Masanet, & Horvath, 2011a).

For CO₂-equivalent as the metric, a lower surface temperature leads to a lower air temperature (Synnefa, et al., 2011) and this in turn leads to a decrease in radiative forcing, which lowers the CO₂-equivalent in the atmosphere (Munoz, Campra, & Fernandez-Alba, 2010). However, if energy consumption is the metric, then cooler temperatures in cold seasons can cause an increase in heating loads because of lower ambient air temperatures (Akbari & Konopacki, 2005). Greater heating loads imply higher CO₂ emissions as a result of burning fossil fuel. However, lower pavement surface temperatures in the warm seasons may actually increase cooling loads as shown in (Yaghoobian & Kleissl, 2012). Because there is no generalized conclusion, a detailed, site-specific analysis is necessary. Based on the results, a higher pavement albedo may not necessarily be the only way to mitigate the impact of the urban environment especially in cooler seasons. Other thermal properties of the pavement layers can also play a significant role in reducing the negative impact of the paved surfaces on the UHI effect by altering the thermal mass of the pavement system.

2.5 ALTERNATIVE CONCRETE PAVEMENT SYSTEM FOR BALANCING SURFACE TEMPERATURE DIFFERENCE

From the preceding analysis, it can be inferred that a higher thermal mass has an impact on surface temperature. In order to increase the thermal mass of the pavement system without changing the albedo, an alternative concrete pavement system was formulated with a higher thermal conductivity at the surface and a base layer with a larger heat capacity. For the new case, the layer thicknesses were the same as the control case P (see Figure 2-1). To increase the thermal conductivity of the surface, steel fiber-Reinforced Concrete (FRC) was proposed. The mean thermal conductivity of 1.53 BTU/hr-ft-°F (2.65 W/mK) for lower temperature ranges 0 to 100°C (32-212°F) as shown in reference (Kodur & Khaliq, 2011) was used. The FRC density, albedo, and heat capacity was assumed to be the same as the control concrete, 150 pcf (2400 kg/m³), 0.30, and 0.28 BTU/lb-°F (1.2 kJ/kgK), respectively. A CTB was used instead of a granular base with the thermal properties taken from Table 2-1.

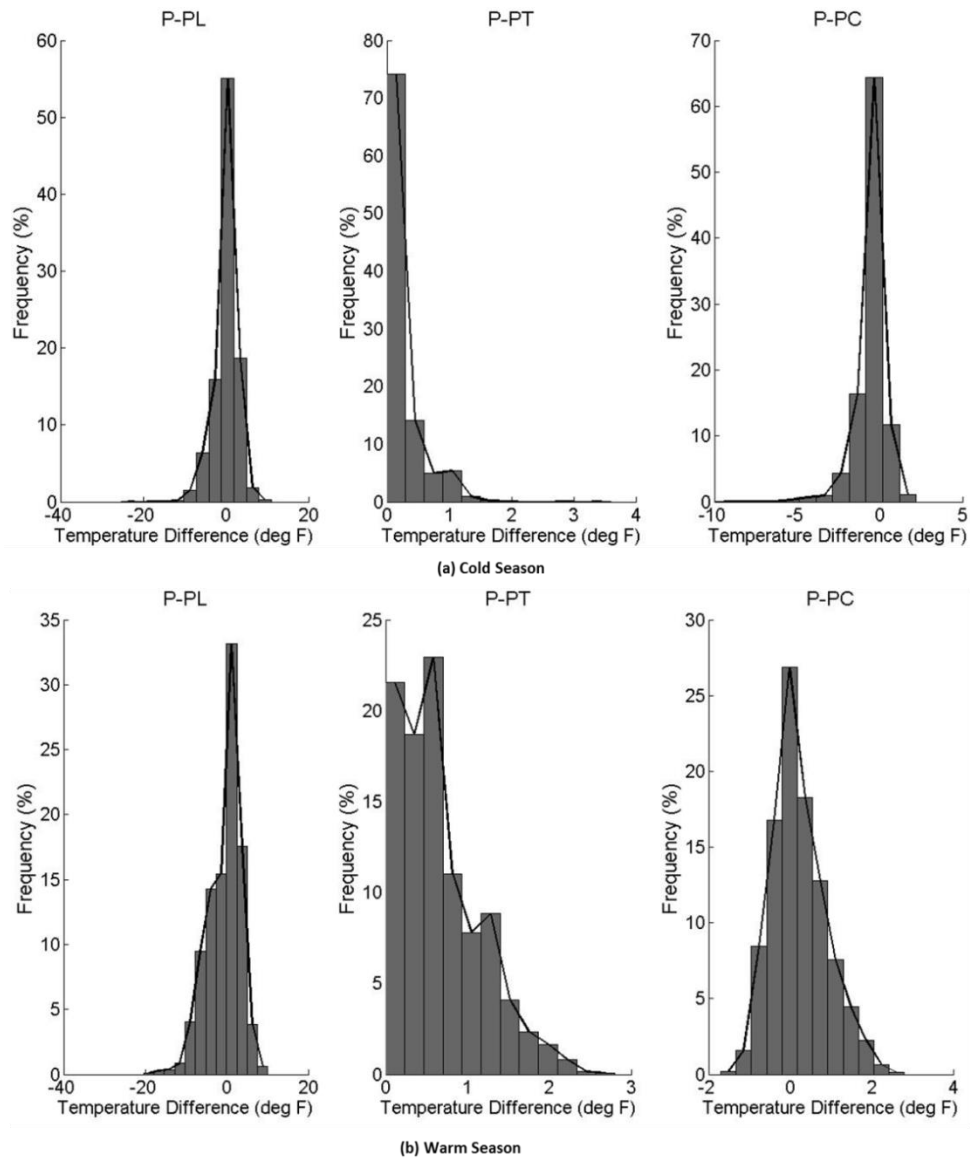


Figure 2-2 Frequency distribution for surface temperature differences (°F) in Chicago
 Table 2-2 Results of concrete pavement surface temperature differences (°F) in Chicago

| Chicago | Cold Season | | | Warm Season | | |
|--------------------|-------------|-------|-------|-------------|-------|-------|
| | P-PL | P-PT | P-PC | P-PL | P-PT | P-PC |
| Minimum | -16.1 | 0 | -5.7 | -22.9 | 0 | -2.2 |
| Maximum | 8.8 | 1.9 | 2.6 | 10.5 | 3.5 | 3.1 |
| Standard Deviation | 2.53 | 0.29 | 0.78 | 4.33 | 0.52 | 0.73 |
| Average | 0.29 | 0.23 | -0.55 | -0.75 | 0.71 | 0.27 |
| % Positive | 47.27 | 59.46 | 17.49 | 46.52 | 90.42 | 52.48 |
| % Negative | 29.03 | 0.00 | 57.15 | 45.25 | 0.00 | 33.36 |
| % Zero | 23.70 | 40.54 | 25.36 | 8.22 | 9.58 | 14.16 |

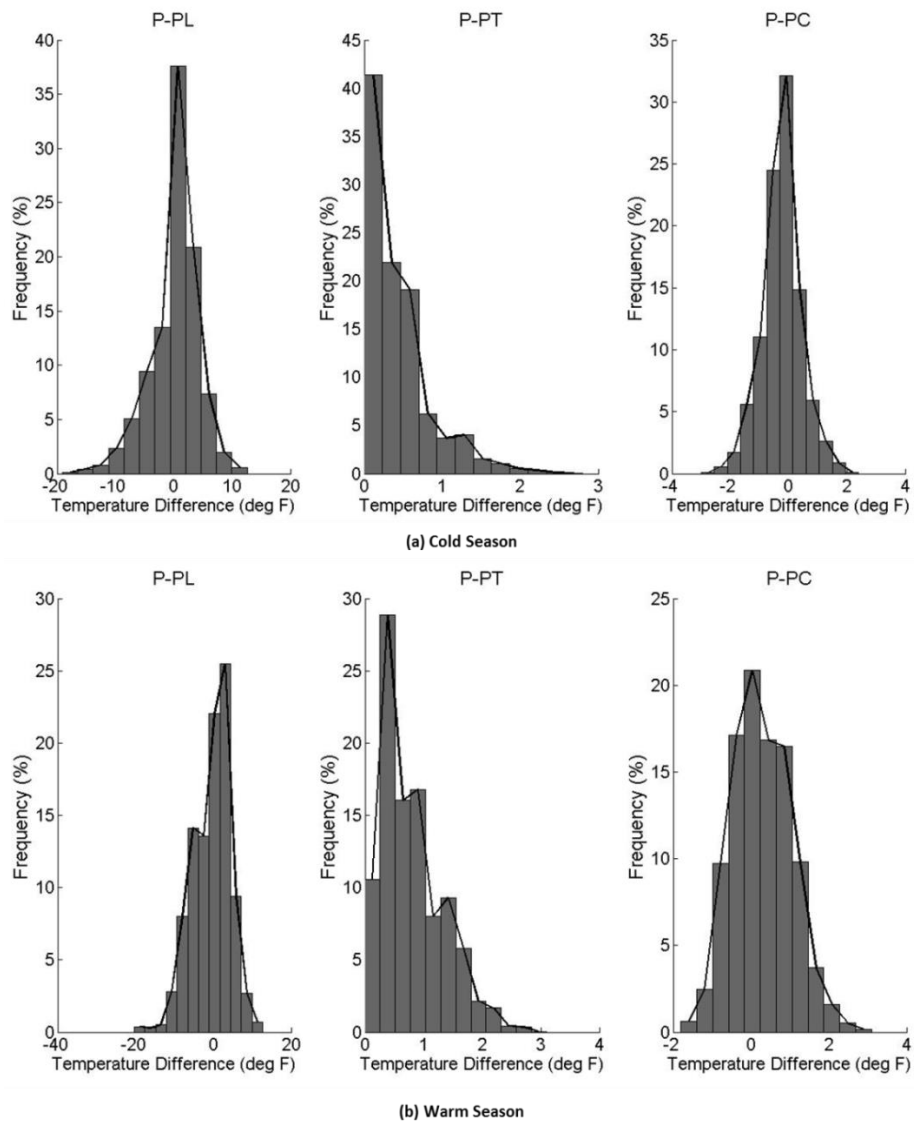


Figure 2-3 Frequency distribution for surface temperature differences (°F) in Austin
 Table 2-3 Results of concrete pavement surface temperature differences (°F) in Austin

| Austin | Cold Season | | | Warm Season | | |
|--------------------|-------------|-------|-------|-------------|-------|-------|
| | P-PL | P-PT | P-PC | P-PL | P-PT | P-PC |
| Minimum | -19.1 | 0 | -3 | -20.3 | 0 | -1.8 |
| Maximum | 12.6 | 2.8 | 2.4 | 12.7 | 3.1 | 2.8 |
| Standard Deviation | 4.13 | 0.42 | 0.69 | 4.95 | 0.53 | 0.75 |
| Average | 0.10 | 0.42 | -0.20 | -0.55 | 0.84 | 0.28 |
| % Positive | 52.46 | 82.86 | 29.58 | 53.26 | 97.74 | 57.78 |
| % Negative | 34.85 | 0.00 | 52.46 | 44.01 | 0.00 | 35.82 |
| % Zero | 12.69 | 17.14 | 17.96 | 2.73 | 2.26 | 6.40 |

The modified case was called PF and was analyzed again for both Chicago and Austin. The surface temperature differences are designated (P-PF) and their frequency distribution for the two cities and two seasons are shown in Figure with the statistical analysis in Table . With the alternative pavement system with higher surface and base thermal conductivity leading to increased base layer thermal storage capacity, Table 4 documents that for both cities, the alternative concrete pavement has warmer surfaces in cooler seasons and cooler surfaces during warmer seasons relative to the control concrete pavement. The minimum and maximum differences vary between the two cities, indicating a dependence on climate with the minimum difference in Chicago in the cold season being -5.4 °F and -2.4 °F for the same season in Austin. On comparing the case (P-PC) from Table 2-2 and Table 2-3 with (P-PF) in Table 2-4, the trends are similar, as expected.

Clearly, thermal mass significantly impacts pavement surface temperature and does it in different magnitudes depending on the season and climate location.

2.6 CONCLUSION

In order to study the UHI effect with respect to pavements, it is important to understand the various factors contributing to change the pavement surface temperature including the pavement layers, materials, and local climatic condition. By using the EICM embedded within the MEDPG, the thermal properties of the entire pavement system, such as albedo, thermal conductivity and heat capacity were studied with respect to the differences in surface temperature relative to a control concrete pavement. Initially, changes were made only to one layer and from the insights gained therein, an alternative system was analyzed.

A change in a single property, such as albedo, thermal conductivity or heat capacity, while fixing the others can lead to significant change in surface temperatures from that of a control case; for example, increasing albedo from 0.30 to 0.35 can cool the surface by as much as 3.5 °F in some cases. While increasing the albedo leads to cooler surface temperatures across seasons, other modifications that change the thermal mass of the pavement system, such as using lower density concrete for the surface layer or a cement treated base or a combination of such strategies, show more variation, which was studied by hour, season, and climate. Lowering the thermal mass using lower density concrete for the surface course can decrease the surface temperature for about 50% of the time but also increase it about 35-40% of the time. Increasing the thermal mass by using a combination of FRC in the surface course and a CTB can lead to warmer surface temperatures in the cold season and cooler surface temperatures in the warm season about 60% of the time. In general, increasing the thermal mass of the system leads to it storing more thermal energy in the lower layers, which can lead to higher or lower surface temperatures depending on the season, which has a bearing on UHI.

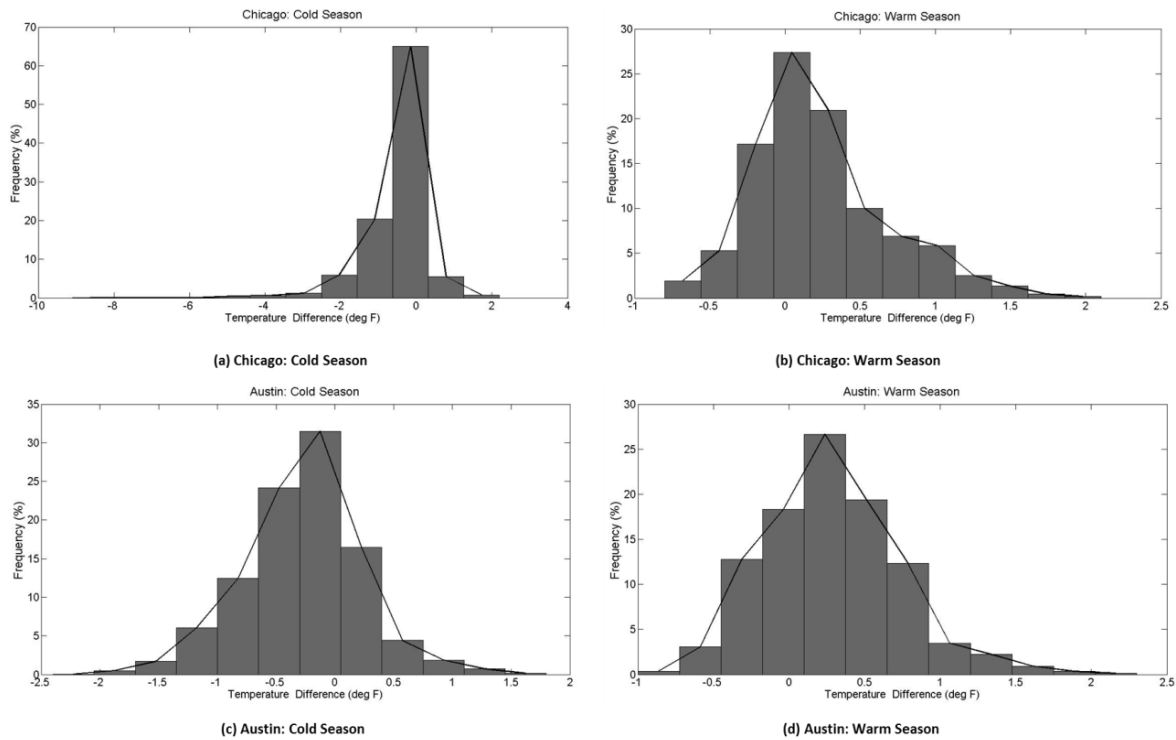


Figure 2-4 Frequency distributions of surface temperature differences ($^{\circ}$ F) for the case P-PF

Table 2-4 Results of a statistical analysis of temperature differences ($^{\circ}$ F) for the case P-PF

| | Chicago | | Austin | |
|--------------------|---------|-------|--------|-------|
| | Cold | Warm | Cold | Warm |
| Minimum | -5.4 | -1.3 | -2.4 | -0.9 |
| Maximum | 2.4 | 2.5 | 1.8 | 2.2 |
| Standard Deviation | 0.73 | 0.49 | 0.53 | 0.45 |
| Average | -0.35 | 0.26 | -0.24 | 0.26 |
| % Positive | 16.09 | 59.58 | 24.17 | 63.63 |
| % Negative | 59.69 | 23.23 | 56.57 | 25.08 |
| % Zero | 24.23 | 17.19 | 19.26 | 11.29 |

As UHI is a key component of a pavement LCA, the thermal properties impact it as well and therefore, should be considered in any pavement life cycle assessment.

The main strengths of this study are: (a) the temporal resolution (one hour) for an entire year; (b) coverage of different seasons and climates; and (c) the use of layers and materials that could be used in pavement construction. It goes beyond previous studies in that it addresses pavement surface temperature differences on an hourly basis and as a percentage of effectiveness of a modification in properties. It also discusses effectiveness with respect to

climate location. In the future, this approach can be used with a climate and building energy model to capture the estimated impact on a pavement LCA.

CHAPTER 3- A HEAT FLUX-BASED APPROACH TO URBAN HEAT ISLANDS IN CONCRETE PAVEMENTS

3.1 INTRODUCTION

The Urban Heat Island (UHI) effect is observed in built-up urban environments as a sustained high temperature difference between urban areas and adjacent rural areas, called the UHI intensity. This difference can be studied at various elevations, e.g., surface, canopy layer and boundary layer UHIs, with Canopy Layer UHIs (CLUHIs) being the most commonly observed and important because this is the layer where people live and work. Typically, the UHI intensity is highest at nighttime (Wong & Hogen, 2011; Goward, 1981) because urban man-made surfaces, i.e., buildings and pavements, absorb and store heat during the day and then gradually release it at night (Shahmohamadi, Che-Anil, Ramly, Maulud, & Mohd-Nor, 2010).

UHI is caused by multiple factors including construction materials and layers used in buildings and pavements, loss of vegetation and anthropogenic heat. In particular, the UHI caused by pavements is assessed for environmental impact in the use-phase of a pavement Life Cycle Assessment (LCA) (Santero, Masanet, & Horvath, 2011b). By absorbing more heat than natural materials, pavements change the earth's heat budget and increase the radiative forcing (RF), which is the imposed change in the rate at which the earth absorbs solar energy. Several studies have focused on the effect of increasing pavement albedo on RF (Menon, Akbari, Mahanama, Sednev, & Levinson, 2010; Akbari, Menon, & Rosenfeld, 2009; Munoz, Campra, & Fernandez-Alba, 2010; Yu & Lu, 2014). They have customarily expressed RF in terms of a Global Warming Potential (GWP) in tons of CO₂-equivalent. This paper proposes a new method to assess the RF and corresponding GWP of a pavement during the use-phase considering all the pavement layer thermal properties. This GWP can be readily integrated into a broader pavement LCA framework.

As a thermal system, pavements consist of a series of material layers with the heat flux through the pavement as well as the temperature profile depending on the following properties: surface layer albedo, thermal conductivity, heat capacity and emissivity. Specifically, the temperature profile $T(x, t)$ through the bound layers, including the surface layer, of a pavement is governed by a 1-D Fourier Equation (Equation 3.1) for transient heat flow (Dempsey & Thompson, A heat transfer model for evaluating frost action and temperature related effects in multi-layered pavement systems, 1970) where x is the depth of the pavement at which the temperature is calculated (positive downwards), t is time, and α is the thermal diffusivity of the material defined by Equation 3.2, where k is the thermal conductivity, C is the heat capacity and ρ is density.

$$\frac{\partial^2 T}{\partial x^2} = \frac{1}{\alpha} \frac{\partial T}{\partial t} \quad (3.1)$$

$$\alpha = \frac{k}{\rho C} \quad (3.2)$$

The temperature profile of the unbound aggregate and soil layers is governed by coupled heat and moisture movements, which is modeled using the Philip-de Vries equations (Dempsey & Elzeftawy, 1976). These processes, which govern heat transfer through a pavement system, are modeled in the Enhanced Integrated Climatic Model (EICM), used in the Mechanistic-Empirical Pavement Design Guide (Larson & Dempsey, 1997). This chapter uses the same principles in a new program called ILLI-THERM to model transient heat flow through pavements.

While thermal diffusivity in transient heat flow determines the rate at which materials can transmit heat, thermal inertia (also called thermal effusivity) is related to the rate at which a material is able to store or lose heat (Jeanjean, Olives, & Py, 2013; Dehdezi, Hall, & Dawson, 2011). Previous studies have shown thermal inertia to be an important property, together with thermal diffusivity, in understanding the thermal behavior of pavements (Kusaka, Kondo, Kikegawa, & Kimura, 2001; Goward, 1981). Thermal inertia I is calculated using Equation 3.3 (Swaid & Hoffman, 1989; Golden, Guthrie, Kaloush, & Britter, 2005).

$$I = \sqrt{k\rho C} \quad (3.3)$$

Thermal inertia causes a pavement layer to have a delayed reaction to changes in meteorological conditions ultimately producing a time lag or delay (Jeanjean, Olives, & Py, 2013) in their thermal response. For example, this thermal delay will result in time lag between the peak surface temperature and peak temperature at other positions in the pavement structure. Previous researchers have described this as a hysteresis lag between daytime and nighttime summer surface temperatures (Golden, Guthrie, Kaloush, & Britter, 2005; Golden, Carlson, Kaloush, & Phelan, 2007).

A previous study (Gui, Carlson, Phelan, Kaloush, & Golden, 2002) varied pavement surface course thicknesses to minimize the average peak surface temperature over a three-day analysis period but without considering what effect those changes had on temperatures at other times of the day. By keeping the thermal diffusivity constant, the increased thickness of the surface course redistributed the heat internally and away from the surface. Thermodynamically, this is equivalent to increasing the thermal inertia of the base course of the pavement so that it can store more of the absorbed heat and keep it away from the surface course. However, this strategy can impact the heat flux and consequently temperatures at other times of the day and night. A heat flux-based approach is proposed to first calculate the RF and GWP of several concrete pavement types and also to demonstrate how thermal inertia and diffusivity for concrete pavement structures can be adjusted to mitigate nighttime CLUHI while keeping the GWP of the pavement nearly the same.

3.2 MATERIALS AND METHODOLOGY

3.2.1 Pavement Cases

Building on Chapter 2, a control case (P) was established, consisting of a hypothetical rigid pavement with a 100 mm PCC surface course, a 150 mm granular base (A-2-4), a 300 mm granular subbase (A-3), and a subgrade (A-6) as shown in Figure . Four independent modifications to the thermal properties of the surface and/or base layers were made to the control case: lower density concrete was used in the surface course (case PL), concrete with titanium dioxide (TiO₂) white cement was used in the surface course (case PT), a cement-treated base (CTB) was substituted for the granular base (case PC), and a CTB was combined

with a steel fiber-reinforced concrete (FRC) surface course (case PF). Relative to the control (case P), case PT increased the albedo of the pavement surface, case PL lowered the concrete's thermal diffusivity and inertia, and case PF increased the concrete's thermal diffusivity. The inclusion of a CTB in cases PC and PF also increased the thermal inertia of the base with respect to case P. All these cases are shown graphically in Figure 3-1.

3.2.2 Thermal Inputs and Analysis

The pavement layer material properties used in these five cases are shown in Table 3-1. The use of steel FRC slightly increased the thermal inertia while lower density concrete greatly reduced it. The thermal emissivity of the surface course in all cases was fixed at 0.93. All other unbound layer properties, namely the grain size distribution and Soil Water Characteristic Curve (SWCC) parameters, are taken as the MEPDG default values (Larson & Dempsey, 1997; ARA, Inc., 2004). The thermal inputs of the unbound layers (aggregate base, subbase and subgrade) were calculated internally by the program. They were a function of the volumetric air and moisture contents and changed over time due to suction. Therefore, no one value could be assigned to them in (Dempsey B. J., 1969). While heat capacity was a weighted average of the three phases, thermal conductivity was based on an empirical function (Dempsey B. J., 1969). Because of their air voids, the thermal diffusivity and inertia of the unbound layers is less than that of the stabilized layers. All other thermal properties were assumed to be constant throughout the analysis.

The 1-D thermal analysis was performed using a program, called the Illinois Thermal Analysis Program (ILLI-THERM), written by the authors and based on the EICM program (Larson & Dempsey, 1997) and in collaboration with its developers. ILLI-THERM calculates the heat flux from the surface and the temperature profile of the pavement at various nodes, for each hour of the analysis period. A positive flux indicates a net absorption of heat while a negative flux is a net heat emission from the pavement surface. All cases were analyzed from October 1, 1999 to September 30, 2004, with the period of April to September each year being classified as the warm season and October to March as the cold season. In this analysis period, no maintenance to the pavement structure were considered and any traffic shading was ignored. As an example of how the UHI can be implemented into a use phase analysis, the thermal analysis was completed for Austin, TX.

| Layer | Dimensions | Case P (Control) | Case PL | Case PT | Case PC | Case PF |
|----------------|---------------|------------------|----------------------|---------------------------|---------------------|---------------------------------|
| Surface Course | 100 mm | Concrete | Low-Density Concrete | TiO ₂ Concrete | Concrete | Steel Fiber-Reinforced Concrete |
| Base Course | 150 mm | Granular (A-2-4) | Granular (A-2-4) | Granular (A-2-4) | Cement-Treated Base | Cement-Treated Base |
| Subbase Course | 300 mm | Granular (A-3) | Granular (A-3) | Granular (A-3) | Granular (A-3) | Granular (A-3) |
| Subgrade | Semi-Infinite | Silty Soil (A-6) | Silty Soil (A-6) | Silty Soil (A-6) | Silty Soil (A-6) | Silty Soil (A-6) |

Figure 3-1 Hypothetical rigid pavement cross sections

3.2.3 Determination of RF and GWP

The Radiative Forcing (RF) of a pavement is defined as the imposed change in the energy budget of the Earth because of the pavement (Intergovernmental Panel on Climate Change (IPCC), 2001). In other words, it is the rate at which energy is absorbed by a pavement over its life by virtue of its construction. This can be expressed in terms of a net heat flux or as a Global Warming Potential (GWP) of an equivalent amount of carbon dioxide released into the atmosphere over the analysis period.

Traditionally, RF of pavements has been calculated through empirical observations of the global surface energy budget (Akbari, Menon, & Rosenfeld, 2009; Cotana, et al., 2014) and global-scale climatological simulations using atmospheric models (Menon, Akbari, Mahanama, Sednev, & Levinson, 2010). For an LCA, other researchers (Yu & Lu, 2014; Susca, 2012) have used empirical values of RF derived from an increase of 0.01 of the earth's albedo to determine the corresponding RF for any albedo change by assuming a linear relationship.

These empirical models fail to take into account differences in the thermal behavior of natural materials such as grass, forests, and snow as well as paving materials like concrete. These RF estimates are primarily used for global policymaking and therefore, only take into account albedo and cannot determine the change in RF caused by changes to other pavement thermal properties. They also cannot incorporate climatic differences between locations where the pavement under consideration is being analyzed because the models are based on global averages. Lastly, the models are valid only at a scale that cannot differentiate between the pavement structure and its surroundings, leading to potentially inaccurate predictions for urban locations.

Table 3-1 Thermal properties of paving materials

| Material | Albedo | Thermal Conductivity | Heat Capacity | Dry Unit Weight | Thermal diffusivity | Thermal Inertia |
|---------------------------------------|----------------|-----------------------|-----------------------|----------------------|---------------------------------------|---------------------------------------|
| | | (W/mK) | (kJ/kgK) | (kg/m ³) | ($\times 10^{-7}$ m ² /s) | (Ws ^{1/2} /m ² K) |
| PCC (JPCP) | 0.30 | 2.16 | 1.17 | 2403 | 7.7 | 2467 |
| A-2-4 (Base) | Not Applicable | Internally calculated | Internally calculated | 1953 | Internally calculated | Internally calculated |
| A-3 (Subbase) | Not Applicable | Internally calculated | Internally calculated | 1922 | Internally calculated | Internally calculated |
| A-6 (Subgrade) | Not Applicable | Internally calculated | Internally calculated | 1615 | Internally calculated | Internally calculated |
| Low-Density Concrete | 0.30 | 0.61 | 1.05 | 1378 | 4.2 | 934 |
| Cement-Treated Base | Not Applicable | 2.16 | 1.17 | 2403 | 7.7 | 2467 |
| TiO ₂ -concrete | 0.35 | 2.16 | 1.17 | 2403 | 7.7 | 2467 |
| Steel Fiber-Reinforced Concrete (FRC) | 0.30 | 2.65 | 1.17 | 2403 | 9.4 | 2730 |

This paper proposes an alternative method to determine RF that can overcome the aforementioned shortcomings. This method takes into account the thermal properties and structure of the pavement layers as well as the service life and climatic conditions where the pavement is constructed. Thus, it overcomes the limitations of the models found in literature and can be readily integrated into a larger pavement LCA framework. The functional unit of this five-year LCA is one square-meter of the pavement, although this can be easily transformed into a more traditional use phase functional unit, e.g., lane-km. The system boundaries are the pavement and the canopy layer immediately above it. Adjacent structures such as buildings are not considered.

The thermal analysis program, ILLI-THERM, used in this paper provides hourly net surface heat flux (positive or negative) over the entire analysis period. This is the rate at which heat is being exchanged with the environment. The total heat stored over that period in the pavement is given by Equation 3.4, where \dot{Q}_i is the surface heat flux at the i^{th} hour, with a total of n hours in the analysis, A is the total area of the pavement under consideration, and Δt is the model time step (one hour).

$$Q_{stored} = \sum_{i=1}^n \dot{Q}_i \Delta t A \quad (3.4)$$

Over the analysis period, the rate at which this heat is stored per unit area is given by Equation 3.5. By definition, this is the RF of the pavement. Mathematically, this is the mean surface heat flux from the pavement. This RF quantity can be thought of as the change in the local surface energy budget of the earth as a result of constructing the pavement.

$$RF = \frac{Q_{stored}}{n \Delta t A} = \frac{\sum_{i=1}^n \dot{Q}_i}{n} \quad (3.5)$$

Previous studies have described how RF can be converted into an equivalent amount of CO₂ (Bird, et al., 2008; Yu & Lu, 2014). An algorithm similar to the one in these studies is used here along with a model to account for decay of atmospheric CO₂ over the analysis period of five years using the function from (Joos, et al., 2001) and averaging it over that period. The GWP or equivalent CO₂, after simplification of constant terms and the value from the decay function, is found using Equation 3.6 in terms of kg CO₂-eq/m².

$$\Delta CO_2 = 1.3556 \times RF \quad (3.6)$$

This equivalent CO₂ can be described as the amount of CO₂ that should be released into the atmosphere over the same analysis period to impose the same RF as the pavement.

3.2.4 Analysis of Heat Flow

For calculating thermal energy stored, three nodes were selected for each case – the surface node, the interface node between the surface and the base, which was assumed to have the same properties as the surface course, and the last node of the base for cases PC and PF, which was assumed to have the same properties as the CTB. The base courses of the cases without a CTB were not analyzed. The thickness of each of the associated nodal elements was 25 mm. These nodes are shown schematically in Figure 3-2(a). The heat stored in each nodal element was calculated every hour based on a reference temperature of 0 °C using Equation 3.7.

$$\text{Heat Stored} = |\text{Nodal Temperature} - 0| \times \rho C \times \text{Thickness} \quad (3.7)$$

The heat conducted per hour through a bound layer (surface course and CTB) was calculated across a layer (and not a nodal element) using Equation 3.8, where T_{top} and T_{bottom} are the

temperatures in °C of the first and last nodes respectively of each layer or sub-layer. The position of these nodes and their associated layers is shown in Figure 3-2(b). A positive value indicates heat conduction into the pavement layers (downward) and a negative value means conduction out of the layers (upward).

$$\text{Heat Conducted} = (T_{top} - T_{bottom}) \times \text{Thickness of layer} \times k \quad (3.8)$$

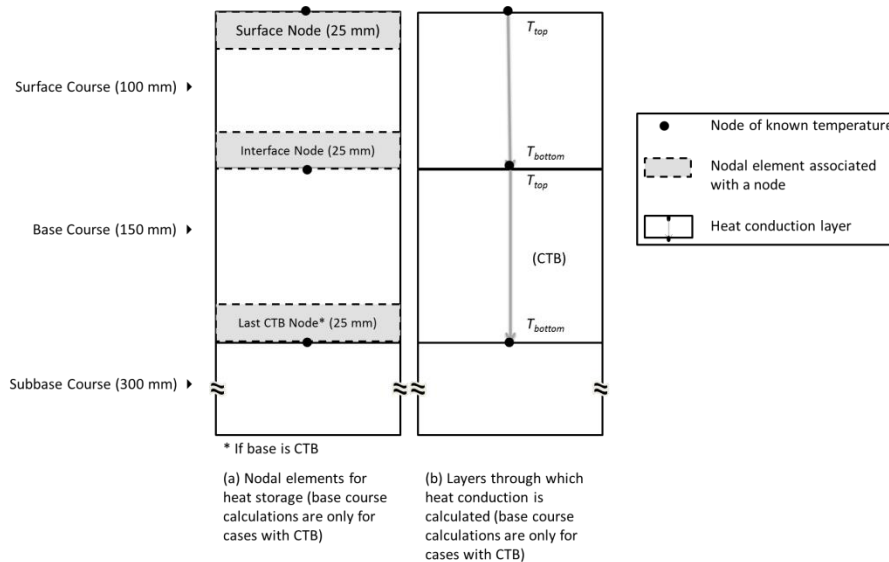


Figure 3-2 Schematic of (a) nodal elements used to calculate heat stored; and (b) layers through which heat conduction is calculated (direction of arrows does not necessarily indicate direction of heat flow. Thickness in brackets

Finally, the net surface heat flux from ILLI-THERM is also analyzed. Incoming radiation depends on the time of day and the albedo of the pavement surface. The albedo of all the cases was the same except for case PT, as shown in Table 3-1. Outgoing radiation is a function of wind speed, thermal emissivity, and surface and air temperatures. The net surface heat flux is the difference between incoming and outgoing radiation, with a positive value indication a net absorption and negative value, net emission and the value always being negative after sunset. The resultant pavement temperature profiles reflect the net heat flux and material thermal properties.

3.2.5 Average Seasonal Day

To observe the time lag in the heat storage and conduction, a new metric called the average seasonal day was developed. With this metric, the data associated with each nodal element and conduction layer or sub-layer for each of the warm and cold seasons is averaged at every given hour with 24 average values obtained that represent an average day in that season. For example, the heat stored in the surface node of Case PT (Figure 3-1(a)) at time 0100 hours is averaged for the entire season and this is repeated for each hour, thereby obtaining the heat stored in an average seasonal day. By restricting the average to a season, it reflects that pavement temperatures vary more between seasons but less so within a season. This same analysis was also performed on the surface heat flux and presented and discussed later in this chapter.

3.2.6 Surface Temperature Difference

To analyze the changes in surface temperatures of all the pavement cases, the hourly difference from the control case at a given node for each modified pavement was statistically summarized. These temperature differences were labeled (P-PL), (P-PT), (P-PC) and (P-PF) for each respective case. The analysis included determining the percentage of effectiveness of the pavements with respect to the control case, i.e., the percentage of hours the differences were positive (the control case is warmer than the modified case), negative (the modified case is warmer) and zero (the two cases have the same surface temperature to the fourth decimal place). The percentage of effectiveness, as used in Chapter 2, quantifies the extent of benefit derived from the pavement in consideration relative to the control pavement in terms of UHI mitigation. This metric provides more insight than reporting only the maximum or minimum surface temperature obtained over the entire analysis period as was the case in a previous study (Gui, Carlson, Phelan, Kaloush, & Golden, 2002).

In addition to analyzing the surface temperature differences separately for two seasons per year (warm and cold), it was also analyzed distinctly for daytime and nighttime, which were defined based on the time of sunrise and sunset of each day from the weather data. This additional temporal level gives more insight into the role of the changes in pavement thermal response because of the changes in thermal properties of the pavement layers.

3.3 RESULTS AND DISCUSSION

3.3.1 Global Warming Potential

Using data from ILLI-THERM and Equations 3.5 and 3.6, the RF and corresponding GWP per unit area of each pavement case is calculated and shown in Figure 3-3. All the pavement cases except case PT have almost the same RF and subsequent GWP of approximately 52 kg CO₂-eq/m². However, case PT has a smaller GWP of about 43 kg CO₂-eq/m². This is a difference of about 9 kg CO₂-eq/m² or, for a typical road width of 7m, about 63 t CO₂-eq/lane-km for a 5 year analysis period.

From this analysis, it can be inferred that a higher albedo (case PT has higher albedo by 0.05) is the most effective way to reduce GWP among the options considered for the assumed system boundaries. Changes to other thermal properties did not lead to any significant change in GWP as seen in Figure 3-3. However, GWP is not a reliable measure of UHI, as it simply describes changes in the earth's heat budget and is a measure of long-term environmental impact quantified in a pavement LCA. The increased heat can be more efficiently redistributed internally and away from the surface for some pavement structures in a more optimal manner to reduce its effects on the UHI, as discussed in the next sections.

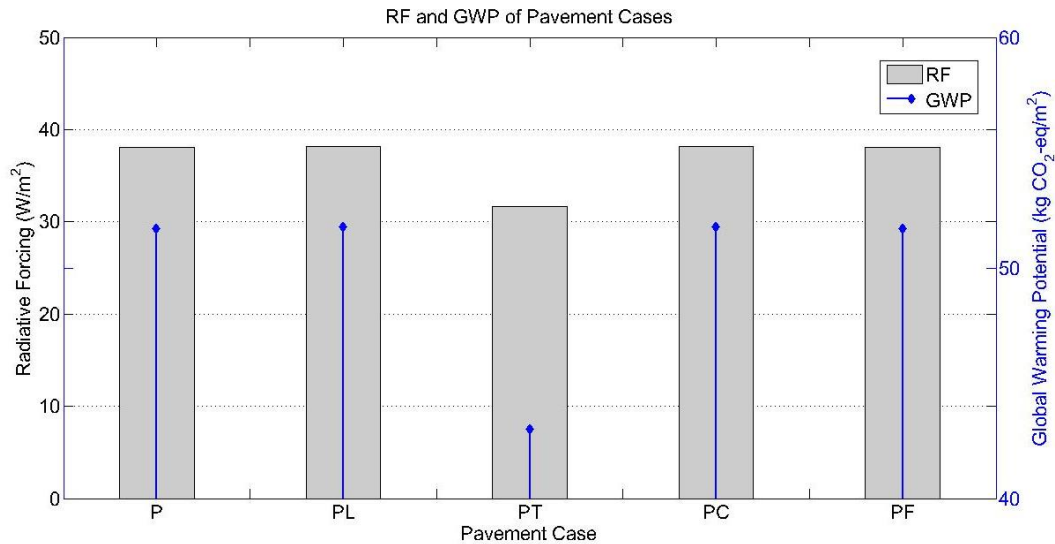


Figure 3-3 RF and GWP of analyzed pavement options for a five-year analysis period

3.3.2 Heat Flux, Storage and Conduction

The net surface heat flux, heat stored and conducted data were analyzed using the average seasonal day metric for both the warm and cold season. The net surface heat flux is plotted in Figure 3-4, heat conducted through each layer for each pavement case is presented in Figure 3-5, and heat stored in specific nodes for each pavement case is shown in Figure 3-6.

Considering Figure 3-4, Figure 3-5 and Figure 3-6, the first observation is that the general thermal behavior of a given concrete pavement case, in terms of the relative magnitude and time of heat flux, storage, and conduction does not change with season but its magnitude does. This is because, in the governing equations of heat flow through the pavement, weather acts only as a boundary condition. The magnitude of heat interacting with the pavement depends on the local climate, but its behavior once inside depends only on material properties and pavement structure. Therefore, the following comparisons made regarding thermal behavior of different concrete pavement systems in the next sections apply to both cold and warm seasons.

3.3.2.1 Effect of Higher Albedo

Observing Figure 3-4, case PT absorbs much less heat at daytime than the control case P, because of its higher albedo, but emits only slightly less heat at nighttime because of its slightly lower surface temperature. This difference is what leads to a lower RF shown in Figure 3-3. From Figure 3-5, it can be observed that the pavement case PT conducts less heat both into and out of the pavement since it absorbs less heat in the first place. Similarly, it stores less heat as well as seen in Figure 3-6. Since PT's granular base course has lower thermal inertia as compared to cases PC and PF, it cannot store heat for a long period at night and it ends up conducting more heat out of the pavement for a part of the night than the cases with a CTB, as seen in Figure 3-5.

3.3.2.2 Effect of Lower Thermal Diffusivity and Inertia

In Figure 3-4, the net surface heat flux of case PL in daytime is always less than that of case P, despite absorbing the same amount of heat on account of the same albedo. This means that a greater part of the heat is emitted out in daytime because of its significantly higher surface temperature. The heat stored and conducted is also lower because the low thermal diffusivity

of the surface course prevents it from conducting much heat to the granular base (Figure 3-5) and the low thermal inertia does not allow the surface course to store much heat either (Figure 3-6). As seen in Figure 3-4, the heat flux of case PL is less than case P during nighttime as well, indicating that a large part of the absorbed heat is emitted out during the daytime, leading to a smaller net heat conducted into the pavement during daytime (Figure 3-5) as well as heat stored in the surface node (Figure 3-6).

3.3.2.3 Effect of Higher Thermal Diffusivity and Inertia

For cases PC and PF, Figure 3-4 shows that the net heat flux is marginally lower than case P in daytime, indicating marginally higher surface temperatures. Figure 3-5 shows that cases PC and PF conduct less heat through the surface course to the atmosphere during the night than the control case P, leading to marginally lower heat flux out of the surface in Figure 3-4. The higher thermal inertia of the CTB in both cases allows them to store a part of the absorbed heat during the daytime, with the CTB of case PF receiving more heat than that of case PC because of the higher diffusivity of the FRC surface course. At night, the thermal inertia of the base course creates a time lag between the behavior of the base and surface courses, such that the heat stored in the base course is not readily given up and is only gradually emitted during the night and also during the early part of the next day.

This time lag can be measured between the two heat waves when they have similar periods. In Figure 3-5, this 4 hour lag occurs between the time when the surface and base courses of case PC begin to conduct heat out of the pavement, i.e., when the heat conduction turns negative. During this time lag, the base course does not conduct heat towards the surface course and into the atmosphere, thus reducing the nighttime UHI. In case PF however, the higher diffusivity of the surface course causes it to conduct heat from the base course faster than case PC but still slower than case P, so that case PF emits marginally more heat at nighttime than case PC but still marginally less than case P, as seen in Figure 3-4. These marginal differences in heat conducted are quantified in per unit area per second units, which sum to a significant amount of heat over a day for a lane-km of pavement.

This time lag is further manifested in the change in heat stored in the surface course and CTB (for cases PC and PF). Choosing the time of maximum heat storage, the time lag between the surface node and interface node and surface node and last node of the CTB for case PC is shown in Figure 3-6 to be 2 and 7 hours, respectively, in both seasons. This demonstrates how the CTB is able to store a part of the heat from the surface course well after the surface course ceases absorbing anymore heat (after sunset) and gradually returns it over the nighttime and early the next day. This is further verified in Figure 3-5 by the heat conduction at the CTB interface which is still negative between the hours of 10:00 and 11:00 in both seasons.

3.3.2.4 Thermal Effects Summary

Pavements with high thermal inertia base course can mitigate nighttime UHI by delaying and moderating the rate at which stored heat is conducted out of the pavement at night and emitted to the atmosphere, thus making the net emission more gradual over the day and reducing peak emissions. Part of this benefit can be lost if the surface course has too high of a thermal diffusivity and is able to conduct the heat out too fast, as was the case with case PF emitting marginally more heat at night as compared to case PC (Figure 3-4). Alternatively, as with case PL, by decreasing the thermal diffusivity and inertia of the surface course, the absorbed heat during the day can be emitted during the daytime (Figure), thus decreasing the heat emitted at night. Finally, increasing the albedo can also mitigate UHI, as is

recommended for developing cool pavements (Santamouris, Synnefa, & Karlessi, Using advanced cool materials in the urban built environment to mitigate heat islands and improve thermal comfort conditions, 2011).

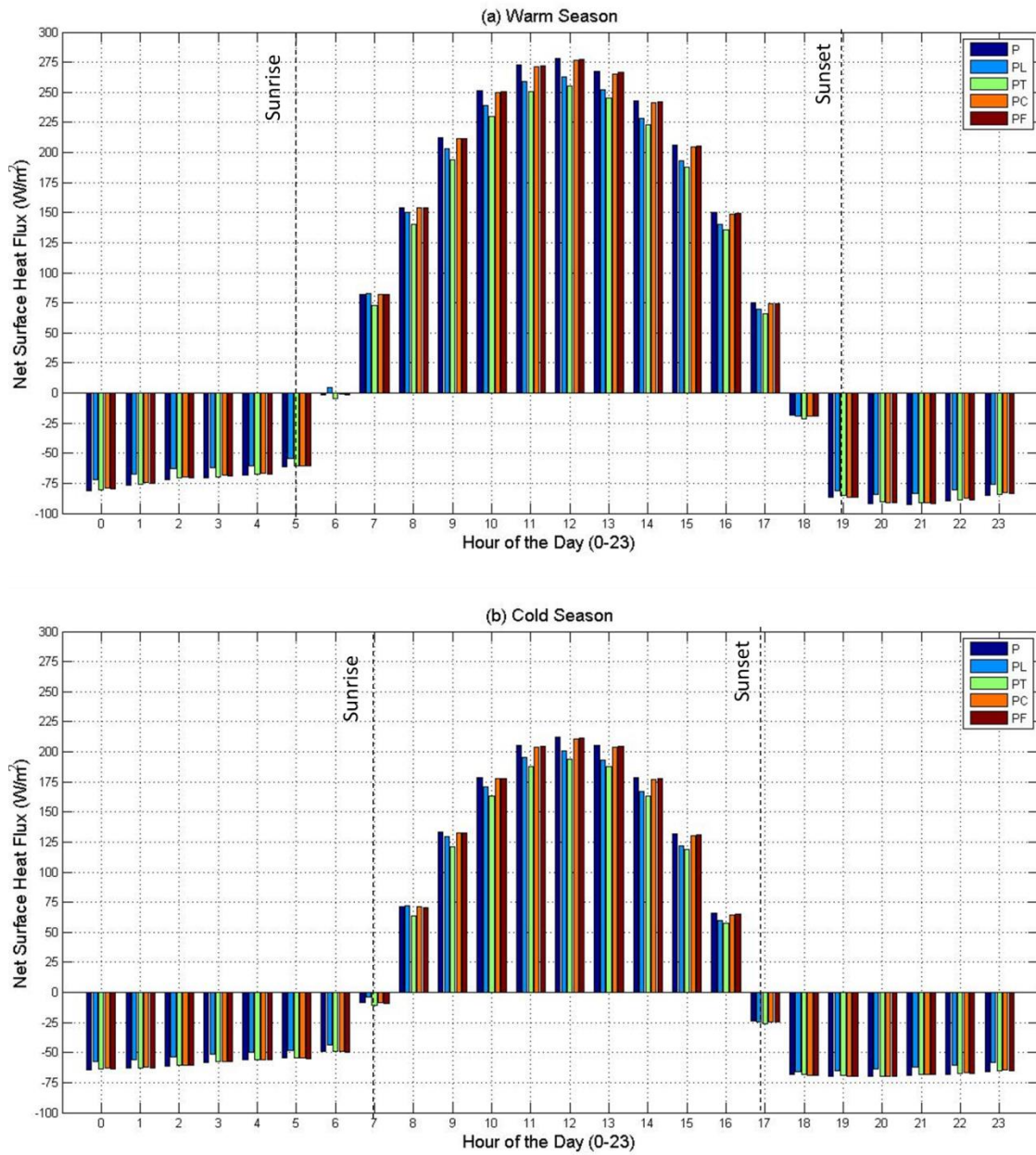


Figure 3-4 Net surface heat flux (in W/m²) for each pavement case in (a) the warm season and (b) the cold season. Times of sunrise and sunset are only indicative

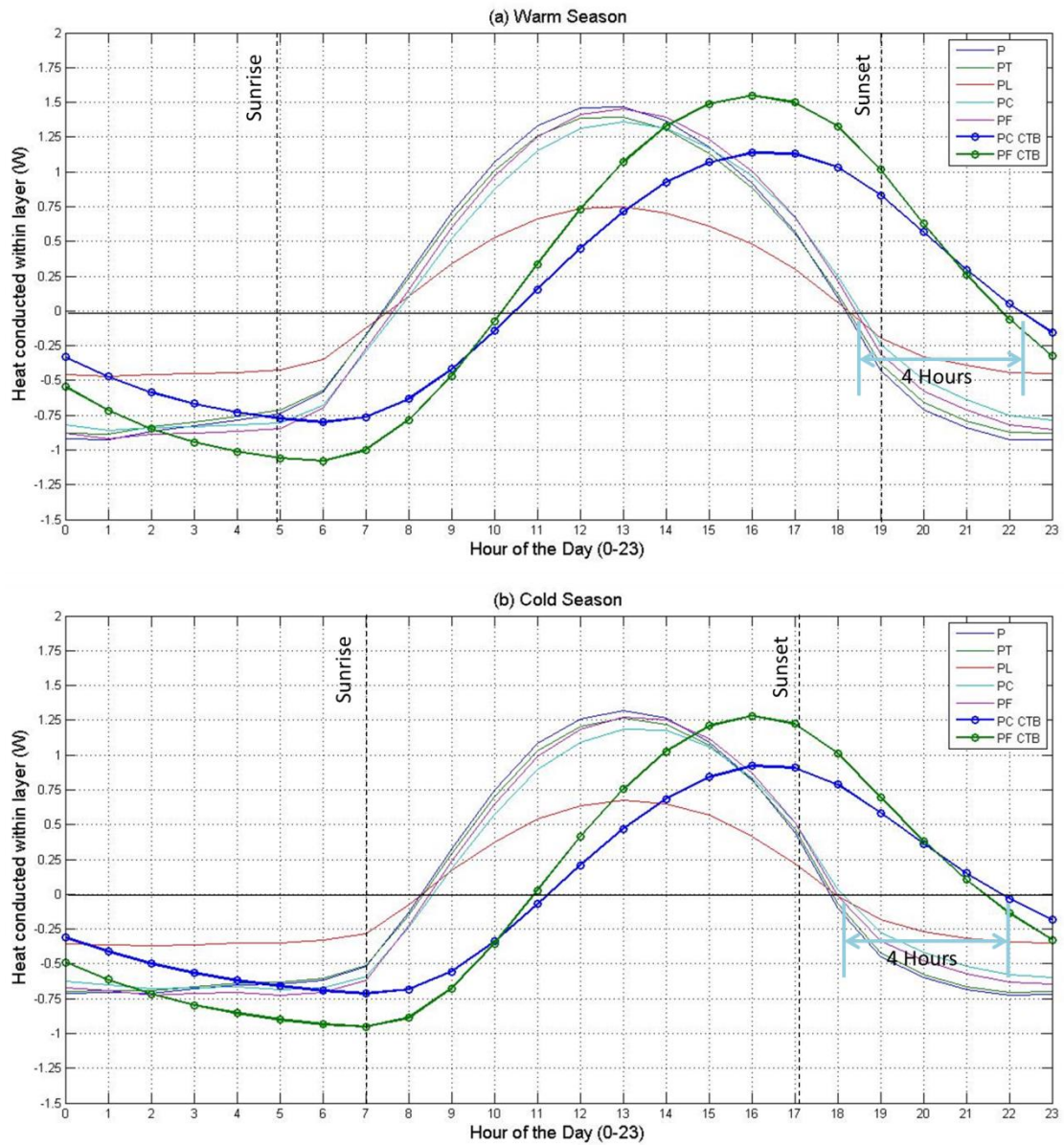


Figure 3-5 Heat conducted (in W) through each layer in an average seasonal day in (a) warm season and (b) cold season. Times of sunrise and sunset are only indicative

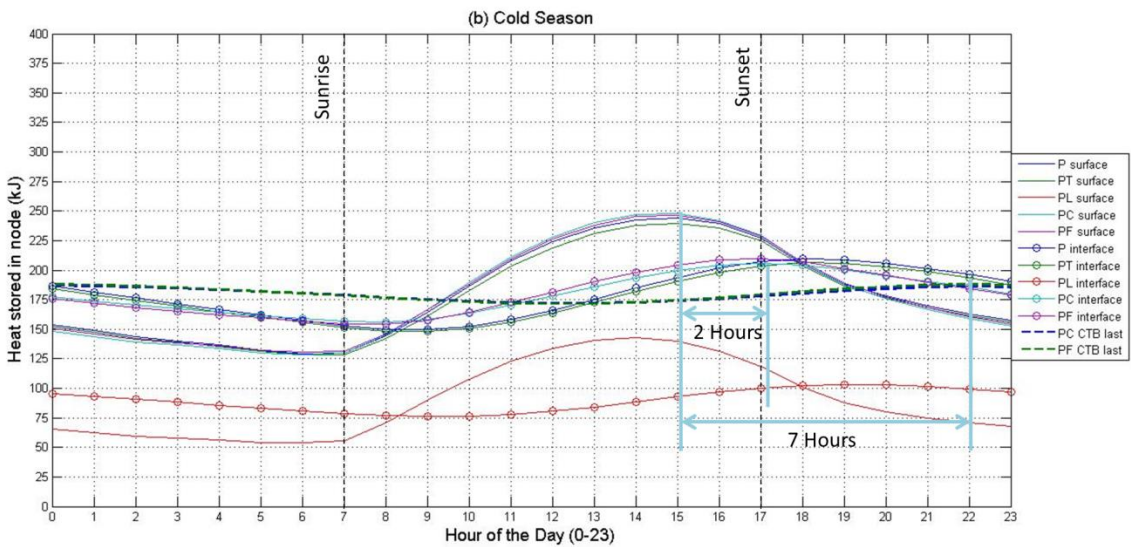
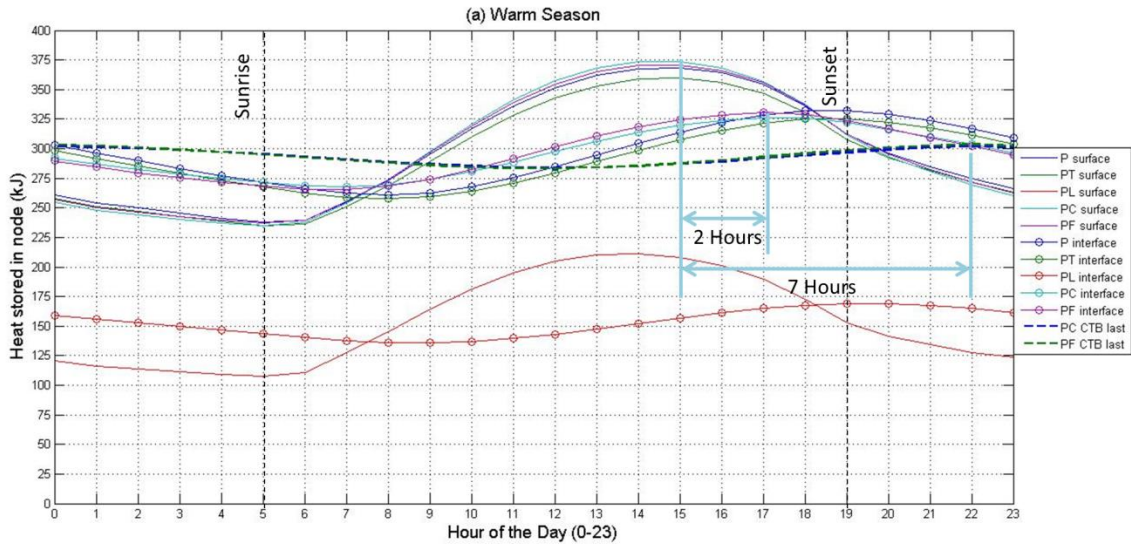


Figure 3-6 Heat stored (in kJ) in specified nodal elements in an average seasonal day in (a) warm season and (b) cold season. Times of sunrise and sunset are only indicative

3.3.3 Surface Temperature Difference

The time lag observed in heat conduction and storage means that there will be a shift in the temperature profile between daytime and nighttime hours for the hypothetical pavement structures relative to the control case. One way to quantify these changes is by comparing the surface temperature differences between the hypothetical pavement structures relative to the control case, as shown in Table 3-2 for the warm season and Table 3-3 for the cold season.

Table 3-2 Statistics of the surface temperature differences (in °C) relative to the control case P for Austin, TX in the warm season; split for daytime and nighttime conditions

| | Daytime | | | | Nighttime | | | |
|------------------------------|---------|------|------|------|-----------|------|------|------|
| | P-PL | P-PT | P-PC | P-PF | P-PL | P-PT | P-PC | P-PF |
| Minimum | -4.8 | 0.0 | -1.4 | -0.7 | -0.1 | 0.0 | -0.6 | -0.7 |
| Maximum | 2.4 | 1.9 | 0.9 | 0.7 | 3.1 | 1.1 | 1.7 | 1.3 |
| Standard Deviation | 0.9 | 0.3 | 0.3 | 0.2 | 0.6 | 0.1 | 0.3 | 0.2 |
| Average | -0.9 | 0.6 | -0.1 | 0.0 | 0.9 | 0.2 | 0.5 | 0.3 |
| Percentage of Hours Positive | 15 | 99 | 28 | 46 | 94 | 94 | 91 | 86 |
| Percentage of Hours Negative | 82 | 0 | 64 | 39 | 0 | 0 | 2 | 5 |
| Percentage of Hours Zero | 3 | 1 | 8 | 15 | 6 | 6 | 7 | 9 |

During nighttime hours, the hypothetical pavement structures resulted in more positive surface temperature differences indicating lower temperatures than the control case (P), especially during the warm season. For most pavement structures, daytime surface temperature differences were more negative, which was strongest in the cold season. Case PT, which has the highest albedo, showed consistently lower surface temperatures relative to the control for both daytime and nighttime hours as well as warm and cold seasons.

For the case PL, the lower thermal inertia and diffusivity of the surface course resulted in higher daytime and lower nighttime temperatures as compared to the control. During daytime hours, the heat remained concentrated in the upper part of the surface course, leading to high temperatures and hence higher emitted heat, which explains the smaller daytime net heat flux as compared to case P in Figure 3-4. Consequently, most of the heat could be quickly conducted out of the surface, leading to lower nighttime temperatures.

Table 3-3 Statistics of the surface temperature differences (in °C) of analyzed pavement systems relative to the control case P for Austin, TX in the cold season; split for daytime and nighttime conditions

| | Daytime | | | | Nighttime | | | |
|------------------------------|---------|------|------|------|-----------|------|------|------|
| | P-PL | P-PT | P-PC | P-PF | P-PL | P-PT | P-PC | P-PF |
| Minimum | -4.2 | 0.0 | -2.1 | -2.0 | -0.4 | 0.0 | -2.0 | -1.9 |
| Maximum | 2.7 | 1.7 | 0.6 | 0.6 | 3.1 | 0.8 | 1.4 | 1.0 |
| Standard Deviation | 0.8 | 0.3 | 0.3 | 0.3 | 0.7 | 0.1 | 0.3 | 0.3 |
| Average | -0.5 | 0.4 | -0.3 | -0.2 | 0.9 | 0.1 | 0.1 | 0.0 |
| Percentage of Hours Positive | 21 | 88 | 10 | 16 | 82 | 79 | 51 | 36 |
| Percentage of Hours Negative | 70 | 0 | 76 | 70 | 0 | 0 | 27 | 41 |
| Percentage of Hours Zero | 9 | 12 | 14 | 14 | 18 | 21 | 22 | 23 |

Case PC shows lower nighttime surface temperatures because the thermal inertia of the CTB allows it to gradually release the daytime heat stored over the night and the early part of the next day, as discussed in Section 3.3.2.3. This resultant time lag, which is beneficial for reducing the nighttime UHI, also causes the heat stored in the CTB from the previous day to be conducted to the surface for a part of the day, leading to higher daytime surface temperatures. Although Case PF also has a CTB and should show similar trends, the higher diffusivity of the surface course allows it to transmit heat faster from the base course to the surface, thereby producing slightly higher nighttime surface temperatures relative to PC especially in the cold season.

3.4 CONCLUSION

In order to develop strategies for UHI mitigation related to the built (horizontal) infrastructure, the transient heat flow processes in pavements must be explicitly modeled. For this analysis, relevant radiative forcing (RF) and the average seasonal day metrics were developed. The RF metric and corresponding GWP represents the overall environmental impact of a constructed pavement in terms of UHI which considers all the pavement layers and thermal properties. Additionally, the average seasonal day metric quantifies the average hourly thermal conduction, storage, and net surface heat flux behavior of the pavement.

For several hypothetical concrete pavement structures in Austin, TX with varying thermal inertia and diffusivity and fixed surface albedo (cases P, PL, PC and PF), 1-D thermal analysis did not produce significantly different GWP between the pavement cases. Only the concrete pavement surface with the highest albedo (case PT) showed a decrease in GWP among the cases analyzed. The GWP in a different climate zone is expected to follow a similar pattern but produce a different GWP magnitude proportional to the incident solar radiation over the analysis period.

Higher GWP does not necessarily mean that the nighttime CLUHI is greater because changes to thermal properties can internally redistribute the absorbed heat. The inclusion of a CTB to increase the thermal inertia was shown in cases PC and PF to decrease the nighttime UHI by storing the heat in the base course during the daytime and delaying and regulating its return to the surface at night and early the next day. Furthermore, the use of low-density concrete (case PL) caused the heat to be stored close to the surface and emitted quickly during daytime, leading to lower nighttime heat emission out of the pavement. Therefore, designing a pavement to mitigate nighttime UHI, besides from just increasing albedo, can also employ combinations of different pavement layers and thermal properties suitable for the specific climate location.

CHAPTER 4-ENVIRONMENTAL BENEFITS OF MULTI-FUNCTIONAL CONCRETE INLAYS²

4.1 INTRODUCTION

In the last decade, pavement preservation has received increasing attention as a cost-effective means to increase service life. Pavements generally perform well with a slow deterioration until a certain point in their service life, after which they deteriorate at a higher rate (Kuennen, 2006). By intervening before that stage is reached through pavement preservation strategies, future rehabilitation and maintenance costs can be lowered. In practice, strategies involving asphalt concrete have been the preferred mode of preservation, with over 60% of State Highway Authorities in the United States and Canada reporting using asphalt and only 20% reporting using concrete solutions i.e., Ultra-Thin Whitetopping on low-volume roads (Peshkin, et al., 2011).

Thin asphalt concrete inlays present several benefits for pavement preservation such as rapid placement, staged construction sequencing, and short opening time to traffic. Recent advancements in concrete technology, particularly the development of Flowable Fibrous Concrete (FFC), have enabled thin concrete inlays to be a pavement preservation option like asphalt concrete. In a previous study (Bordelon & Roesler, 2011), the constructability of a thin FFC inlay with rapid consolidation and high construction productivity was demonstrated along with verifying the FFC's high material toughness in the laboratory. Moreover, by incorporating titanium dioxide (TiO₂) nanoparticles into the cement, concrete inlays can provide significant environmental benefits by increasing the pavement surface albedo and reducing the near road side vehicular emissions, e.g., nitrogen oxides (NO_x).

The surface albedo of a pavement is an important determinant of surface temperature and hence the impact of pavements on the surrounding environment. When incorporated into a Pavement Life Cycle Assessment framework, concrete with higher albedo has been shown to reduce the urban air temperature (Synnefa, et al., 2011) and hence the Urban Heat Island (UHI), as well as the Global Warming Potential (GWP) (Munoz, Campra, & Fernandez-Alba, 2010). The effect of an FFC mix incorporating polymer fibers and fly ash, as well as TiO₂-containing cement, has not yet been studied.

This paper presents a preliminary study of the application of a multi-functional FFC inlay with TiO₂-containing cement for pavement preservation as well as its environmental sustainability impact based on laboratory testing of cylindrical and beam specimens. The structural properties are quantified through fracture and strength testing. Surface albedo of samples is measured and used to demonstrate surface temperature mitigation over a ten-year period as compared to the existing asphalt pavement. Together with the potential for reduction in greenhouse gases from vehicular emissions, this FFC inlay can be an environmentally-sustainable option for pavement preservation.

²Adapted from:

Sen, S, King, D, and Roesler, J (2015). *Structural and Environmental Benefits of Concrete Inlays for Pavement Preservation*. Airfield and Highway Pavements 2015, doi: [10.1061/9780784479216.062](https://doi.org/10.1061/9780784479216.062), pp. 697-707

4.2 MATERIALS AND METHODOLOGY

The concrete mix designs developed for this study were based on the combined principles of Self-Consolidating Concrete (SCC) and polymer fiber reinforcement (Bordelon & Roesler, 2011). More details on the mix design can be found in (King, 2015) and is reproduced in Table 4-1. A fracture beam of size 450 mm x 150 mm x 150 mm was cast with this concrete mix.

Table 4-1 TiO₂ FFC mix designs

| Mix Component | Unit | Mix Proportion |
|--------------------------------------------|-------------------|----------------|
| Sand | kg/m ³ | 857 |
| Limestone Chip (9.5 mm NMAS) | kg/m ³ | 1052 |
| TiO ₂ -containing Type I Cement | kg/m ³ | 328 |
| Type C Fly Ash | kg/m ³ | 140 |
| HRWR | ml/m ³ | 1700-2000 |
| AEA | ml/m ³ | 107 |
| Water | kg/m ³ | 187 |
| Synthetic Macro-fibers | kg/m ³ | 4.6 |
| w/cm | NA | 0.40 |

NMAS = Nominal Maximum Aggregate Size

NA = Not Applicable

AEA = Air Entraining Admixture

HRWR = High Range Water Reducing Admixture (superplasticizer)

Albedo was measured using one of the FFC flexure beam specimens with a Kipp & Zonen[®] CMA 6 Albedometer (also called a double pyranometer) according to the standard procedure ASTM E1918 (ASTM Standard E1918, 2006), as seen in Figure 4-1(a) at a height of 0.5 m above the specimen, except that the pyranometer did not have to be flipped in this case. The specimen was placed on an aged concrete ramp. Measurements were made on September 3, 2014 between 11:30 AM and 12:30 PM CDT outside Newmark Civil Engineering Building of the University of Illinois at Urbana-Champaign (at 40°6'52" N, 88°13'36" W) to obtain a conservative estimate of albedo (Li, Harvey, & Kendall, 2013). Weather data covering the period of study is shown in Table 4-2.

Reflected, diffuse radiation was recorded over three parts of the smooth surface of the beam, left, center, and right, as shown in Figure 4-1(b). Care was taken to ensure that shadows did not fall on the surface. The Albedometer measured radiation every second and logged an average value every five seconds. Measurements were taken for 3 to 4 minutes over each part of the surface to demonstrate spatial and temporal variation of albedo. These measurements however, included some radiation received from the background surface on which the

specimen was placed, which has an effect on the calculated values of albedo. Eliminating this background radiation is beyond the scope of this paper however, and is left for future study. An average of all values was used for further analysis of UHI mitigation potential through a reduction in the surface temperature over a ten-year analysis period.

Table 4-2: Weather data for September 3, 2014 at Willard Airport, Champaign station
(Source: (National Climatic Data Center, n.d.))

| Time (CDT) | Sky Conditions | Temperature (°C) | | |
|------------|----------------------------|------------------|----------|-----------|
| | | Dry Bulb | Wet Bulb | Dew Point |
| 10:53 AM | Scattered clouds at 1300 m | 27.2 | 21.0 | 17.8 |
| 11:53 AM | Few clouds at 1400 m | 27.2 | 21.0 | 17.8 |
| 12:53 PM | Few clouds at 1400 m | 27.2 | 21.0 | 17.8 |

To calculate surface temperatures, a typical aged asphalt pavement (Case 1) was considered and compared with the FFC inlay (Case 2) milled onto it. The cross sections of the pavement in both cases are shown in Figure 4-2. The thermal properties of all layers were the default values published in the Mechanistic-Empirical Pavement Design Guide (MEPDG) documentation (National Cooperative Highway Research Program Report 1-37A, 2004) as shown in Table 4-3, unless otherwise specified. The surface temperatures were calculated using a heat transfer analysis program similar to the Enhanced Integrated Climatic Model (EICM), from January 2000 to December 2010 with weather data from Chicago, IL (O’Hare International Airport). The temperature differences between Case 1 and Case 2 were analyzed at each hour as a whole as well separately for daytime and nighttime conditions based on time of sunrise and sunset for each day of the analysis period.

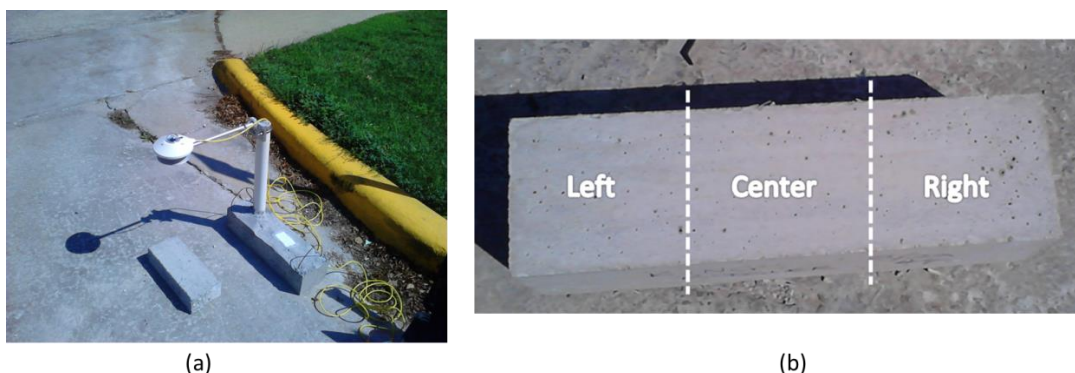


Figure 4-1 Reflected and incident solar radiation (a) being measured using a CMA 6 albedometer over (b) the three areas of the smooth surface of the beam

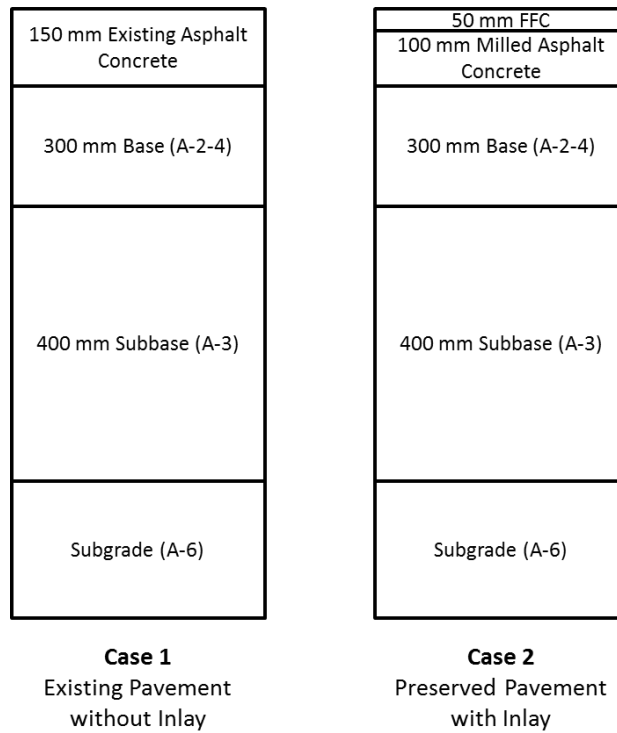


Figure 4-2 Pavement structures for surface temperature analyses

Table 4-3 Thermal properties of layer materials are the MEPDG level 3 default values unless otherwise noted

| Material | Albedo | Thermal Conductivity (W/mK) | Heat Capacity (kJ/kg) | Dry Unit Weight (kg/m³) |
|------------------|-------------------|----------------------------------------|----------------------------------|-----------------------------------------------|
| Asphalt Concrete | 0.15 ¹ | 1.18 | 0.98 | 2400 |
| FFC | 0.26 ² | 2.20 | 1.20 | 2226 ² |
| Base (A-2-4) | NA | IC | IC | 1950 |
| Subbase (A-3) | NA | IC | IC | 1920 |
| Subgrade (A-6) | NA | IC | IC | 1600 |

NA = Not Applicable, IC = Internally Calculated

¹ Typical value for aged asphalt concrete (Santamouris, Synnefa, & Karlessi, Using advanced cool materials in the urban built environment to mitigate heat islands and improve thermal comfort conditions, 2011)

² Measured values from laboratory FFC beams

4.3 RESULTS AND DISCUSSION

Albedo values tend to vary over time and space for the same sample. Field measurements made between 9 AM and 3 PM in summer tend to give conservative results (Li, Harvey, & Kendall, 2013). Five-point summary statistics for the Left, Center and Right positions, as defined in Figure 4-1(b), are shown in Figure 4-2 and other statistics in Table 4-4. For all the measurements, there was no change in the background material on which the specimen was placed.

Table 4-4 Statistics of albedo measurements

| | Position on Beam Surface | | |
|-------------------------|--------------------------|--------|--------|
| | Left | Center | Right |
| Sample Size | 56 | 52 | 49 |
| Mean | 0.26 | 0.26 | 0.26 |
| Sample Std. Dev. | 0.0026 | 0.0039 | 0.0037 |

The average of the mean values for the three surfaces was 0.26, and this value was used for the surface temperature analysis (as mentioned in Table 4-3). From Figure 4-2, the albedo appears to follow different distributions for the three positions on the surface of the beam, although the mean values are the same to two significant figures. The reason for this is possibly because of the diffuse radiation from the background surface on which the specimen was placed, some of which is detected by the Albedometer. While this background radiation does alter the true value of albedo, a method to eliminate it is beyond the scope of this paper. For subsequent analysis, the mean value of 0.26 is used.

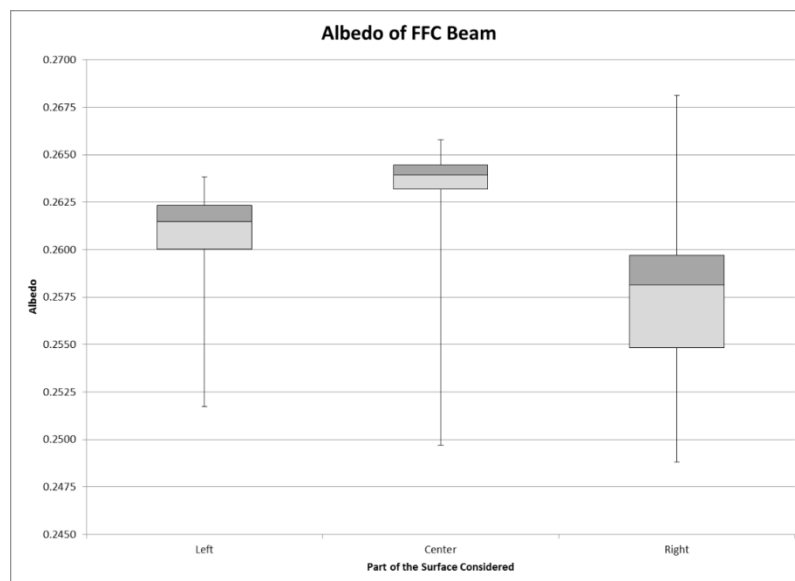


Figure 4-2 Five point summary statistics for the albedo of FFC beam surfaces

The surface temperatures for Case 1 and Case 2 were analyzed using a heat transfer analysis program. The difference in surface temperature between Case 1 and Case 2 was evaluated for each hour as well as for daytime and nighttime temperatures based on the time of sunrise and sunset for each day. The statistics of these temperature differences are given in Table 4-5 and shown in Figure 4-3. In Table 4-5, the percentage of hours when the difference is positive (Case 1 has a higher temperature than Case 2), negative (Case 2 is higher than Case 1) and zero (both the cases have the same temperature to the fourth decimal place) is also shown.

The surface temperature analysis clearly shows that, about 54% of the time, the addition of an FFC inlay (Case 2) with TiO₂-containing cement leads to the lower pavement surface temperature as compared to the pavement without an FFC inlay (Case 1). This is on account of lower temperatures during 94% of daytime hours and 15% of nighttime hours. The lower temperatures are a result primarily of the higher albedo, which also explains the low magnitude of differences in nighttime hours because less heat is absorbed during the day in Case 2; while the higher temperatures at night are because of the higher thermal inertia of the pavement in Case 2, as explained in Chapter 3. Additionally, a quarter of nighttime hours show no temperature difference because the two pavement types have reached thermal equilibrium with the environment. Lower surface temperatures during daytime reduce the air temperatures (Synnefa, et al., 2011), which in turn lowers the radiative forcing, and subsequently reduces the Global Warming Potential (GWP) of the pavement (Munoz, Campra, & Fernandez-Alba, 2010). Hence, the FFC inlay can potentially decrease the Urban Heat Island effect in daytime. During nighttime hours however, the higher surface temperatures, albeit of lower magnitude, can have the reverse effect. This means that this inlay is not as effective in tackling nighttime UHI as daytime. The impact on building energy consumption is not clear, because a lower air temperature in winter can increase heating loads in adjacent buildings (Akbari & Konopacki, 2005). In order to estimate the impact of inlays on UHI from the perspective of building energy consumption, a site-specific analysis (i.e., local climate dependent) is necessary, which is beyond the scope of this study.

Table 4-5 Statistics for hourly surface temperature differences between case 1 and case 2 (in °C) over the period of study (cumulative) as well as between daytime and nighttime hours.

| Statistic | Cumulative | Daytime | Nighttime |
|--------------------------------|-------------------|----------------|------------------|
| Minimum Difference | -3.09 | -2.49 | -3.09 |
| Maximum Difference | 7.36 | 7.36 | 2.54 |
| Average Difference | 0.66 | 1.44 | -0.14 |
| % of Hours Positive Difference | 54.53 | 94.14 | 14.86 |
| % of Hours Negative Difference | 31.90 | 3.62 | 59.45 |
| % of Hours Zero Difference | 13.57 | 2.24 | 25.69 |

4.4 CONCLUSION

Flowable fibrous concrete (FFC) inlay technologies are a promising option for pavement preservation. Moreover, by incorporating TiO₂-containing cement in the mix, additional environmental benefits can also be derived. The albedo of a beam made of this mix was measured with an albedometer at three different positions on the side of the beam to account for spatial variations of concrete surfaces. The testing was done between 11:30 AM and 12:30 PM on a sunny day to obtain a conservative estimate. A time- and space-averaged value of 0.26 was obtained, which is higher than the typical value of 0.15 for the underlying aged asphalt pavement. This higher albedo was expected to lower the overall surface temperature of the roadway. The albedo value includes some background radiation picked up by the Albedometer, which was not isolated in this study.

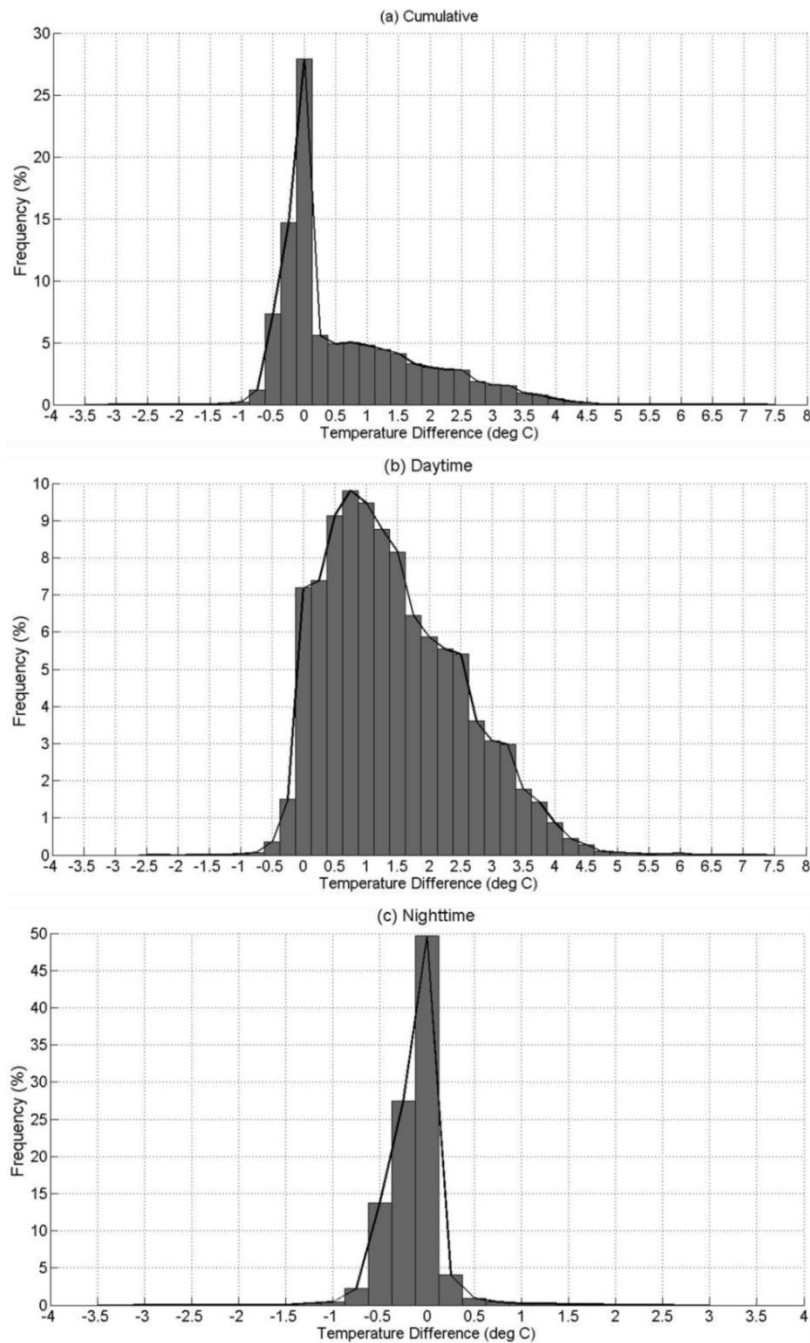


Figure 4-3 Frequency distribution of surface temperature differences over (a) the entire analysis period (b) daytime hours (c) nighttime hours

To calculate the predicted surface temperature, a hypothetical pavement was assumed for a 50mm FFC inlay over 100 mm aged asphalt concrete and compared to just a 150mm aged asphalt concrete pavement over the same pavement foundation layers. Typical values for thermal properties of construction materials were assumed, except for the albedo of the FFC inlay and its density. By comparing the surface temperatures over a 10-year period from 2000 to 2010 for weather data from Chicago, IL as an illustration, the Urban Heat Island-related benefits of using the inlay as compared to not adopting any preservation strategy could be quantified. The surface temperature of the inlay was less than that of an existing asphalt surface for about 54% of the hours analyzed and higher for about 32%, with no temperature difference about 14%. The lower surface temperature decreases the radiative forcing and

hence the Global Warming Potential. The impact of higher pavement albedo from the FFC on building energy loads must be analyzed with site-specific data and features.

CHAPTER 5-AGING ALBEDO MODEL FOR ASPHALT PAVEMENT SURFACES

5.1 INTRODUCTION

Rapid urbanization around the world in the last century has led to the replacement of natural materials by man-made ones through the construction of buildings and pavements. This has had consequences for the urban heat budget and local climate. The Urban Heat Island (UHI), characterized by high urban temperatures with respect to adjacent rural areas, is one such consequence that has been studied in great detail (Pichierri, Bonafoni, & Biondi, 2012; Kleerekopera, van Esch, & Salcedo, 2012; Memon, Leung, & Chunho, 2008; Oke, 1982). Previous studies have demonstrated that temperature increases because of the UHI leads to potentially higher water consumption (Aggarwal, Guhathakurta, Grossman-Clarke, & Lathey, 2012; Guhathakurta & Gober, 2007) and building energy usage (Taha, Akbari, Rosenfeld, & Huang, 1988).

With respect to UHI mitigation, cool pavements, among other solutions, have been the subject of extensive research, with several materials having been proposed to lower pavement temperatures (Santamouris, Synnefa, & Karlessi, 2011; Santero, Masanet, & Horvath, 2011b; Li, Harvey, & Kendall, 2013). The common feature of all these proposed materials is that they increase the albedo of the pavement, which is the average reflectance of the material over the solar spectrum and varies from 0 (no reflection) to 1 (perfect reflector). Studies have shown that the impact of albedo on UHI can vary from about 1 to 100 t CO₂-eq/lane-km of pavement (Santero & Horvath, 2009) and a global adoption of cool roofs and pavements can lead to a potential offset of 44 Gt CO₂-eq (Akbari, Menon, & Rosenfeld, 2009). As expected, the surface layer albedo assumes a prominent position in the study of UHI mitigation.

In general, pavement surfaces are either made of Asphalt Concrete (AC) or Portland Cement Concrete (PCC) with several studies measuring the albedos of both kinds of pavements. The albedo of freshly-paved asphalt has been measured to be 0.04 to 0.06 (Taha, Sailor, & Akbari, 1992; Li, Harvey, & Kendall, 2013), which rises to 0.09 to 0.18 after environmental aging (Santamouris, Synnefa, & Karlessi, 2011). As noted, asphalt pavements initially have a very low albedo, but with aging and aggregate exposure, it eventually increases significantly (Tran, Powell, Marks, West, & Kvasnak, 2009). There has been little effort to understand how quickly this aging occurs and consequently, most UHI studies assume a single, static value of albedo over the service life of the asphalt pavement (Li, Harvey, & Jones, 2014; Menon, Akbari, Mahanama, Sednev, & Levinson, 2010; Munoz, Campra, & Fernandez-Alba, 2010; Yu & Lu, 2014; Yaghoobian & Kleissl, 2012). Even the new AASHTO (2011) pavement design guide recommends a default value (static) of 0.15 for AC and 0.30 for PCC.

The albedo of a newly cast concrete pavement is higher than that of a new asphalt pavement, at about 0.20 to 0.30 (Li, Harvey, & Kendall, 2013). This albedo value is highly sensitive to the choice of cement, aggregates and supplementary cementitious materials, which can increase the albedo of new concrete to 0.50 to 0.70 (Boriboonsomsin & Reza, 2007; Levinson & Akbari, 2002). While carbonation initially increases the albedo of concrete, it eventually decreases by about 0.06 to 0.19 because of weathering, soiling, and abrasion (Levinson & Akbari, 2002). Thus, concrete albedo has the opposite trend to asphalt pavement with higher albedo at construction and decreasing over time (Santero, Masanet, & Horvath, 2011b).

In addition, supplementary materials used in concrete can alter the surface characteristics and potentially the albedo of the pavement. In particular, fiber-reinforced concrete has been extensively used to improve the toughness and achieve higher durability of the concrete mix

(Balaguru & Shah, 1992; Bordelon & Roesler, 2011). Organic fibers have been used in cementitious roof tiles for cheaper construction in rural areas with measured albedos of 0.30 (Roma, Jr., Martello, & Savastano, Jr., 2008). No research has been reported on the albedo of fiber-reinforced concrete pavements where the fibers are visible at the slab surface.

From the literature, albedo for both concrete and asphalt pavements is found to be a property that depends on a variety of factors including age and surface material constituents. Pavement albedo can vary spatially as well as temporally but this is not currently incorporated in the use phase analysis of pavement life cycle assessment (LCA) studies (Santero, Masanet, & Horvath, 2011b). This paper reports the results of albedo measurements for a set of asphalt and concrete pavement test sections of varying ages in Rantoul, IL. From the asphalt pavements, a non-linear aging albedo model is proposed and used to determine the Global Warming Potential (GWP) of a hypothetical pavement as compared to one with a static albedo. In addition, a spectrophotometer is used to determine the approximate AM 1.5G albedo of polymer fibers used in and visible on the surface of one of the concrete pavements to understand whether this surface modification has a significant impact on the albedo of the pavement.

5.2 MATERIALS AND METHODOLOGY

5.2.1 Test Sections

The University of Illinois operates the Advanced Transportation Research and Engineering Laboratory (ATREL) in Rantoul, IL, which includes several full-scale test sections, each about 150 m in length. The full-scale test sections, seen in Figure 5-1, include both concrete and asphalt and were built over the past 8 years in what is called the Accelerated Transportation Loading Assembly (ATLAS) facility.



Figure 5-1 Google Earth™ screenshot of the ATLAS facility with the five sections under study labeled AC 1-3 and PCC 1-2

As of October 2014, the ATLAS facility had five sections – three asphalt and two concrete – that were constructed over the years and exposed to continuous weathering. These sections are named AC1 to AC3 for the asphalt sections and PCC1 and PCC2 for the concrete, as shown in Figure 5-1. Towards the east end of AC2 is an asphalt overlay that was recently constructed. PCC1 is a 5 cm concrete inlay made of Flowable Fibrous Concrete (FFC) (Bordelon & Roesler, 2011) over an old asphalt pavement. Polymer fibers used in PCC1 are visibly embedded in the surface (Figure 5-2). In addition, at the time of construction, a curing compound was applied on the surface, which likely impacted the final color of the section. PCC2 consists of a short segment, about 12m in length, that was built separately and for a different purpose than the rest of the section. The majority of PCC2 underwent repeated loading until fatigue failure and therefore only limited testing could be performed on it. The albedo of all these sections was not previously measured.

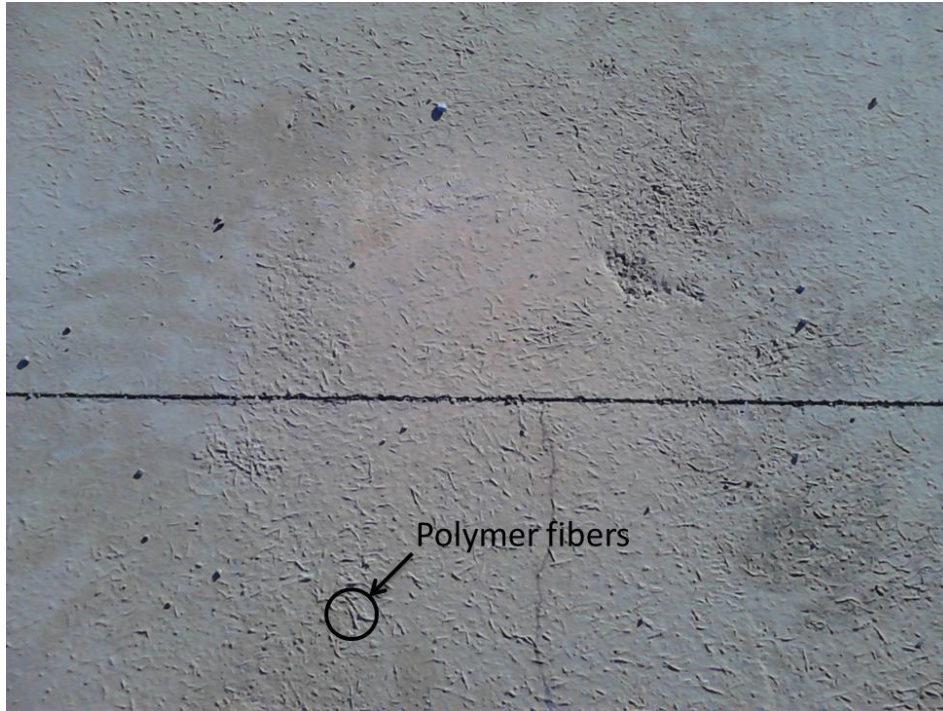


Figure 5-2 Top view of PCC1 with polymer fibers on the surface

Table 5-1 lists the type of pavement, year of construction of the sections, and a reference with more details about paving materials, construction, and testing results. For the purpose of sampling albedo, each section was divided into subsections of about 15m each. The designation of each is also shown in Table 5-1.

5.2.2 Albedo Measurement

There are two methods reported in literature to measure albedo: field testing using an albedometer (also called a double pyranometer) (Li, Harvey, & Kendall, 2013) as per ASTM E1918 (ASTM Standard E1918, 2006), which gives an accurate value for the location but is strongly dependent on size of the sample and weather conditions; and laboratory testing using spectral reflectance obtained from a spectrophotometer (Santamouris, Synnefa, & Karlessi, 2011), to obtain an approximate estimate of the albedo as per ASTM E903 (ASTM International, 2012).

Table 5-1 Year of construction and other details of the test sections

| Section | Type of Pavement | Year of Construction | Reference | Subsection(s) |
|---------|----------------------|----------------------|---------------------------------------------------------|---------------|
| AC1 | Asphalt overlay | 2008 | (al-Qadi, Carpenter, Leng, Ozer, & Trepanier, 2009) | 1-8 |
| AC2 | Asphalt overlay | 2007 | (Dave, Ahmed, Buttlar, Bausano, & Lynn, 2010) | 1-5 |
| | Newer overlay | 2014 | Unpublished | 6-9 |
| AC3 | Asphalt | 2013 | (al-Qadi, Abuawad, Dhasmana, Coenen, & Trepanier, 2014) | 1-8 |
| PCC1 | FFC Inlay | 2009 | (Bordelon & Roesler, 2011) | 1-6 |
| PCC2 | Concrete – first 15m | 2008 | Unpublished | 1 |
| | Concrete | 2007 | (Cervantes & Roesler, 2009) | 2-3 |

The field method is used to estimate the albedo of each of the test sections at the ATLAS facility. The albedo is measured with readings taken every two seconds for at least one minute for each subsection (as designated in Table 5-1) and averaged to reach a representative value for that section. Thus, each section had a minimum sample size of 30. Measurements were done per ASTM E1918 (ASTM Standard E1918, 2006) using a Kipp & Zonen[®] CMA6 Albedometer, except that the device did not have to be flipped. The standard calls for a minimum dimension of 4m x 4m of the sample, whereas the test sections were all approximately 4m wide and each sampling section was approximately 15m in length, so that the results meet the requirements. Since the results are sensitive to sky conditions, testing was only done on clear and sunny days. Representative weather data for the measurement period was obtained from the Rantoul Elliott Field National Aviation Center through the National Climatic Data Center (NCDC), which is less than 2 km from the ATREL facility.

The PCC1 section was made of polymer fiber reinforced, self-consolidating concrete called flowable fibrous concrete. The specific fiber used was a translucent polymer 40 mm in length with an aspect ratio of 90 and this was visible on the concrete surface but covered by the cement paste. A sample of the fiber, though not covered by the paste, was tested for combined diffused and specular spectral reflectance on a Cary 5000 UV-Vis-NIR Spectrophotometer from 280 nm to 2600 nm. The spectral reflectance is averaged over the standard AM 1.5G solar spectrum from ASTM G173 (ASTM International, 2003) to obtain an approximate value of albedo for the fiber. This creates two sources of error: the air mass in Rantoul is not exactly 1.5 (it is actually about 1.3), so the actual solar spectrum is slightly different but not by much; and the spectrum extends all the way to 4000 nm but the spectrophotometer can only detect reflectance up to 2600 nm, leading to a small loss of about 0.8% of the spectrum by irradiance between 2600 and 4000 nm. These errors cause some error in the results, which should be considered approximate.

5.2.3 Aging Albedo Model

Data obtained from the asphalt sections – AC1 to AC3 and the newer overlay on AC2 – was used to develop a non-linear, three-parameter model for aging albedo calibrated for this area. The functional form of the model is shown in Equation 5.1.

$$\alpha(N) = \alpha_0 + AN^B \quad (5.1)$$

Where α_0 is the ‘at-construction’ albedo of the section, N is the age of the pavement in years and A and B (both less than 1) are constants that depend on the local climate and weathering. The functional form of the model implies that the pavement starts out at the at-construction albedo and then undergoes weathering, with a majority of the weathering effects taking place in the first few years and the rate of increase in albedo decreasing over time. A previous study (Richard, Dore, Lemieux, Bilodeau, & Haure-Touze, 2015) found similar results but used a two-parameter logarithmic model instead of a power model. However, that model was not valid at $N = 0$ i.e., at construction and would need a third parameter added to make it continuous at that point, thus making it equivalent to the model proposed in this study.

An important assumption of this model is that the sections have the same (or at least similar) at-construction albedo, which can be justified by the fact that the aggregates and binder used for these sections are obtained from the same sources. Furthermore, as the various sections are located at the same site, the general climate and sections can be assumed to have undergone similar patterns of weathering over the years.

5.2.4 Radiative Forcing and Global Warming Potential Analysis

The role of radiative forcing (RF) in determining the environmental impact of a pavement in terms of UHI was discussed in Chapter 3. RF is an important parameter that explains the environmental impact of UHI induced by pavements in terms of the change induced in the earth’s energy budget over the pavement, although it is not necessarily the only parameter that can be used to characterize it. In that study, a method to calculate the RF using a heat analysis program called ILLI-THERM was developed and was subsequently converted into an equivalent Global Warming Potential (GWP), which can be integrated into the use phase of a pavement Life Cycle Assessment (LCA) program. The functional unit for this LCA is a square meter of pavement area.

In this paper, a similar analysis was performed on a hypothetical pavement section taken from Chapter 4, which was assumed to have been constructed in January 1999. A cross section of the hypothetical pavement is shown in Figure 5-3. The same, typical thermal properties except the surface albedo were assumed as in the previous study. The analysis was performed over the five-year period of January, 1999 to December, 2003 for Chicago, IL, which was assumed to undergo similar weather cycles as Rantoul because of geographical proximity. Two cases of albedo were considered:

- (a) Static albedo: The albedo was assumed to remain fixed at the construction value throughout the analysis period. This represents the current practice of pavement LCA studies for UHI.
- (b) Aging albedo: The model developed from the experimental data of the test sections was applied, starting at the at-construction albedo and increasing from there because of weathering. This represents a more realistic scenario than the current practice.

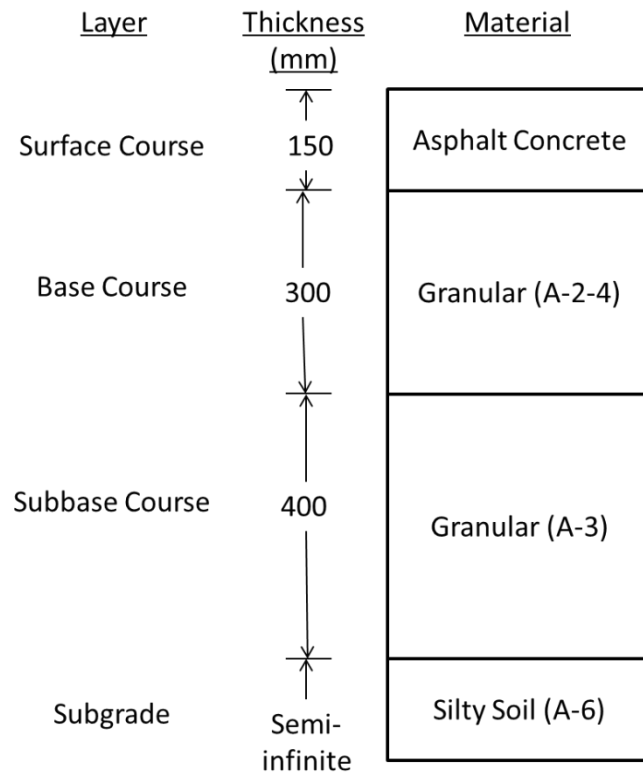


Figure 5-3 Hypothetical pavement section

The RF of these two cases was determined using ILLI-THERM. This represents the change in heat budget of the part of the earth covered by the pavement by virtue of its construction over the analysis period. The equivalent GWP represents the amount of CO₂ that would have to be released into the atmosphere to achieve the same radiative forcing. The conversion to a GWP was done using the method used in Chapter 3. The corresponding relationship between GWP (in kg-CO₂-eq/m²) and RF (in W/m²) is as shown in Equation 5.2.

$$GWP = 1.3556 * RF \quad (5.2)$$

The GWP of the two cases was then compared to indicate the difference in the pavement LCA between static and aging albedos.

5.3 RESULTS AND DISCUSSION

5.3.1 Weather Conditions

Albedo measurements on the test sections were performed over three days when sky conditions were favorable. Representative weather data for that period for Rantoul is presented in Table 5-2 (National Climatic Data Center, 2014). At all times, sky conditions were clear with almost no clouds and plenty of sunshine and testing was done within the recommended time as per ASTM E1918. The instrument was oriented such that the shadow fell away from the area where albedo is being measured so as not to cause significant errors.

5.3.2 Albedo of Sections

The albedo of each section varied over time as well as spatial location. The five point summary statistics for the subsections defined in Table 5-1 are shown as box and whisker plots in Figure 5-4 to Figure 5-6 for AC1 to AC3 and Figure 5-7 to Figure 5-8 for PCC1 and PCC2.

Spatially, albedo shows a lot of variation between subsections in sections AC1 and AC3, while the values for AC2 (except the new overlay), PCC1 (except the original AC layer) and PCC2 (in which Section 1 is from a different mix) show less variation. A previous field study (Li, Harvey, & Kendall, 2013) showed similar variation in the albedo between subsections of a section, possibly because of variations during construction. The albedo values for PCC1 and PCC2 in this study also agree with those measured in other studies for similar mixes (Li, Harvey, & Kendall, 2013; Boriboonsomsin & Reza, 2007; Levinson & Akbari, 2002).

It is useful to assign a single representative value for each section. This is done by taking the average of the albedo of each of the sampling subsections, except for those that came from a different mix, namely the new AC overlay of AC2 and Section 1 of PCC2. These representative values are summarized in Table 5-3.

Table 5-2 Representative weather data for the period of measurement for Rantoul, IL
(National Climatic Data Center, 2014)

| Date | Time (CDT) | Sky Conditions | Temperature (°C) | | | Cases covered |
|---------------|------------|----------------|------------------|----------|-----------|----------------------|
| | | | Dry Bulb | Wet Bulb | Dew Point | |
| Nov. 3, 2014 | 11:53 AM | Clear | 18.0 | 10.3 | 3.0 | AC1 subsections 1-2 |
| | 12:53 PM | Clear | 19.0 | 11.2 | 4.0 | AC1 subsections 3-7 |
| | 1:53 PM | Clear | 20.1 | 12.2 | 5.2 | AC1 subsections 8 |
| Nov. 5, 2014 | 9:53 AM | Clear | 11.5 | 9.1 | 6.9 | AC2 subsections 1-4 |
| | 10:53 AM | Clear | 13.9 | 10.2 | 6.7 | AC2 subsections 5-9 |
| | 11:53 AM | Clear | 15.5 | 10.0 | 4.2 | AC3 subsections 1-4 |
| | 12:53 PM | Clear | 16.1 | 9.8 | 3.6 | AC3 subsections 5-8 |
| | 1:53 PM | Clear | 16.9 | 10.0 | 3.1 | PCC1 subsections 1 |
| | 2:53 PM | Clear | 16.7 | 10.5 | 4.2 | PCC1 subsections 2-3 |
| Nov. 10, 2014 | 12:53 PM | Clear | 17.3 | 11.6 | 6.9 | PCC1 subsections 4-7 |
| | 1:53 PM | Clear | 18.5 | 12.4 | 7.0 | PCC2 subsections 1-3 |

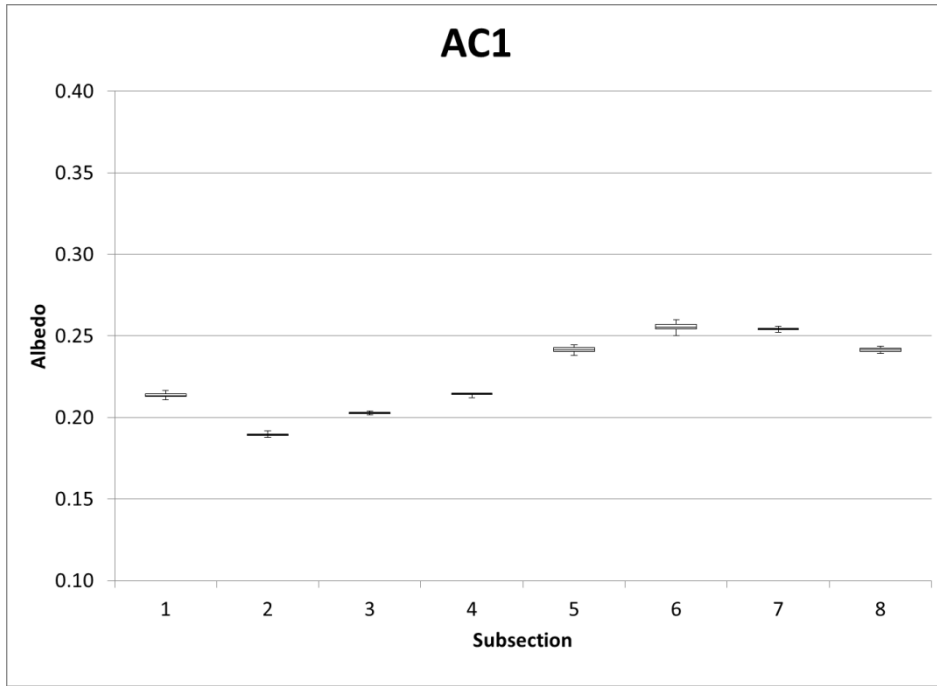


Figure 5-4 Albedo of subsections of AC1

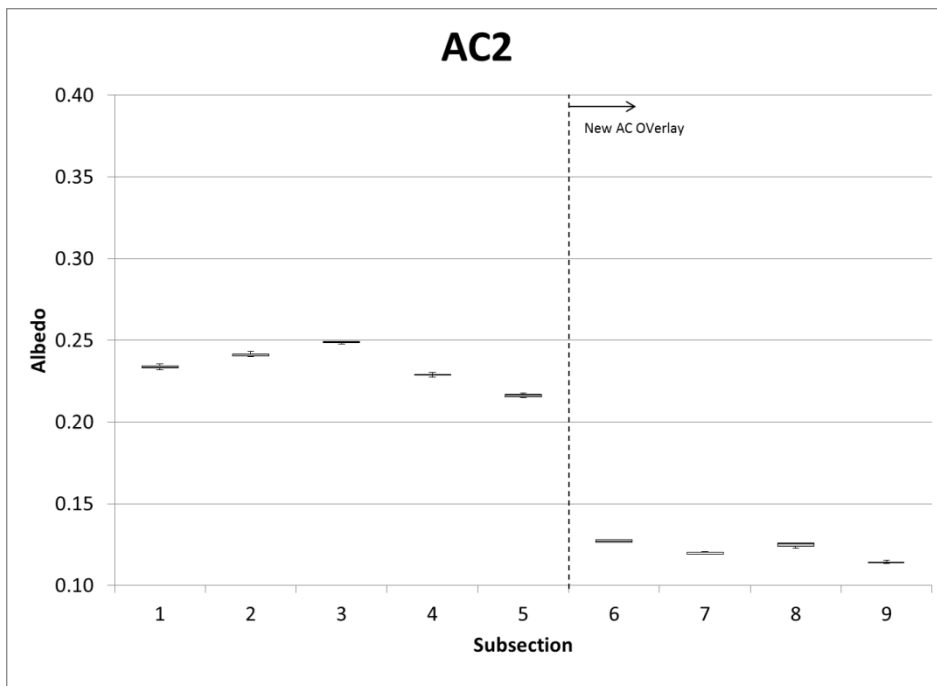


Figure 5-5 Albedo of subsections of AC2

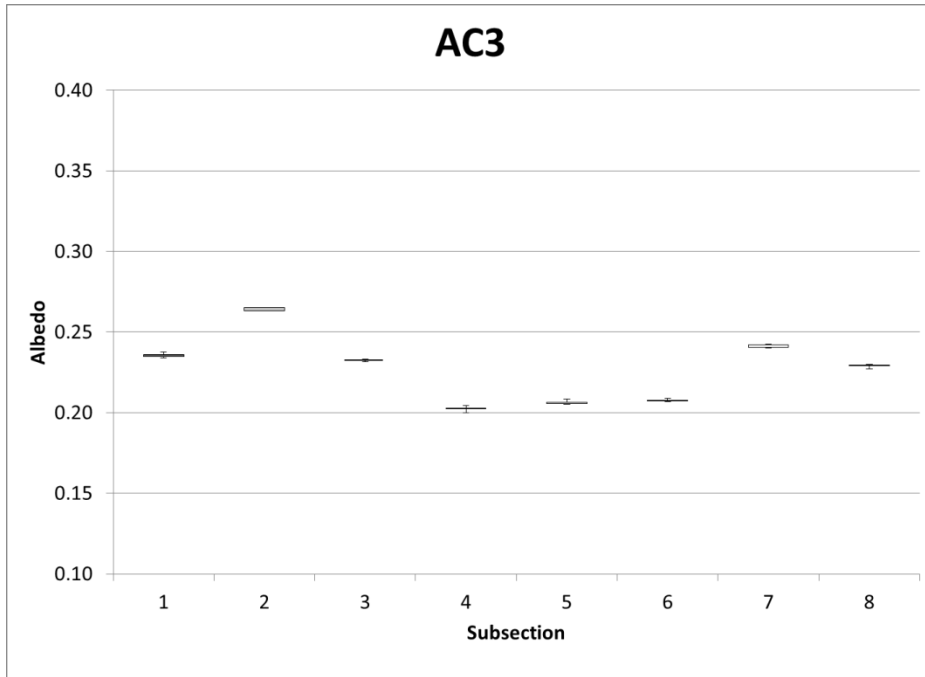


Figure 5-6 Albedo of subsections of AC3

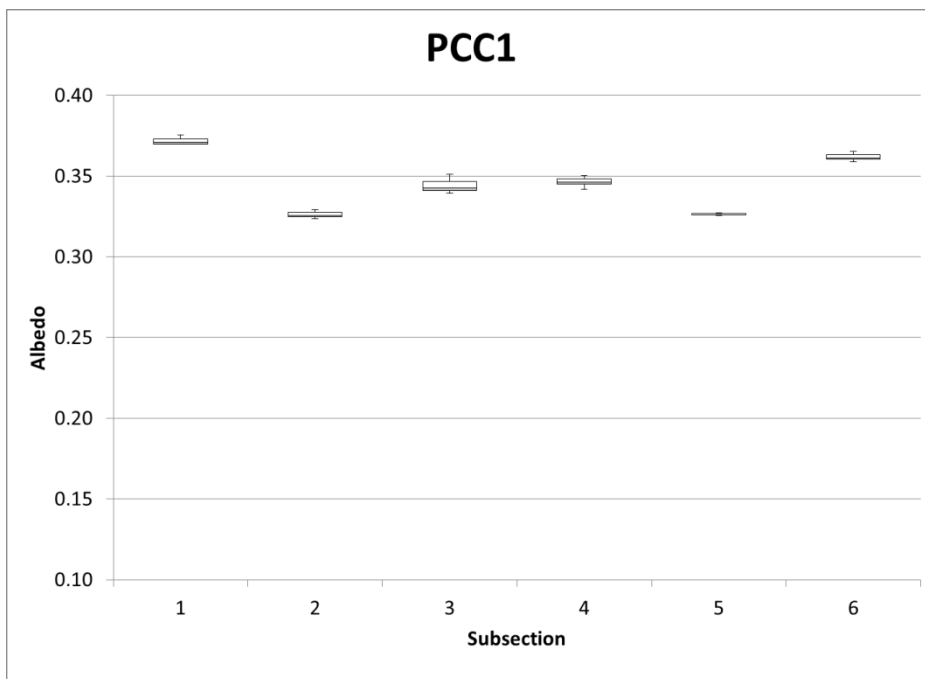


Figure 5-7 Albedo of subsections of PCC1

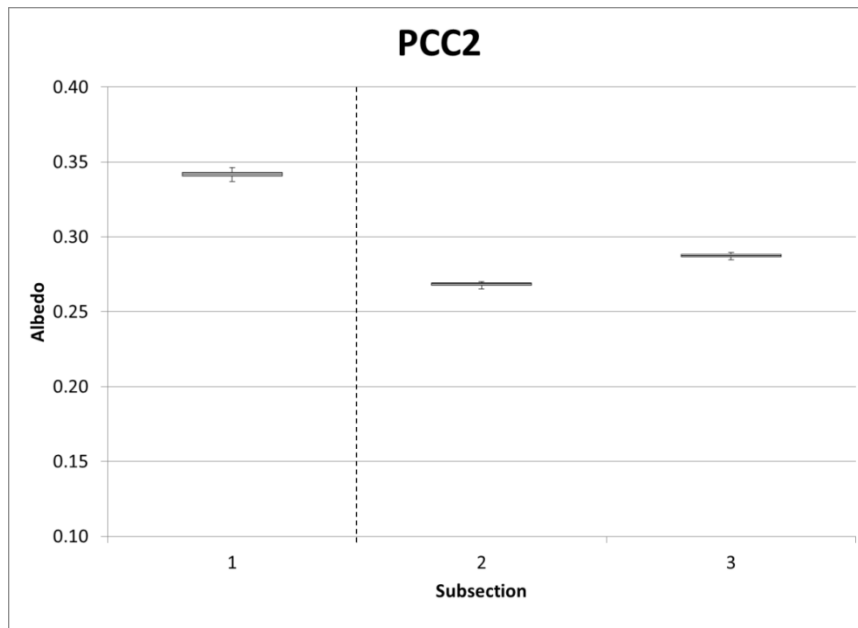


Figure 5-8 Albedo of subsections of PCC2

Table 5-3 Mean albedo of the ATLAS test sections

| | AC1 | AC2 | | AC3 | PCC1 | PCC2 | |
|--------|--------|--------------|----------------|--------|--------------|-----------|--------------|
| | | Sections 1-5 | New AC Overlay | | Sections 1-6 | Section 1 | Sections 2-3 |
| Albedo | 0.2266 | 0.2338 | 0.1214 | 0.2272 | 0.3455 | 0.3420 | 0.2779 |

5.3.3 Calibration of Aging Albedo Model

The general functional form of Equation 1 is calibrated using the representative albedos of AC1, AC2 (including the new AC overlay) and AC3 from Table 5-3. Measurements were taken in 2014 and the age was calculated based on the year of constructions as shown in Table 5-4.

The calibrated aging albedo model is shown in Equation 5.3.

$$\alpha(N) = 0.1214 + 0.1056N^{0.0152} \quad (5.3)$$

Because of the limited data, the most suitable measure of goodness of fit for this model is the Root Mean Square Error (RMSE), which is 0.0025. A graphical representation of the data and the fitted model is shown in Figure 5-9. The RMSE is much less than the accepted precision of 0.01 for albedo per ASTM E1918 and thus, can be described as having a good fit. The measured ‘at-construction’ albedo of 0.1214 will be the constant albedo assumed during the analysis period in the static albedo case. Figure 5-9 also includes some data obtained from literature. These are from a variety of different asphalt pavements with varying binders and aggregates at locations all over the US. Therefore, they are not necessarily comparable to values from this study. Moreover, many studies in literature (Taha, Sailor, &

Akbari, High-albedo materials for reducing building cooling energy use, 1992) report an albedo of around 0.20 for ‘weathered’ pavements without quantifying the age of the pavement, which is why they could not be included in Figure 5-9. Overall, there is a lack of long-term data relating albedo with age for a given pavement or at least pavements with similar materials and mix design.

Table 5-4 Age and albedo data for aging albedo model calibration

| Section | Year of Construction | Age at measurement (in years) | Representative albedo | |
|---------|----------------------|-------------------------------|-----------------------|--------|
| AC1 | 2008 | 7 | 0.2266 | |
| AC2 | Sections 1-5 | 2007 | 8 | 0.2338 |
| | New AC Overlay | 2014 | 0 | 0.1214 |
| AC3 | 2013 | 1 | 0.2272 | |

5.3.4 RF and GWP

As described in Section 2.4, the RF (or equivalently the GWP) of a pavement is a measure of its environmental impact and can be used to quantify the UHI component of the use phase in a pavement LCA. Existing models, which consider a single value of albedo throughout the analysis period, are represented by the static albedo case, while the aging albedo case uses the predictions from Equation 5.3. The RF and corresponding GWP of each case are calculated using ILLI-THERM program and Equation 5.2, respectively, and plotted in Figure 5-10.

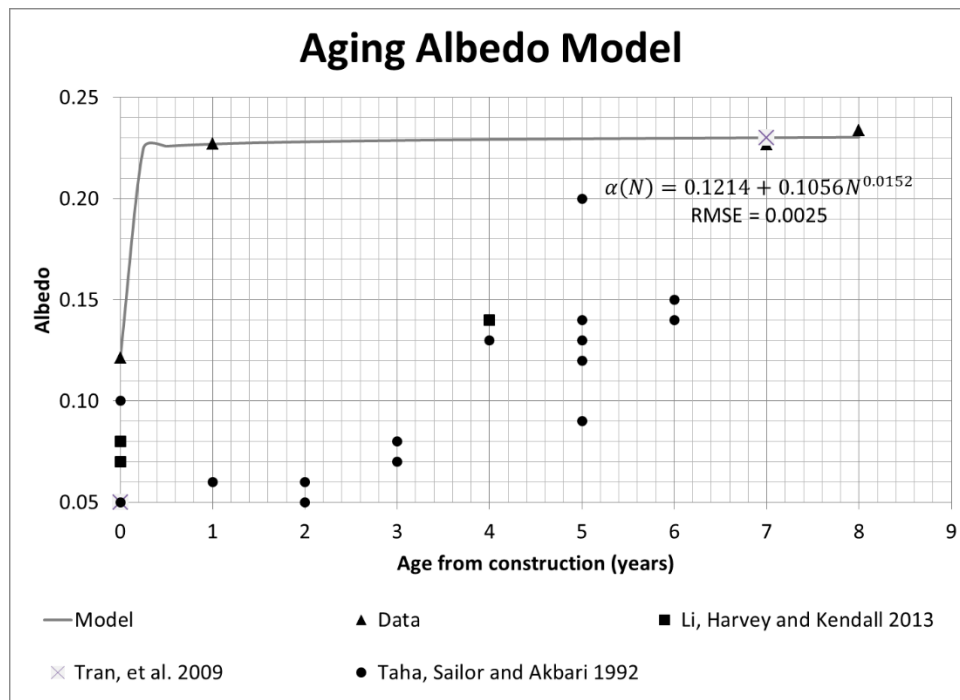


Figure 5-9 Aging albedo model

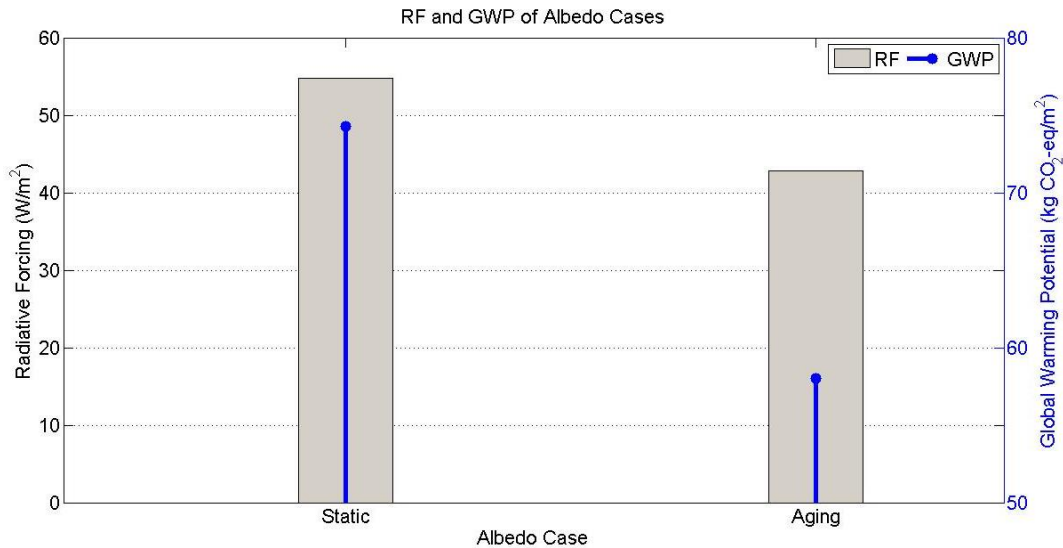


Figure 5-10 RF and GWP of albedo cases

The GWP according to the static albedo case is about 75 kg CO₂-eq/m² while the same pavement under the aging albedo case is about 58 kg CO₂-eq/m², a difference of 25%. For a typical lane-km, this is a difference of nearly 119 ton CO₂-eq/lane-km over a 5-year period. Two important conclusions can be made: first, a large part of the aging or weathering takes place in the first one or two years and after that, there is not much change in the albedo. This is based on limited data and would need to be verified with a larger dataset including different climate zones and asphalt concrete mixes. Second, the current practice of assuming a static albedo in LCAs is highly conservative and significantly overestimates the actual GWP of pavements. Models like ILLI-THERM using an aging albedo model can be used for more accurate LCAs because the local climate and pavement structure is captured reasonably accurately in the analysis.

5.3.5 Albedo of Polymer Fibers

Since PCC1 section was made of FFC, polymer fibers were clearly visible on the surface as seen in Figure 5-2. Although the fibers are covered in cement paste and are thus not expected to directly impact the surface albedo, it is possible that they become exposed in service because of abrasion. Measurements were taken on the individual fibers to determine their maximum theoretical contributions to the surface albedo. The fibers used were the same from the original FFC mix and test section. The spectral reflectance of a single fiber was determined according to the procedure outlined in Section 2.2. The resultant spectrum was found to have some noise from about 780 to 800 nm and again from 2000 to 2600 nm. To eliminate the noise, two corrective procedures were applied to the data:

- (a) Any values above 100% were reduced to 100% and those below 0% were corrected to 0%.
- (b) An exponential smoothing function was applied so as to minimize the error. A damping factor of 0.9 was found to return the lowest sum of squared errors (SSE).

The AM 1.5G standard solar spectrum from ASTM G173 as well as the smoothed spectral reflectance of a single polymer fiber are shown in Figure 5-11.

The calculated value of albedo of the fibers was 0.07 after the two corrective procedures noted above were applied. This albedo does not affect the pavement as long as the fibers remain coated with cement paste; only on abrasion will they become exposed to incoming solar radiation and have a thermal impact on the pavement. On exposure, a low albedo of 0.07 will have an impact, but it will depend on the area of the pavement covered by the exposed fibers, which is difficult to predict. Measurements on fiber reinforced concrete pavement sections and those without fibers is required to validate this laboratory finding, but is not further considered in the paper.

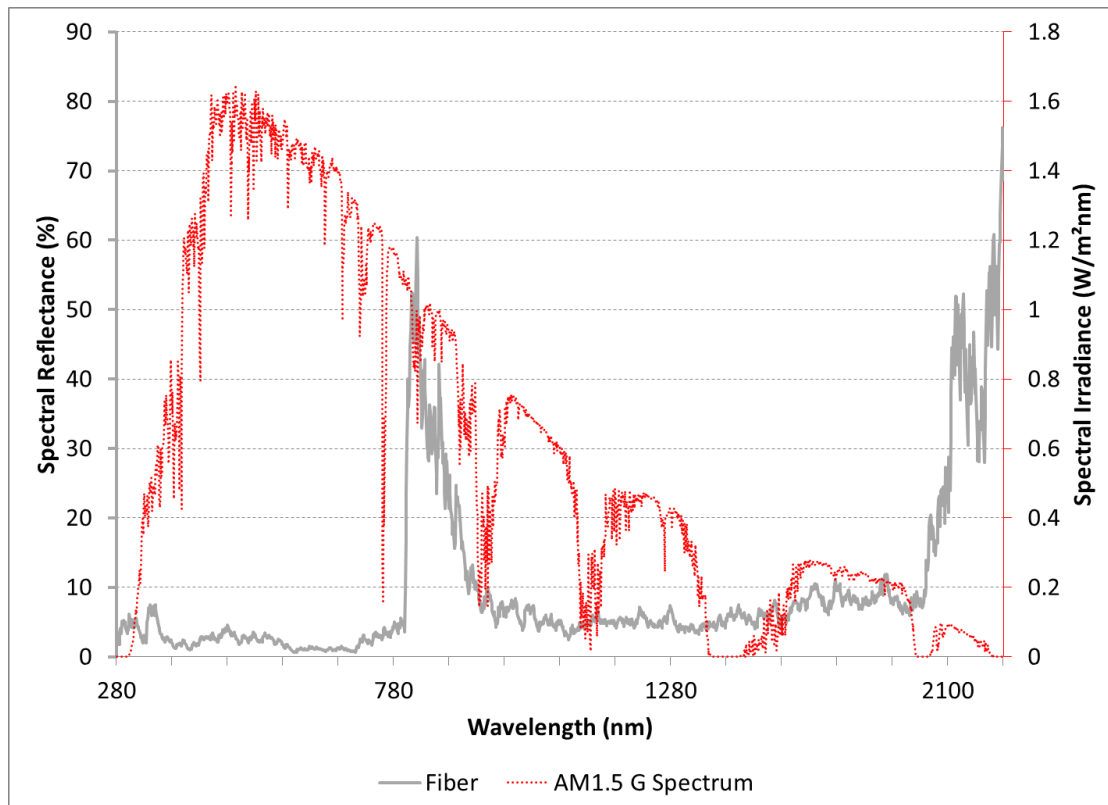


Figure 5-11 Smoothed spectral reflectance of polymer macrofiber. Standard AM 1.5G solar spectrum is also shown on the secondary axis

5.4 CONCLUSION

The albedo is a key factor affecting the UHI and environmental impact of pavement structures. Studies have measured the albedo of pavement surfaces made of a variety of materials but no work has been reported quantitatively expressing how pavement albedo ages with time. The albedo of three asphalt and two concrete sections at the ATREL facility in Rantoul, IL was measured with an albedometer. The measured albedos were used to calibrate a three-parameter aging albedo model for asphalt pavements with ages ranging from 0 to 8 years. The results of this model showed that asphalt concrete albedo increases and reaches a steady state value in one or two years. This aging albedo model was implemented into the 1-D heat transfer model called ILLI-THERM to determine the RF and GWP of a hypothetical pavement structure in Chicago, IL. A static albedo assumed over the analysis period overestimated the GWP of an asphalt pavement by approximately 25% for the asphalt

materials tested. The results of this first locally calibrated aging albedo model will allow for more accurate use phase LCAs.

This albedo testing on concrete pavements found values that largely agree with those reported in the literature. Additional spectrophotometer testing was completed to quantify the effect of macrofibers observed on one test section on surface albedo. Based on the spectral reflectance of a single fiber, it was found that the translucent fibers had a very low albedo of 0.07. As long as they remain covered with cement paste however, this will not affect the concrete pavement albedo. If there is abrasion of the paste due to vehicles however, this low albedo will have an impact that will depend on the area of the exposed fibers.

CHAPTER 6-CONCRETE ALBEDO MEASUREMENT FOR FINITE SIZED SPECIMENS

6.1 INTRODUCTION

The growth of urban agglomerations around the world has led to several impacts that affect the environment and human well-being. Among these impacts, the Urban Heat Island (UHI) has been studied extensively and can be observed as a significant temperature difference between urban agglomerations and adjacent rural areas (Kleerekopera, van Esch, & Salcedo, 2012) Aside from other factors, such as anthropogenic heat and loss of natural vegetation, a major cause of UHI is the extensive use of man-made materials in buildings and pavements.

For pavements in particular, UHI is studied in the use phase of Life Cycle Assessment (LCA) of concrete and asphalt pavements (Santero, Masanet, & Horvath, 2011a). In a pavement LCA, UHI is controlled by thermal properties of pavement layers, such as albedo, thermal conductivity, heat capacity and emissivity. Many studies have considered the impact of pavement albedo on UHI (Akbari, Menon, & Rosenfeld, Global cooling: increasing worldwide urban albedos to offset CO₂, 2009; Menon, Akbari, Mahanama, Sednev, & Levinson, 2010; Santamouris, Synnefa, & Karlessi, 2011) while a few have also considered pavement thermal properties as a whole (Gui, Phelan, Kaloush, & Golden, 2007). In chapter 3, it was shown that the effect of albedo in pavement LCA analysis relative to other thermal properties of concrete pavements is significant. Therefore, measuring albedo of existing and future concrete pavements is an important step towards achieving more sustainable pavement structures.

Accurately measuring the albedo of concrete pavement surfaces can be challenging. While the incoming solar radiation is a combination of diffuse and direct radiation, the radiation reflected by the concrete pavement is diffuse in nature (Levinson, Akbari, & Berdahl, 2010). A field method based on ASTM E1918 (ASTM Standard E1918, 2006) uses a single or double pyranometer (a double pyranometer is also known as an albedometer) and has been used in previous studies on large surfaces (Li, Harvey, & Kendall, 2013; Lin, Matzarakis, Hwang, & Huang, 2010; Krimpali & Karamanis, 2015; Pisello, Pignatta, Castaldo, & Cotana, 2014; Tran, Powell, Marks, West, & Kvasnak, 2009; Kaloush, Carlson, Golden, & Phelan, 2008). ASTM E1918 recommends a surface size of at least 4m x 4m. With respect to concrete in civil engineering applications, however, it is not practical to cast such large specimens to measure albedo, particularly as the albedo varies by mix design and choice of constituent materials (Levinson & Akbari, Effects of composition and exposure on the solar reflectance of portland cement concrete, 2002; Boriboonsomsin & Reza, 2007), and it may be necessary to attempt several material designs. The ASTM E1918 method is also limited by cloud conditions and zenith angle of the sun during measurement. A detailed discussion of additional shortcomings ASTM E1918 can be found elsewhere (Levinson, Akbari, & Berdahl, 2010).

Despite these limitations, ASTM E1918 is useful and even preferred because it can measure albedo quickly in the field and is inexpensive. Attempts have been made to refine the technique using the concept of view factors (or configuration factors) from radiative heat transfer (Reifsnyder, 1967). The view factor of a surface with respect to another surface is the proportion of the radiation from the surface that reaches the other surface. One study (Matthias, et al., 1999) made use of simple view factors for square-shaped soil samples while another (Sailor, Resh, & Segura, 2006) used a shade curtain and complex geometric analysis

over grass to determine albedo. Even with the proposed algorithms, neither of these studies was able to validate their results with an independent method. In addition, neither study considered stray reflections from other surfaces, such as trees or buildings, although both tried to avoid interference by careful choosing of the test location. A third study (Akbari, Levinson, & Stern, 2008) developed an alternative method, named E1918A, that used a series of measurements based on ASTM E1918 and standardized black and white masks of pre-determined albedo to determine the surface albedo, which eliminated the need to calculate view factors. However, in practice it is difficult to maintain such masks without damaging or needing to regularly recalibrate them and the E1918A method also did not take into account any stray reflections.

An alternate laboratory method, utilizing a spectrophotometer, has been used that employs smaller samples and is based on the spectral reflectance of the sample per ASTM E903 (ASTM International, 2012) in conjunction with a standard air mass 1.5 global (AM 1.5G) solar spectrum from ASTM G173 (ASTM International, 2003). This method has been used in previous studies to determine the albedo of small colored concrete tiles (Synnefa, et al., 2011; Santamouris, Synnefa, & Karlessi, 2011; Synnefa, Santamouris, & Apostolakis, 2007) and other concrete samples (Krimpali & Karamanis, 2015). As discussed in (Levinson, Akbari, & Berdahl, 2010), this method is not representative of the reflection from non-concentrated sunlight, even with clear skies in most parts of the US, and it is only suitable to obtain an approximate value of albedo. The spectral reflectance represents a very small area of the sample, about 10 mm². Moreover, the spectrophotometer equipment required for the test is very expensive and not generally available for most agencies. Therefore, it is necessary to develop a field or lab method that overcomes the disadvantages of the current methods presented in the literature such as specimen geometry and adjacent radiation reflectors along with an independent laboratory estimate of the material's albedo.

In general, the albedo of concrete is known to decrease over time (Santamouris, 2013) with many studies reporting albedo of weathered concrete (Santamouris, 2013; American Concrete Pavement Association (ACPA), 2002). There is very little reported literature that explicitly studies concrete albedo with weathering under controlled conditions, with only one study showing how different factors, such as soiling and abrasion, affect the albedo (Levinson & Akbari, 2002). The present study also examines weathering of a concrete sample over one winter in the Midwestern US to estimate the contribution to change of albedo by dust and dirt accumulated on the surface as well as possible chemical or physical changes in the concrete.

This chapter summarizes work performed in two stages (I and II) and serves three objectives:

- (a) In Stage I, a new method is presented that combines simple geometric analysis with statistical methods to determine the albedo of concrete samples of finite size and contributing background. The measured albedo is then independently validated in the laboratory per ASTM E903. The proposed method eliminates the need for large specimen sizes and can be used with virtually any specimen size, including those that are typically used in civil engineering testing. It also accounts for reflection from background materials without the need for standardized masks, increasing the number of test sites where albedo can be measured.
- (b) Using the new method for albedo for finite sized specimens, Stage II determined the impact of one full winter of weathering on the albedo of the concrete.
- (c) Lastly, the concrete tested in this study used white Portland cement incorporated with titanium dioxide (TiO₂) nanoparticles, a material that not only increases albedo but also acts as a photocatalyst to reduce greenhouse gas emissions from vehicles

(Guerrini & Peccati, 2007; Boonen & Beeldens, 2013; Osborn, Hassan, & Dylla, 2012). Aside from the value measured in chapter 4, only one other study (National Concrete Pavement Technology Center, 2012) has reported albedos for this kind of concrete.

6.2 METHODOLOGY

6.2.1 Experimental Design

This investigation is part of a larger study on the development of multi-functional concrete inlays that provide structural, functional and environmental benefits. The goal of this paper was restricted to determining the albedo of a concrete sample of any size using an albedometer. Specifically, this study utilized a Kipp & Zonen[®] CMA 6 albedometer. A 1 m square concrete slab was cast based on a mix design outlined in Section 2.2. In Stage I of the study, the slab was placed on a test site described in Section 2.3 and black paper was used to cover parts of the slab surface so as to vary the size of the slab area exposed to sunlight. Measurements from the albedometer were used to develop a method to determine the albedo of the concrete for a finite size exposed area with background interference. During Stage I, the slab was covered whenever it was not being tested so as to minimize environmental exposure.

Following Stage I, the slab was left exposed to the environment from December 2014 to April 2015 to allow for one winter season of weathering. During this time, the slab underwent multiple cycles of precipitation (rain and snow) and exposure to sunlight, dust, debris, freezing/thawing cycles, and wetting/drying cycles but no vehicular traffic. In April 2015, the slab was moved to another site for Stage II measurements, which is described in Section 2.3. The albedo of this weathered concrete was determined using the new method discussed in Sections 2.5-2.7. Afterward, the slab was cored and washed thoroughly. ASTM E903 was used to independently estimate the albedo of this weathered and washed sample of concrete. Thus, in Stage II, the effect on the concrete albedo of atmospheric weathering of the slab and weathering without dust or other particulate matter was quantified. This provides a short-term insight into whether any chemical or physical changes in the concrete induced changes in the albedo because of the ambient environment.

6.2.2 Concrete Mix Design

The concrete mix design was controlled by the structural and construction requirements of multi-functional concrete inlays based on a previous design (King, 2015). This is discussed in chapter 4 and reproduced below in Table 6-1. The mix design was changed to remove the fly ash and macro fibers so that the albedo would depend only on the aggregates and cement. The 1 m² concrete slab was then cast and subsequently cured under wet burlap for 24 hours before moving it to the test site for Stage I testing. To independently validate the slab albedo with the spectrophotometer, two 100 mm cubes were also cast with the same constituents except with slightly higher w/cm ratio and cured the same.

Table 6-1 Concrete mix design

| Mix Component | Unit | Mix Proportion |
|------------------------------------------------------------------------|-------------------|----------------|
| Natural Sand | kg/m ³ | 857 |
| Limestone Aggregate | kg/m ³ | 1052 |
| Type I white Portland cement containing TiO ₂ nanoparticles | kg/m ³ | 468 |
| Class C Fly Ash | kg/m ³ | - |
| High Range Water Reducer | ml/m ³ | 1715 |
| Air-Entraining Admixture | ml/m ³ | 107 |
| Synthetic Macro-Fibers | kg/m ³ | - |
| Water | kg/m ³ | 187 |
| w/cm | - | 0.40 |

6.2.3 Test Sites

In Stage I, the slab was placed on the south lawn of Newmark Civil Engineering Laboratory in Urbana, Illinois, on grass adjacent to a large concrete ramp (Figure 6-1). In Stage II, after weathering, the slab was moved to a location outside the Traffic Operations Laboratory (TOL) at the Advanced Transportation Engineering and Research Laboratory (ATREL) in Rantoul, Illinois, just northeast of Urbana (Figure 6-2). In both cases, the slab was placed at least 4m from adjacent buildings and trees. Google Earth images of the sites are shown in Figure 6-3 along with the location where the slab was placed.



Figure 6-1 TiO₂ concrete slab on the site for stage I testing



Figure 6-2 TiO₂ concrete slab on the site for stage II testing

In Stage I, the slab was placed on the grass with a concrete ramp and sidewalk on two sides. The dimensions of these are shown in Figure 6-4. Dimensions exceeding 4 m were considered to be theoretically infinite and shown simply as '> 4 m'. This value comes from ASTM E1918, which considers a surface of size 4 m x 4 m to be 'large'. There were also some trees and buildings as well as an old asphalt pavement in the area, as visible in Figure 6-3(a). In Stage II, the slab was placed in an old asphalt parking lot with two buildings on the south and east of the slab and some trees on the north, but all of these were 'far' (more than 4 m) away from the slab.

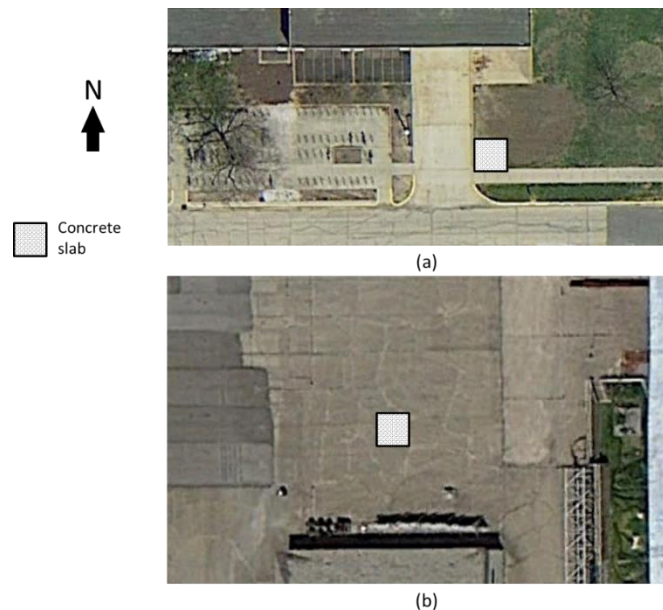


Figure 6-3 Test site for (a) stage I testing in Urbana, Illinois and (b) stage II testing in Rantoul, Illinois. Pictures are taken from Google Earth™.

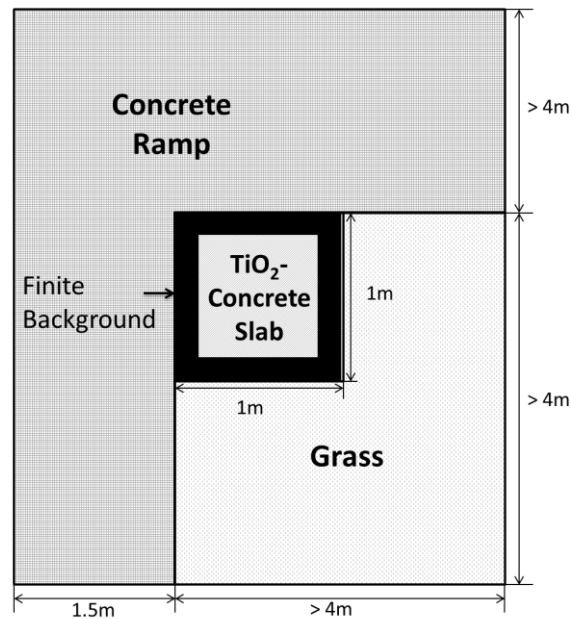


Figure 6-4 Schematic diagram of the concrete slab in stage I and its adjacent surfaces.

6.2.4 Albedo Measurement: Laboratory Method

Albedo measurements using a spectrophotometer were performed according to ASTM E903 and the AM 1.5G standard solar spectrum from ASTM G173 to satisfy two objectives. The first was to measure the albedo of the constituent materials used to make the concrete as well as the black paper used in Stage I. The second objective was to validate the results from the field measurements.

Two spectrophotometers were used for this study. Cement and sand were tested using a Cary 5G UV-Vis-NIR instrument and their combined specular and diffuse spectral reflectance were obtained from 280 nm to 3300 nm. This covers the ultraviolet (UV, 280-400 nm), visible (Vis, 400-700 nm) and near infrared (NIR, 700-3300 nm) bands of the spectrum. This instrument is suited for measuring the spectral reflectance of powder materials. Limestone aggregate, black paper, and concrete cubes/cores were also measured for combined specular and diffuse spectral reflectance from 280 nm to 2600 nm using a Cary 5000 UV-Vis-NIR spectrophotometer, which is well-suited for such non-powder samples. The Cary 5G and Cary 5000 could not detect spectral reflectance up to 4000 nm, so part of the spectral irradiance was neglected, leading to some error. This spectral irradiance was only 0.6% and 0.8% of the solar spectrum for the two instruments, respectively, so the error is considered negligible.

The standard solar spectrum from ASTM G173 corresponds to the AM 1.5 G. Air mass is a measure of the length of the atmosphere that a beam of light has to go through before reaching the earth's surface, which is related to the level of attenuation of the beam's energy. Air mass varies with latitude Z as $1/\cos(Z)$ for mid-latitude regions, and in Champaign County, it is approximately 1.3. Thus, AM 1.5 G does not correspond exactly to the expected solar spectrum over the tests sites in this study, but it is expected to be similar, leading to some small, but systemic, error between field and laboratory measurements of albedo.

6.2.5 Albedo Measurement: Field Method

Field measurements of the concrete slab albedo were conducted under clear skies using an albedometer. Although ASTM E1918 recommends a slab size of at least 4 m x 4 m and for measurements to be taken at a height of 0.5 m, this study measured albedo at 0.25, 0.50, 0.75, 1.00, 1.25 and 1.50 m above the center of the TiO₂-concrete slab. In Stage I, the size of the exposed surface of the slab was varied incrementally in steps of 0.2 m from 1.0 m to 0.0 m (i.e., the whole slab was covered as shown in Figure 6-5 by covering parts of the slab with black paper, as shown in Figure 6-6. This is shown in Figure 6-4 as a ‘finite background’. Thus, a variety of combinations of height and slab size were used. The albedo of the background ramp and grass surfaces was also measured at those heights (Figure 6-7).

A similar procedure was performed in Stage II, except that the entire exposed surface of the slab was considered without any black paper covering it (Figure 6-8). In all cases in stages I and II, measurements were taken over the center of the slab for at least three minutes and averaged every five seconds so that the sample size of albedo measurements for each case was at least 30.

In each case, the measured albedo was a composite value that included diffuse radiation reflected from the slab and finite / infinite background as well as other background surfaces not explicitly considered. The composite albedo does not represent the albedo of any one surface except in those cases where the albedo was measured over an ‘infinite’ surface with no other background interference or external surfaces. A method to determine the relative contribution of reflected radiation of each surface is described in the next section.



Figure 6-5 Albedo being measured at a height of 0.50 m when the exposed slab size is 0.0 m i.e., when it is fully covered in the ‘finite background’ (black paper)



Figure 6-6 Slab covered with the 'finite background' (black paper) with an exposed size of 0.6 m



Figure 6-7 Measurement of albedo over (a) grass surface and (b) concrete ramp surface. An average of these two is called a composite 'infinite' background albedo



Figure 6-8 Stage II measurement of albedo over the TiO₂ concrete slab with asphalt pavement background surface

6.2.6 View Factors

To determine the albedo of the concrete slab alone, it was necessary to eliminate the fraction of reflected solar radiation coming in from surrounding surfaces. This fraction is called the view factor of the albedometer with respect to the surfaces in question and describes the proportion of reflected solar radiation received from the slab and from background surfaces by the albedometer (Reifsnyder, 1967). The view factor is obtained through geometric analysis, assuming that the area of the albedometer was very small as compared to the slab and surrounding surfaces. In Stage I of this study, there were two such surfaces:

- (a) The black paper, which is named the finite background (*bg-fin*).
- (b) A composite background made up of equal proportions of the ramp and grass, which is called the infinite background (*bg-inf*). The albedo of this composite background at any height was defined as the average albedo of the grass and ramp as measured at that height. A simple average was used because the view factor of both the surfaces with respect to the albedometer was equal by symmetry (See Figure and Figure), so an average albedo could be used together with the view factor of the combined infinite background.

In Stage II of the study, the slab was placed on top of an old asphalt pavement, which was designated as the infinite background (*bg-inf*), and there was no finite background. In all cases involving the concrete slab, the albedometer was placed over the center of the slab at various heights.

Next, the view factors of all the surfaces being explicitly considered were determined. If s represents the concrete slab and dA the albedometer, and a and h are the length of the side of the exposed square slab surface and height of measurement respectively and $0.0\text{ m} \leq a \leq$

1.0 m, then the relationship between the view factors of the albedometer with respect to the slab and the finite and infinite backgrounds is given in Equation 6.1, where $F_{dA \rightarrow i}$ is the view factor of the albedometer with respect to any surface i and is a function of a and h . $F_{dA \rightarrow s}$ represents the view factor of the square slab with respect to the albedometer placed over its center and can be evaluated using Equation 6.2 (Matthias, et al., 1999), where the constant A is given by Equation 6.3. This is only valid for this shape of the slab and the position of the albedometer, but can be calculated for any specimen geometry and albedometer position (Reifsnyder, 1967).

$$F_{dA \rightarrow s}(a, h) + F_{dA \rightarrow bg-fin}(a, h) + F_{dA \rightarrow bg-inf}(a, h) = 1 \quad (6.1)$$

$$F_{dA \rightarrow s}(a, h) = \frac{4}{\pi} * \frac{A}{\sqrt{1 + A^2}} * \tan^{-1} \left(\frac{A}{\sqrt{1 + A^2}} \right) \quad (6.2)$$

$$A = \frac{a}{2h} \quad (6.3)$$

Determining $F_{dA \rightarrow bg-fin}$ involves determining the view factor of the finite background when it covers the entire slab, which is numerically equal to $F_{dA \rightarrow s}(a = 1.0m, h)$, and subtracting from it the view factor of an imaginary surface covering the exposed slab, as shown mathematically in Equation 6.4 and graphically in Figure 6-9.

$$F_{dA \rightarrow bg-fin}(a, h) = F_{dA \rightarrow s}(a = 1.0m, h) - F_{dA \rightarrow s}(a, h) \quad (6.4)$$

Finally, the view factor of the infinite background is calculated using Equation 6.5.

$$F_{dA \rightarrow bg-inf}(a, h) = 1 - F_{dA \rightarrow bg-fin}(a, h) - F_{dA \rightarrow s}(a, h) \quad (6.5)$$

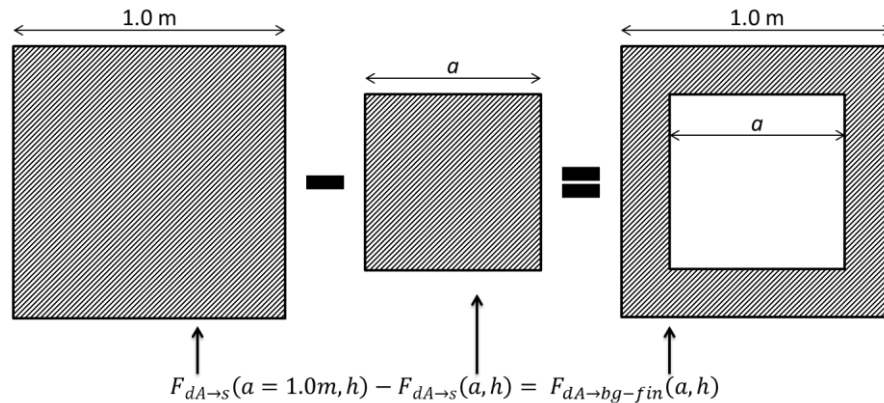


Figure 6-9 Graphical representation of Equation 4 to calculate the view factor of the finite background

The relationship between the albedo of the slab and finite and infinite backgrounds with the measured (composite) albedo α_m is given by Equation 6.6, where α_i is the 'true' albedo of any surface i at a specific site.

$$\alpha_s F_{dA \rightarrow s}(a, h) + \alpha_{bg-fin} F_{dA \rightarrow bg-fin}(a, h) + \alpha_{bg-inf} F_{dA \rightarrow bg-inf}(a, h) = \alpha_m(a, h) \quad (6.6)$$

In Stage II of the study, no finite background (black paper) was used, and hence, Equation 6.6 was used with $F_{dA \rightarrow bg-fin}(a, h) = 0$. Furthermore, as no finite background was used to partially cover the slab, the exposed side was also constant at $a = 1.0$ m.

There are two important facts pertaining to Equation 6.6 that should be noted. First, the contribution of the slab and finite and infinite backgrounds are explicitly considered, while those from other sources such as buildings or trees are implicitly considered by measuring albedo at various heights. Thus, any variation in albedo as a function of height with the infinite background was on account of this stray interference and had to be statistically minimized. Second, unlike some previous studies (Matthias, et al., 1999; Sailor, Resh, & Segura, 2006), but similar to another (Li, Harvey, & Kendall, 2013), the shadow of the albedometer is not considered in the view factor analyses and care was taken to ensure that it did not fall on the slab surface itself, except at a height of 0.25 m where it was unavoidable. As the area of the shadow as compared to the other surfaces was very small, the error was neglected.

6.2.7 Albedo Estimation

Albedo was estimated using Equation 6.6 based on the assumed number of surfaces where the albedo is not known. The albedo of the finite-sized slab α_s is unknown, but that of the finite and infinite backgrounds may be determined. The following two methods can be employed to determine α_s :

- (a) If the measured albedo of the infinite background α_{bg-inf} does not vary significantly with height, there is little interference from other surfaces and thus it can assumed to be a known quantity. In this case, an average value of the infinite background albedo at different heights can be used. Furthermore, if the albedo of the finite background α_{bg-fin} can also be determined separately so that it also is known, then Equation 6.7 can be used to find values of α_s for each albedo height and exposed slab area measurement and then averaged.

$$\alpha_s = \frac{\alpha_m(a, h) - [\alpha_{bg-fin}F_{dA \rightarrow bg-fin}(a, h) + \alpha_{bg-inf}F_{dA \rightarrow bg-inf}(a, h)]}{F_{dA \rightarrow s}(a, h)} \quad (6.7)$$

- (b) If either or both of α_{bg-inf} and α_{bg-fin} are unknown, Equation 6.6 can be written in the form of a matrix as shown in Equation 6.8. This is an over-determined system of equations and a least-squares solution can be obtained using Equation 6.9. This solution statistically minimizes errors due to interference from other background surfaces to provide the best estimate of albedo for all surfaces.

$$\begin{aligned} [F_{dA \rightarrow s}(a, h) \quad F_{dA \rightarrow bg-fin}(a, h) \quad F_{dA \rightarrow bg-inf}(a, h)] * \begin{Bmatrix} \alpha_s \\ \alpha_{bg-fin} \\ \alpha_{bg-inf} \end{Bmatrix} \\ = \{\alpha_m(a, h)\} \end{aligned} \quad (6.8)$$

$$\text{Or, } [F] * \{\alpha\} = \{\alpha_m\}$$

$$\{\alpha\} = ([F]^T * [F])^{-1} * ([F]^T * \{\alpha_m\}) \quad (6.9)$$

The proof for Equation 6.9 is as follows. As there is no exact solution, any solution has an error, which is represented by the residual vector r in Equation 6.9a.

$$\{r\} = \{\alpha_m\} - [F] * \{\alpha\} \quad (6.9a)$$

The least squares solution is one that minimizes the sum of the square of the residuals, $\sum_{i=1}^n r_i^2$, where n is the number of equations. This is achieved by setting $\frac{\partial(\sum_{i=1}^n r_i^2)}{\partial \alpha_j} = 0$, where $\alpha_j, j = \{1,2,3\}$ is one of the three unknown albedos in the vector $\{\alpha\}$. The result of this is shown in the series of equations marked 6.9b.

$$\begin{aligned} \frac{\partial(\sum_{i=1}^n r_i^2)}{\partial \alpha_j} &= \frac{\partial(\sum_{i=1}^n [\alpha_{m,i} - \sum_{j=1}^3 F_{ij} * \alpha_j]^2)}{\partial \alpha_j} \\ &= \sum_{i=1}^n -2F_{ij} \left[\alpha_{m,i} - \sum_{j=1}^3 F_{ij} * \alpha_j \right] = 0 \end{aligned} \quad (6.9b)$$

Expressing Equation 6.9b in matrix form and simplifying the terms gives the necessary solution in Equation 6.9c.

$$\begin{aligned} [F]^T * (\{\alpha_m\} - [F] * \{\alpha\}) &= \{0\} \\ ([F]^T * [F]) * \{\alpha\} &= [F]^T * \{\alpha_m\} \\ \{\alpha\} &= ([F]^T * [F])^{-1} * ([F]^T * \{\alpha_m\}) \end{aligned} \quad (6.9c)$$

If one of α_{bg-inf} and α_{bg-fin} are known with reasonable certainty, then its contribution to the measured albedo, $\alpha_{bg-inf} F_{dA \rightarrow bg-inf}(a, h)$ and $\alpha_{bg-fin} F_{dA \rightarrow bg-fin}(a, h)$, respectively, can be subtracted from the measured value of α_m in Equation 6.8 so that the left side is a matrix of unknown terms and the right side contains one of known terms. For example, without loss of generality, the equation for this case is shown in Equation 6.10 when the value of α_{bg-inf} is known. Equation 6.10 can be solved for $\{\alpha\}$ using a least-squares solution from (Equation 6.9).

$$\begin{aligned} [F_{dA \rightarrow s}(a, h) \quad F_{dA \rightarrow bg-fin}(a, h)] * \left\{ \begin{array}{c} \alpha_s \\ \alpha_{bg-fin} \end{array} \right\} \\ = \{ \alpha_m(a, h) - \alpha_{bg-inf} F_{dA \rightarrow bg-inf}(a, h) \} \end{aligned} \quad (6.10)$$

$$\text{Or, } [F] * \{\alpha\} = \{ \alpha_m - \alpha_{bg-inf} F_{dA \rightarrow bg-inf} \}$$

To summarize the methodology, the measured albedo of various combinations of the finite-sized slab with finite and infinite backgrounds at different heights and size of the exposed slab was experimentally determined. In order to isolate the contributions of each of these surfaces as well as any external surfaces not explicitly considered in the measured albedo, the concept of view factors was used. While the actual albedo of the concrete slab (α_s) is

unknown, the finite and infinite backgrounds may or may not be known. Depending on the number of unknown albedos, methods were proposed to calculate the unknown albedos. Measured composite albedos of the finite-sized slab specimens and the results of each of these methods are discussed in the following sections.

6.3 RESULTS AND DISCUSSION: STAGE I

6.3.1 Albedo of Constituent Materials

The spectral reflectance of sand and TiO₂ white cement were obtained using the Cary 5G spectrophotometer as shown in Figure 6-10. For comparison, the spectra of some other materials typically used in concrete as well as a sample of the TiO₂ (anatase) are also shown. The limestone aggregates and finite background (black paper, both sides) spectral reflectances, obtained using a Cary 5000 spectrophotometer, are shown in Figure 6-11. The AM 1.5G solar spectrum used to find albedo is also shown in both the figures. There is some noise in these measurements, particularly in Figure 6-11, because the samples could not be placed perfectly flat against the instrument. The albedo was calculated using Equation 6.11, taken from ASTM E903, where $R_s(\lambda)$ is the spectral reflectance, $E(\lambda)$ is the spectral irradiance of the standard AM 1.5G solar spectrum from ASTM G173 and λ is the wavelength.

$$\alpha = \frac{\int R_s(\lambda)E(\lambda)d\lambda}{\int E(\lambda)d\lambda} \approx \frac{\sum R_s(\lambda)E(\lambda)\Delta\lambda}{\sum E(\lambda)\Delta\lambda} \quad (6.11)$$

An integration was performed over the applicable range of the spectrum for which $R_s(\lambda)$ is measured by the spectrophotometers. The calculated albedos are shown in Figure 6-12. This value is only approximate and not necessarily the ‘true’ value of albedo at a given location since the AM 1.5G spectrum is not valid for the test location, as discussed in Section 1. The albedo of the TiO₂ cement and the sand were comparable to values corresponding to white cement and tan beach sand from another study for the same air mass of 1.5 (Levinson & Akbari, 2002), which were 0.87 and 0.45 respectively. Relative to conventional (gray) Portland cement, which has a reported albedo of 0.32 (Levinson & Akbari, 2002) and 0.25 as measured in this study, it can be noted that the TiO₂-containing white cement tested in this study has a much higher albedo of 0.80.

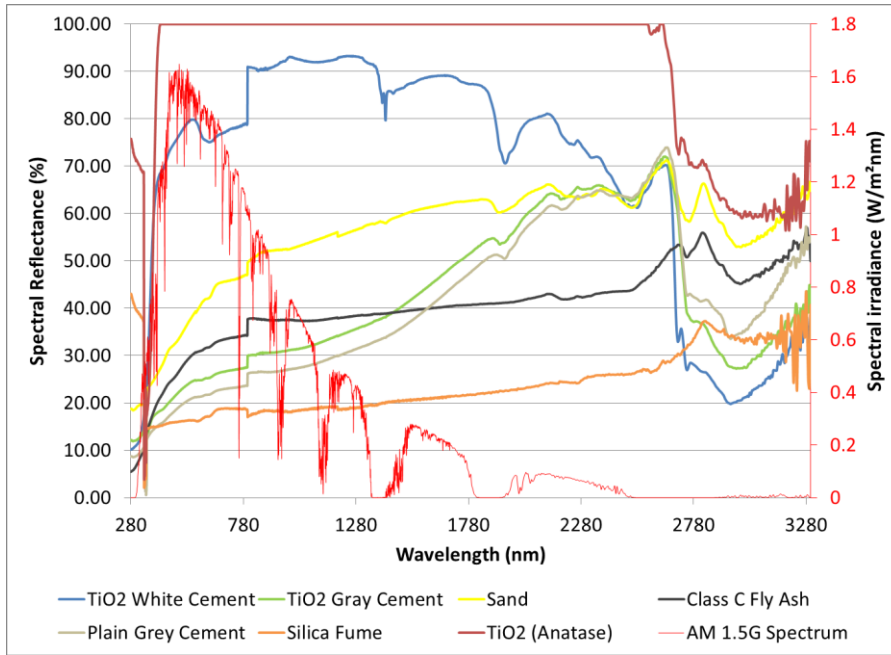


Figure 6-10 Spectral reflectance of various materials from the Cary 5G spectrophotometer with AM 1.5 G spectrum on the secondary axis

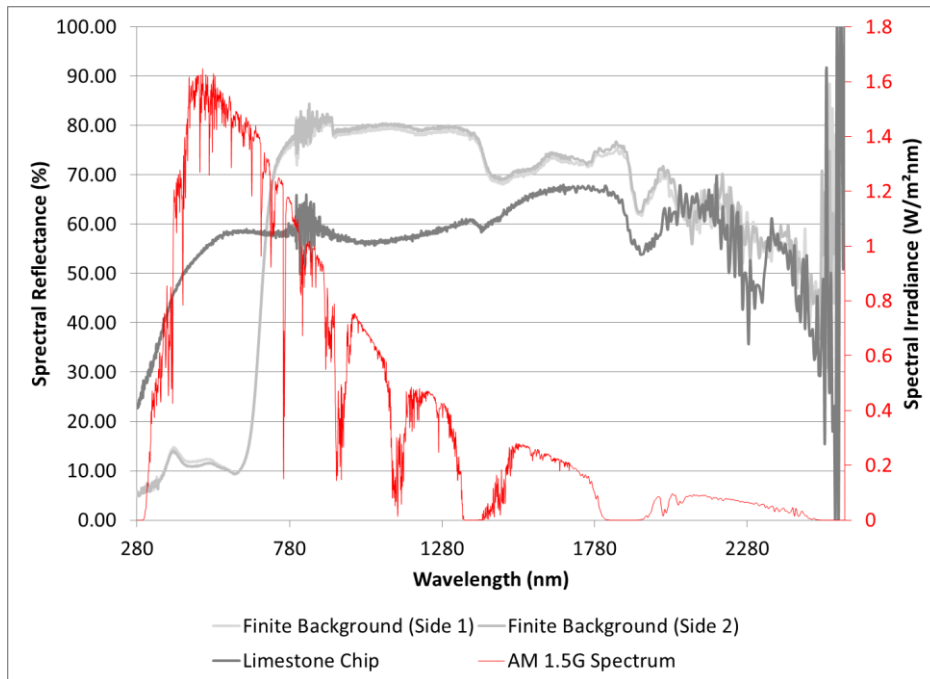


Figure 6-11 Spectral reflectance of black paper and limestone aggregate chip from the Cary 5000 spectrophotometer with AM 1.5 G spectrum on the secondary axis

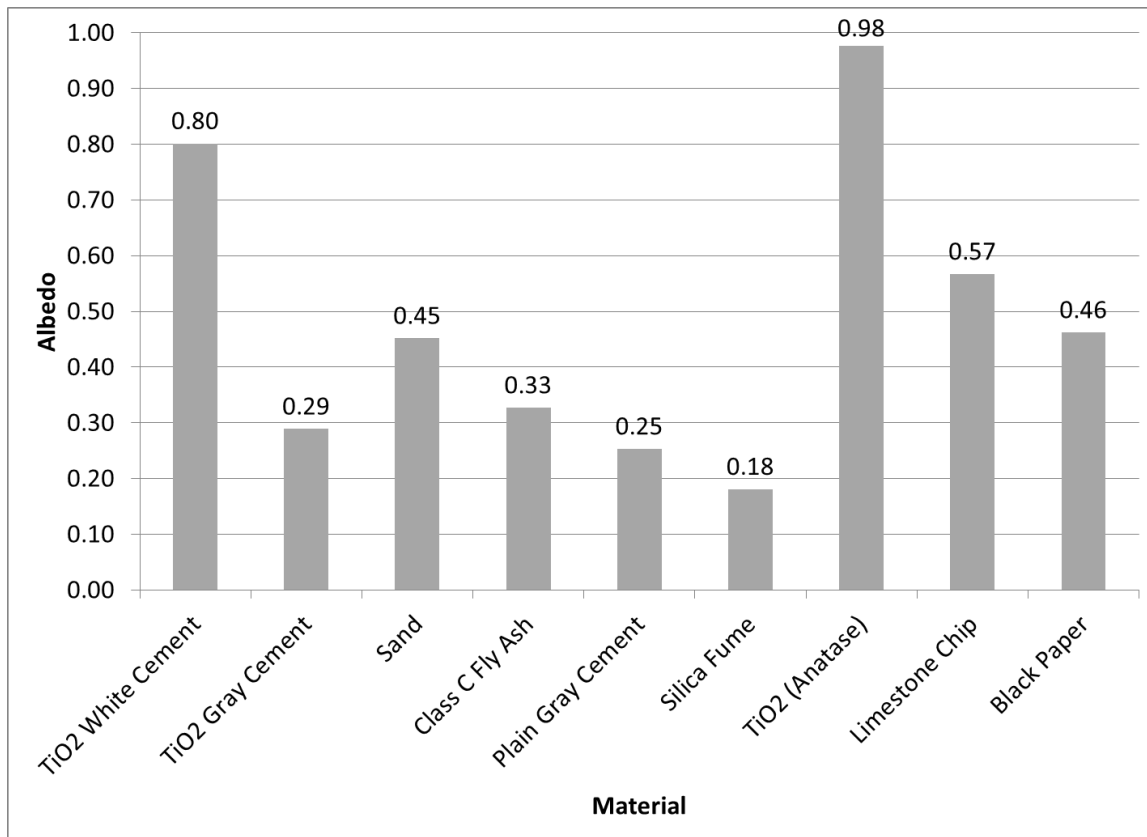


Figure 6-12 Calculated albedo of TiO₂ white cement, sand, limestone aggregate and the black paper (average of two sides)

The albedo of the black paper, used for the finite background, had a high value of 0.46. The cause of this finding is clear in Figure 6-12, where the black paper exhibits a high reflectance in the NIR region of the spectrum (700 – 2600 nm) and very low reflectance in the visible region (400-700 nm). Thus, color is not necessarily the best indicator of albedo.

6.3.2 Weather Conditions

Field measurements of concrete slab albedo were performed between 10:00 AM and 3:00 PM CDT whenever there were little or no clouds in the sky. No measurements were taken when clouds were covering the solar disc. A summary of the weather conditions from the nearby Champaign Willard Airport, obtained through the National Climatic Data Center (NCDC) (National Climatic Data Center, 2014), is presented in Table 6-2. Under the column ‘Cases Covered’ in Table 6-2, the cases are referred to with respect to the size of the exposed slab (1.0m, 0.8m, etc.) and the ramp or grass in the infinite background.

6.3.3 Albedo Measurements

Five-second averaged albedometer results are shown in box and whisker diagrams for each height case in Figure 6-13(a)-(h). An exposed slab size of 0.0m corresponding to Figure 6-13(f) refers to the case when the entire slab is covered by the finite background of black paper. There was very little variation within a given combination of exposed surface size and height, but there was significant variation as the height of the albedometer changed over the exposed surface of any size. The mean value of each case can be taken as a representative value and the variation of mean albedo with height and exposed size is summarized in Figure 6-14. The mean albedo of the infinite background represents the combined mean of the ramp and grass as discussed in Section 2.6.

Table 6-2 Weather data for stage I field measurements from (National Climatic Data Center, 2014) at Champaign Willard Airport

| Date | Time (LST) | Sky Conditions | Temperature (°C) | | | Cases Covered |
|------------|------------|---------------------|------------------|----------|-----------|------------------------------|
| | | | Dry Bulb | Wet Bulb | Dew Point | |
| 10/20/2014 | 10:53 | Clear | 18.3 | 12.9 | 8.3 | 1.0m and 0.8m at all heights |
| | 11:53 | Clear | 19.4 | 13.3 | 8.3 | |
| | 12:53 | Clear | 20.0 | 13.3 | 7.8 | |
| | 13:53 | Few clouds at 1250m | 20.0 | 13.3 | 7.8 | |
| | 14:53 | Few clouds at 1250m | 20.0 | 13.3 | 7.8 | |
| 10/21/2014 | 12:53 | Few clouds at 1500m | 15.6 | 9.5 | 3.3 | 0.6m at all heights |
| | 13:53 | Clear | 15.6 | 9.5 | 3.3 | |
| | 14:53 | Few clouds at 1400m | 15.0 | 9.5 | 3.9 | |
| 10/22/2014 | 9:53 | Clear | 10.6 | 7.1 | 3.3 | 0.4m and 0.2m at all heights |
| | 10:53 | Clear | 12.2 | 7.7 | 2.8 | |
| | 11:53 | Clear | 13.3 | 8.3 | 2.8 | |
| | 12:53 | Clear | 14.4 | 9.0 | 3.3 | |
| | 13:53 | Clear | 15.0 | 9.1 | 2.8 | |
| | 14:53 | Clear | 15.6 | 9.3 | 2.8 | |
| 10/26/2014 | 10:53 | Clear | 17.2 | 8.5 | -1.7 | 0.0m at all heights |
| | 11:53 | Clear | 19.4 | 9.7 | -1.1 | |
| | 12:53 | Clear | 20.0 | 9.5 | -2.8 | |
| 10/28/2014 | 13:53 | Clear | 16.7 | 10.5 | 4.4 | Grass at all heights |
| | 14:53 | Clear | 16.7 | 10.3 | 3.9 | |
| 11/02/2014 | 9:53 | Few clouds at 3300m | 6.1 | 2.7 | -2.2 | Concrete ramp at all heights |
| | 10:53 | Clear | 7.8 | 3.1 | -3.9 | |

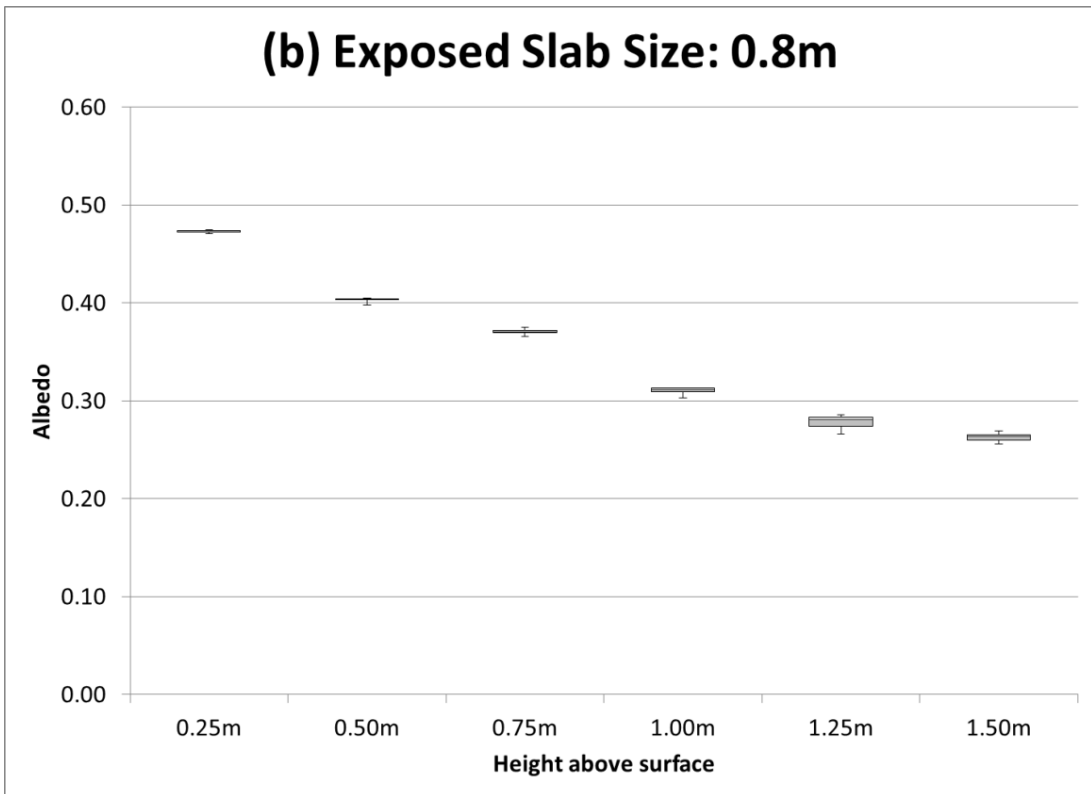
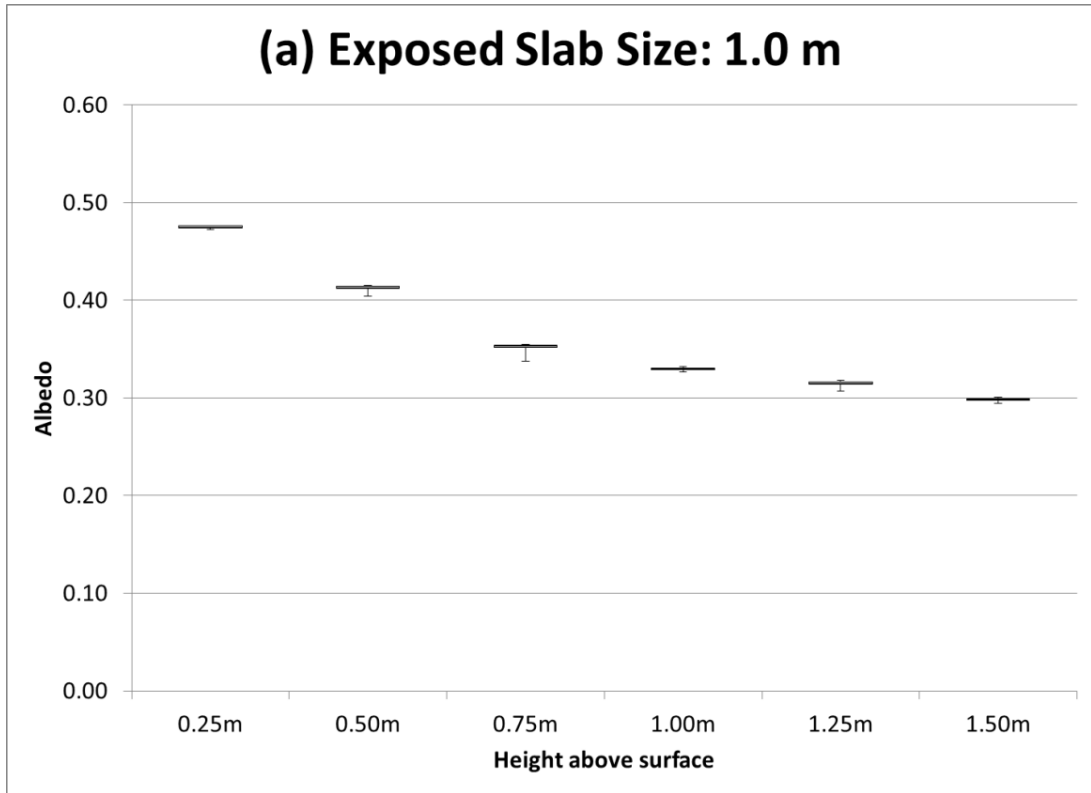


Figure 6-13 Box and whisker plots of the measured albedo of (a)-(e) the slab with various exposed sizes (f) the slab fully covered in the finite background and (g)-(h) the components of the infinite background

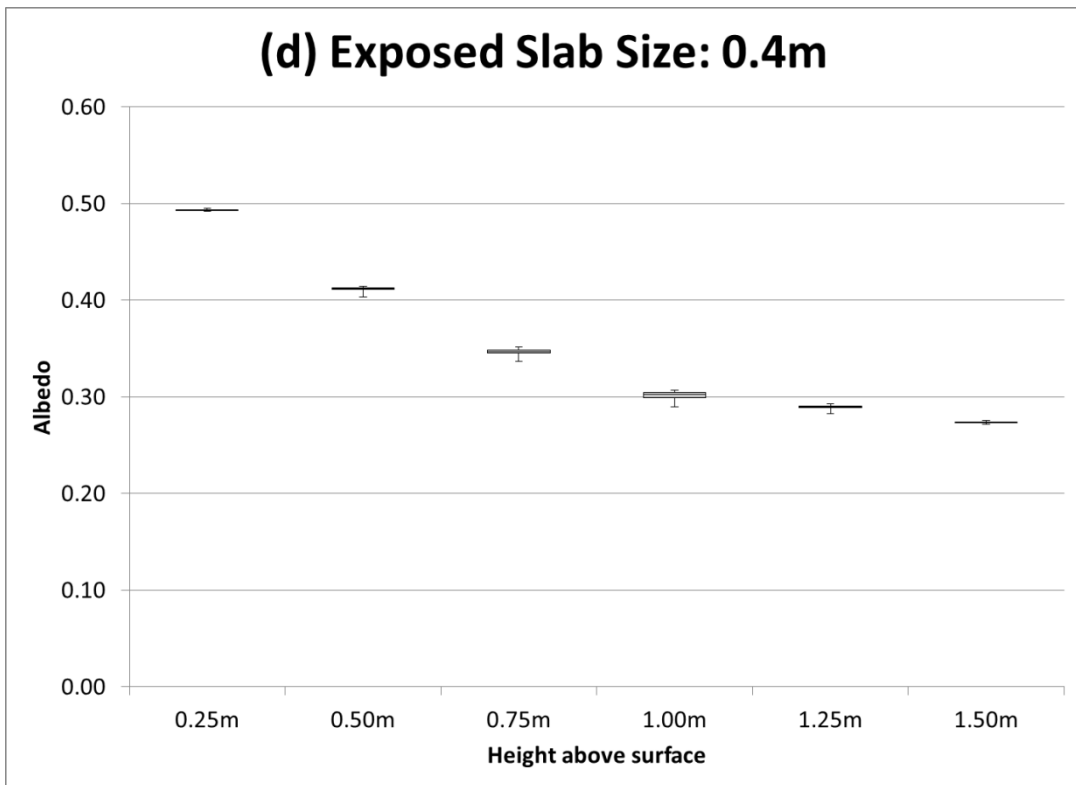
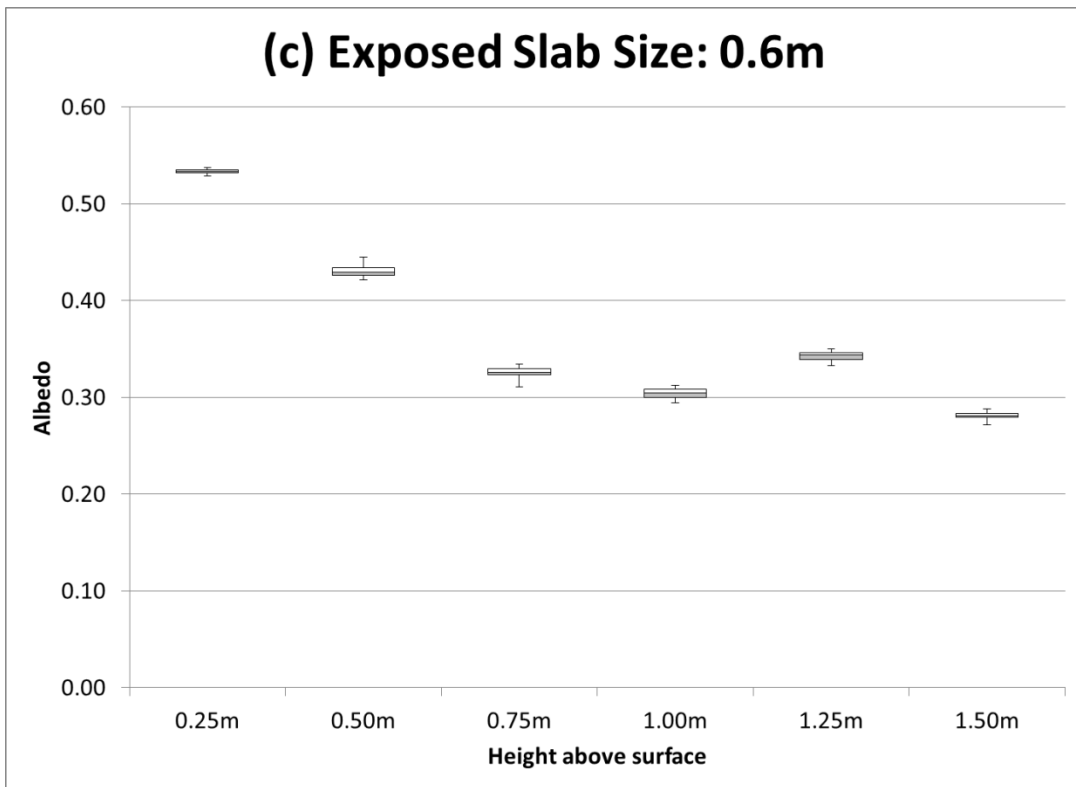


Figure 6-13 (cont.)

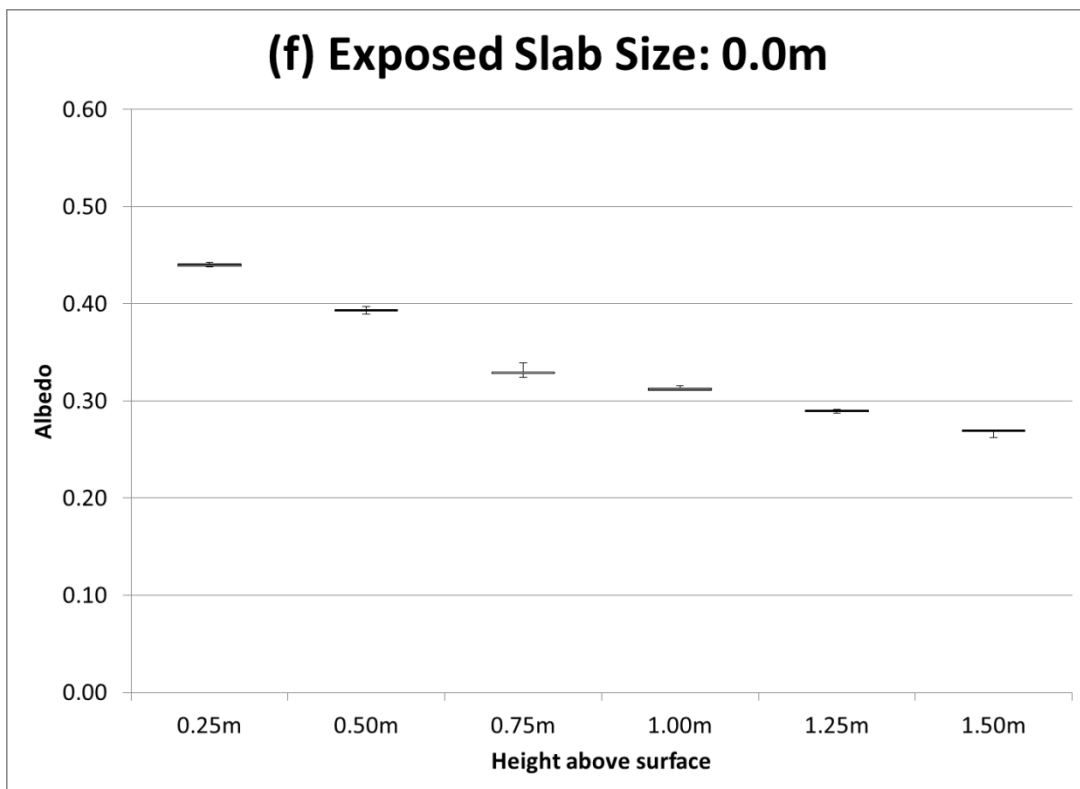
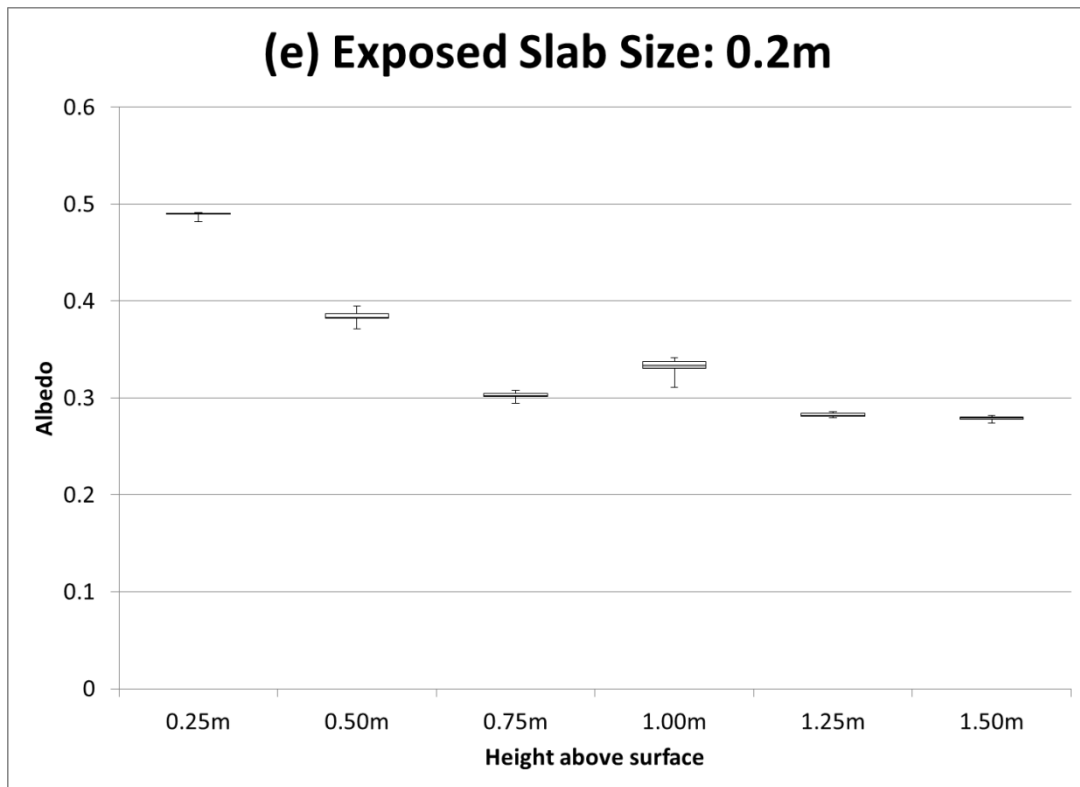


Figure 6-13 (cont.)

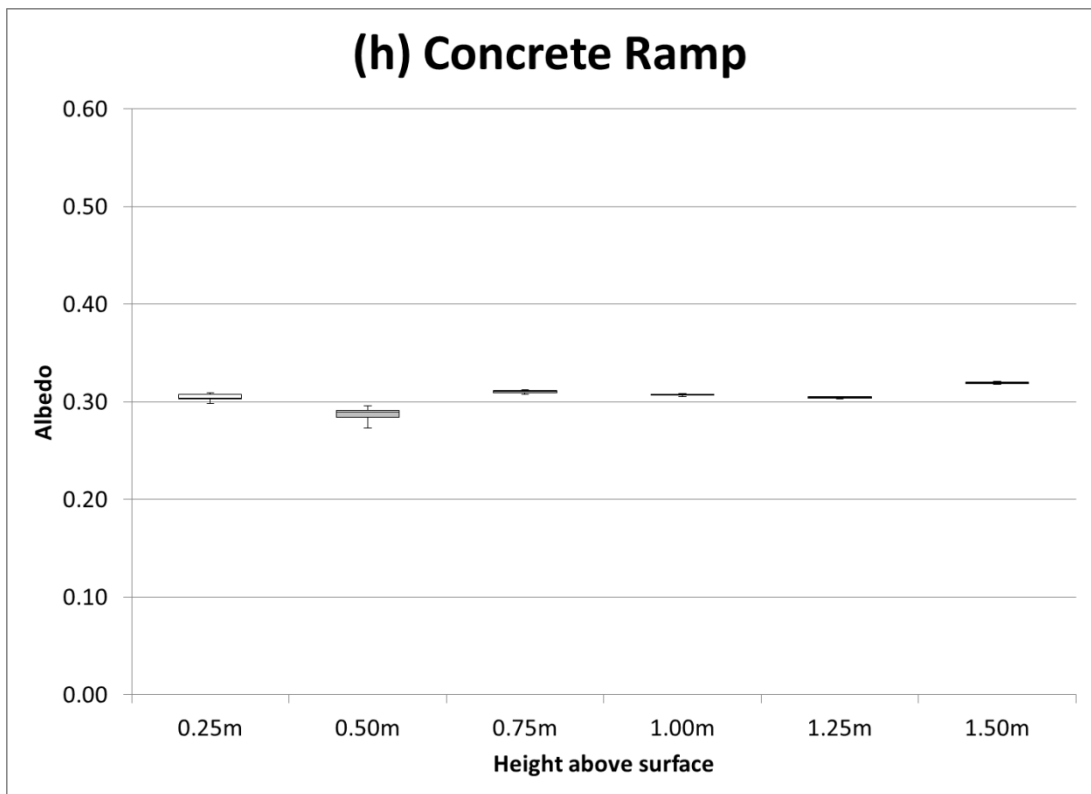
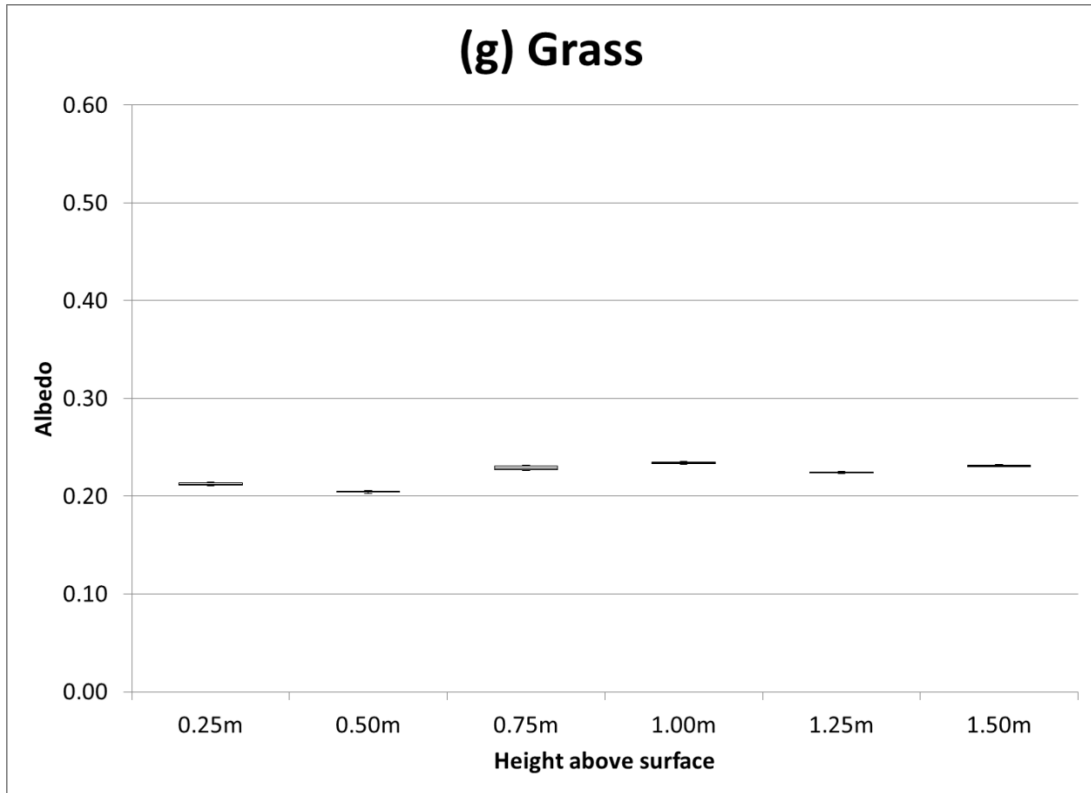


Figure 6-13 (cont.)

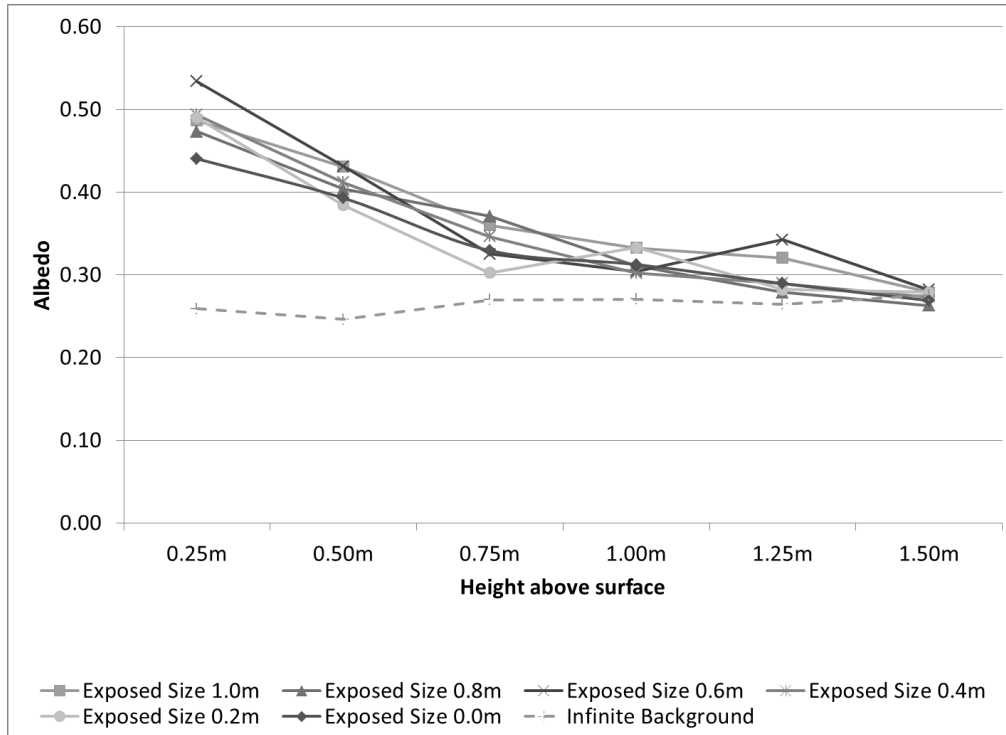


Figure 6-14 Variation of mean albedo with height of albedometer and exposed slab size

From Figure 6-14, there was some variation in the albedo of the infinite background. Based on the discussion pertaining to Equation 6.6 in Section 2.6, this finding indicates that reflections were present from external surfaces that were not explicitly considered, but the resultant variation was also not too significant. Therefore, the variation in the albedo of the infinite background is small and can be assumed to be fixed value for any height. Second, the albedo of all cases converged to the infinite background as the measurement height increased. This means the view factor of the infinite background should be increasing with height, which is discussed further in Section 3.4.

6.3.4 View Factors

In order to calculate the albedo of the TiO₂ concrete slab, the view factors for each case were evaluated according to the procedure outlined in Section 2.6 and summarized in Figure 6-15(a)-(c). The view factors for the infinite background are calculated without the concrete slab in view which then results in the curve presented in Figure 6-15 (c). Changing the exposed concrete slab size a only redistributes the view factors between the slab and the finite background. Therefore, for this setup and testing methodology, Equation 6.12 holds true.

$$F_{dA \rightarrow bg-inf}(a, h) = F_{dA \rightarrow bg-inf}(h) \quad (6.12)$$

From Figure 6-15(c), at a height of 1.50 m, the view factor of the infinite background is close to 88% while it is about 12% for the TiO₂ concrete slab when there is no finite background. This explains why albedos appear to converge to that of the infinite background with increasing height in Figure 6-14.

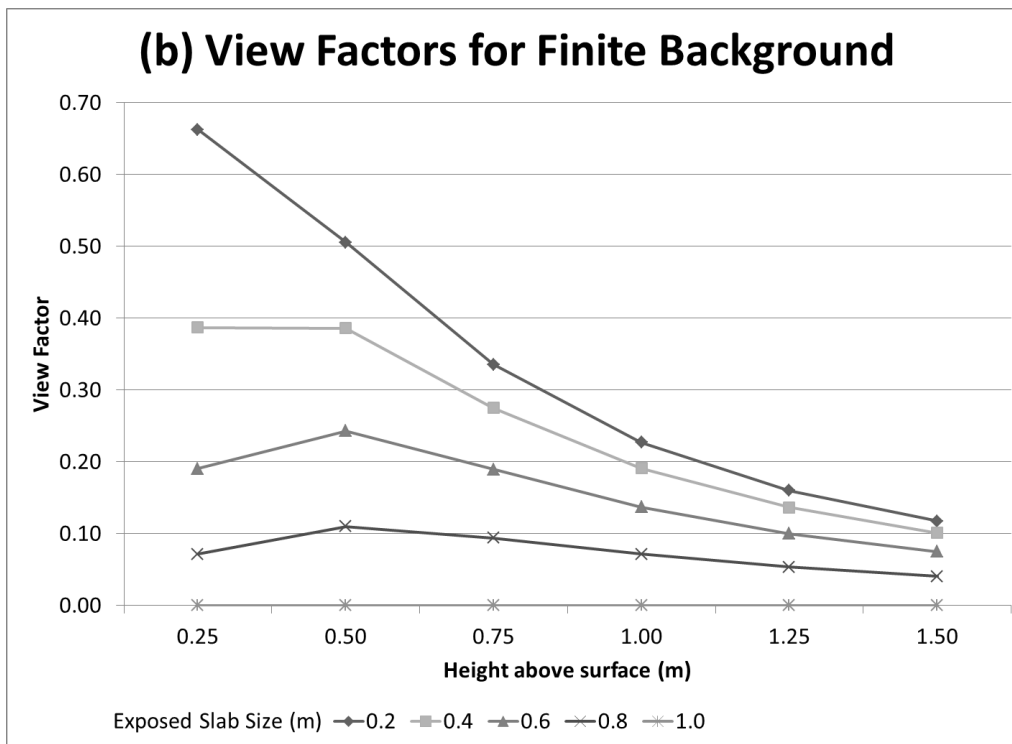
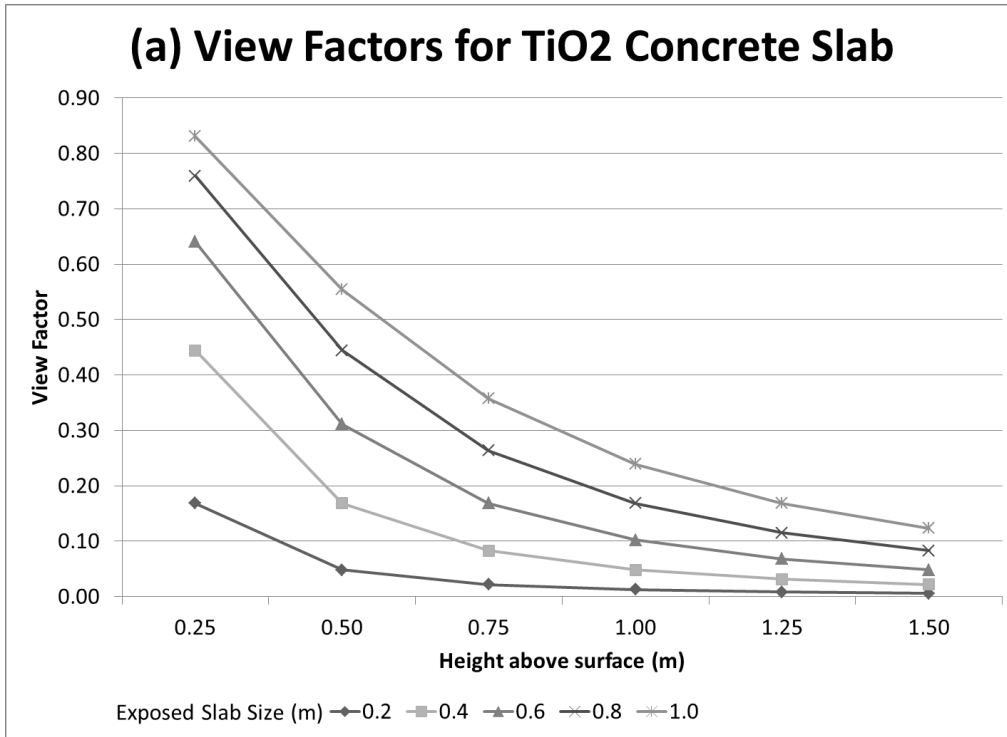


Figure 6-15 View factors for each case for (a) TiO₂ concrete slab (b) finite background and (c) infinite background

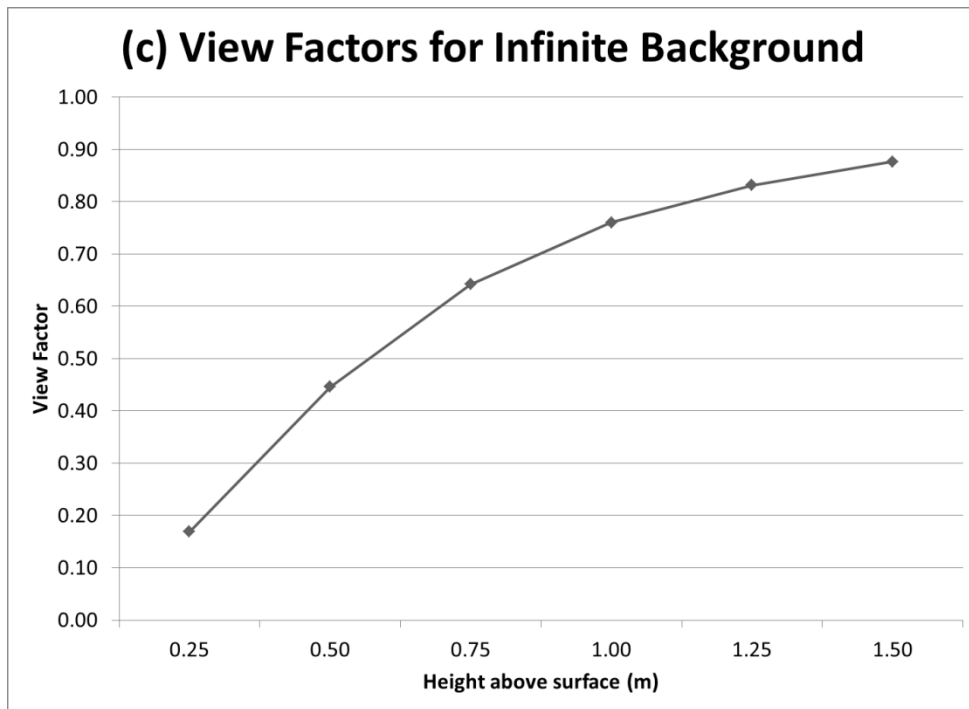


Figure 6-15 (cont.)

6.3.5 Albedo Calculation

Section 2.7 described two methods to determine albedo of the TiO₂ concrete slab depending on the number of unknowns in the albedo measurement such as the finite and infinite backgrounds. This section applies those methods.

6.3.5.1 Only Slab Albedo is Unknown (Case 1)

For this calculation, the albedo of the finite background and infinite background were assumed to be known. The albedo of the finite background (black paper) is equal to 0.46 from the spectrophotometer (Figure 6-12) and the albedo of the infinite background is equal to the mean of the grass and adjacent concrete values, shown in Figure 6-14, which is 0.26. In reality, the measured values from this study are not exact. The albedo of the finite background determined per ASTM E903 does not accurately represent the albedo at the given location because of the reasons outlined in Section 1, while there was some minor variation in albedo of the infinite background with height as seen in Figure 6-14.

The albedo of the slab α_s for each combination of exposed slab size and height of measurement was calculated using Equation 6.7. Some of the calculated values of α_s were found to be negative or greater than 1, which implied some possible error, which could be experimental or as a result of the incorrect assumptions. These values were discarded as outliers and the average slab albedo was 0.50 with a high standard deviation of 0.16. The possibility of obtaining extraneous values for albedo as well as the high standard deviation leads to the conclusion that this technique with only one unknown could give an unreliable albedo for the finite-sized slab.

6.3.5.2 Slab and Finite Background Albedos are Unknown (Case 2)

Results from the previous case were unreliable because the contribution of the finite background albedo was not accurately known at the testing location. In this case, both the

slab and the finite background albedos were assumed to be unknown, while that of the infinite background was fixed at the average value of 0.26. Using Equations 6.9 and 6.10, the albedo of the slab and finite background were calculated as 0.54 and 0.49, respectively. The RMSE was a low 0.02, indicating a good fit.

6.3.5.3 All Albedos are Unknown (Case 3)

Case 3 takes into account variation because of the background surfaces, such as buildings and trees that were not explicitly considered. This interference was relatively small, and therefore, the results from this case and those from the previous case were not expected to be very different. Using Equations 6.8 and 6.10, the albedo of the slab and finite and infinite backgrounds were found to be 0.55, 0.50 and 0.25, respectively. The albedo of the slab and infinite background differed from case 2 by just 1.9% and 3.9% respectively, representing a very small error due to interference from surfaces that were not explicitly considered. The RMSE in this case was also found to be a low 0.02.

6.3.5.4 Stage I Summary

A summary of the three cases is presented in Table 6-3. As discussed in Section 3.5.1, the assumptions in Case 1 are not reasonable, and therefore, its results are rejected. Between Case 2 and Case 3, the results are quite similar and a conservative value of 0.54 can be selected as the most likely ‘true’ albedo of the TiO₂ concrete mix, based on these calculations and assumptions.

Table 6-3 Summary of albedo calculation for varying number of unknowns for stage I

| | TiO ₂ Concrete Slab | | Finite Background | | Infinite Background | |
|--------|--------------------------------|------------|-------------------|------------|---------------------|------------|
| | Albedo | | Albedo | | Albedo | |
| Case 1 | 0.50 | Calculated | 0.46 | Known | 0.26 | Known |
| Case 2 | 0.54 | Calculated | 0.49 | Calculated | 0.26 | Known |
| Case 3 | 0.55 | Calculated | 0.50 | Calculated | 0.25 | Calculated |

There is a case wherein the albedo of the finite background is known and that of the background is not. However, as previously discussed in Section 3.5.1, the albedo of the finite background is in fact not known with reasonable certainty, and therefore, this possible case is neglected for the sake of brevity.

6.3.6 Validation

To validate the Stage I field method described previously, the albedo of two cubes with the same concrete mix design (described in Section 2.2) were estimated as per ASTM E903 using a Cary 5000 UV-Vis-NIR spectrophotometer and Equation 6.11. The spectral reflectance of the cubes is shown in Figure 6-16 together with the AM 1.5G standard solar spectrum from ASTM G173.

The average albedo of the cubes was determined to be 0.58 with a standard deviation of 0.04. This differs from the value estimated from field measurements by 7.5%. This cannot however, be called an ‘error’ because, as previously discussed, the albedo determined from

ASTM E903 is not necessarily representative of the ‘true’ albedo at a given location, and therefore, the field and lab methods need only be similar but not necessarily the same in order to validate the field method. A previous study (Krimpelis & Karamanis, 2015) measured the albedo of a reflective concrete slab by ASTM E1918 and ASTM E903 and found a similar difference (6.2%) between the two methods. Therefore, since the lab and field methods gave similar results, the field method was deemed validated and a conservative estimate of the albedo of the TiO₂ white cement concrete mix was determined to be 0.54.

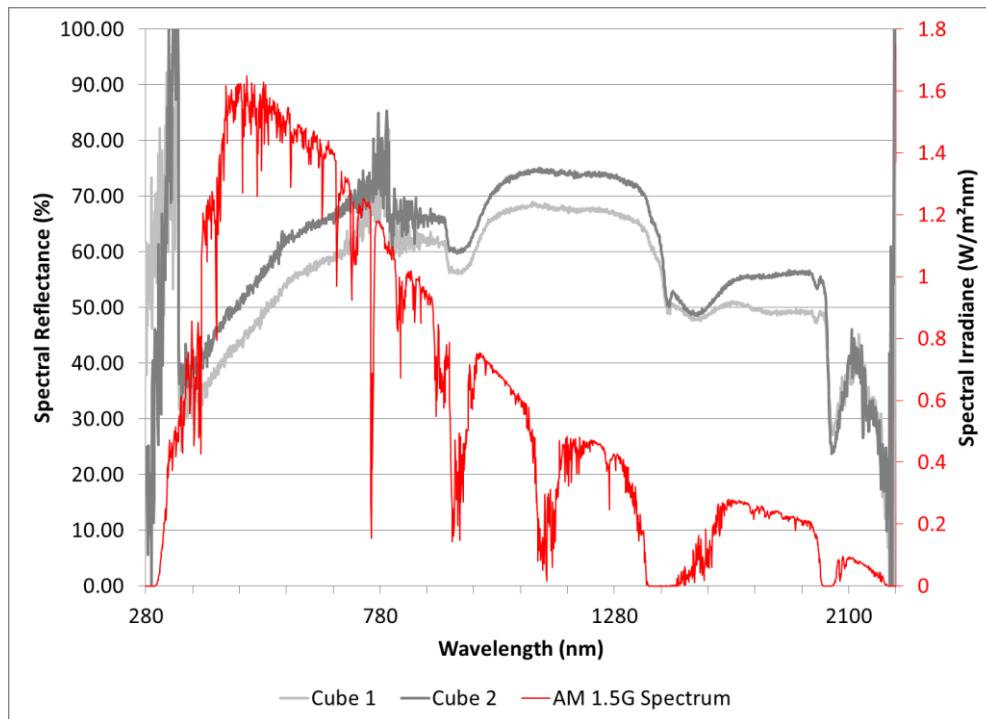


Figure 6-16 Spectral reflectance of cubes made of TiO₂ concrete with AM 1.5 G spectrum on the secondary axis

6.4 RESULTS AND DISCUSSION: STAGE II

As described in Section 2.1, following Stage I measurements, the slab was left exposed to the environment for the entire winter in Urbana, Illinois, and then moved to Rantoul, Illinois. The albedo of the weathered slab was measured in the field with the finite-size albedo algorithm using the view factor, after which a core was taken, washed thoroughly to remove dust and dirt on the surface, and the albedo was measured again in the laboratory.

6.4.1 Weather Conditions

Field measurements of the slab and the old asphalt pavement on which it was placed (Figure 6-7) were performed between 10:00 AM and 2:00 PM CST on April 17, 2015. Weather data from the nearby Rantoul Elliot Field National Aviation Center for that period was obtained from (National Climatic Data Center, 2015) and summarized in Table 6-4. No measurements were taken when the solar disc was covered by clouds.

Table 6-4 Weather data for stage II field measurements from (National Climatic Data Center, 2015) at Rantoul Elliot Field National Aviation Center

| Time (LST) | Sky Conditions | Temperature (°C) | | |
|------------|-----------------------------|------------------|----------|-----------|
| | | Dry Bulb | Wet Bulb | Dew Point |
| 10:35 | Clear | 12.6 | 6.9 | 0.0 |
| 11:35 | Scattered clouds at 2,500 m | 13.9 | 7.1 | -0.9 |
| 12:35 | Clear | 15.2 | 6.8 | -4.0 |

6.4.2 Albedo Measurements

Albedo was measured in the field in a manner similar to Section 3.3, but only one case was considered with the slab fully exposed at heights ranging from 0.25 m to 1.50 m in increments of 0.25 m. There was no finite background as in Stage I field testing. The albedo of the infinite background (aged asphalt pavement about 20-25 years old) was measured at the same heights, which are shown in Figure 6-17 (a) and (b).

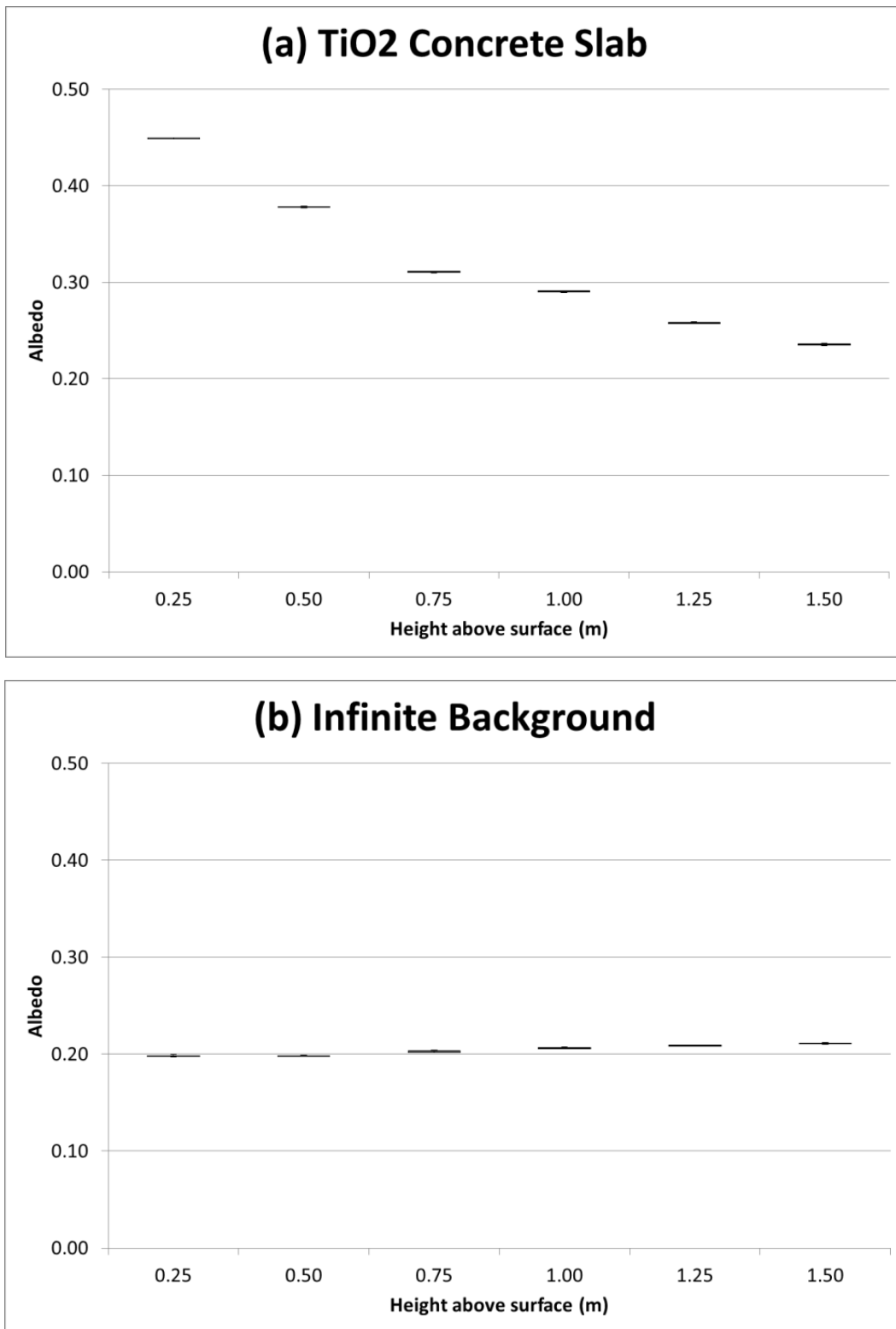


Figure 6-17 Box and whisker plots of the measured albedo of (a) TiO₂ concrete slab after weathering and (b) the infinite background

The infinite background was of a single surface and met the 4 m x4 m minimum requirement from ASTM E1918. There was very little variation in albedo of the aged asphalt pavement with height, indicating that there was little interference from surfaces that were not explicitly

considered. The mean values of the measured albedos at each height of measurement are shown in Figure 6-18.

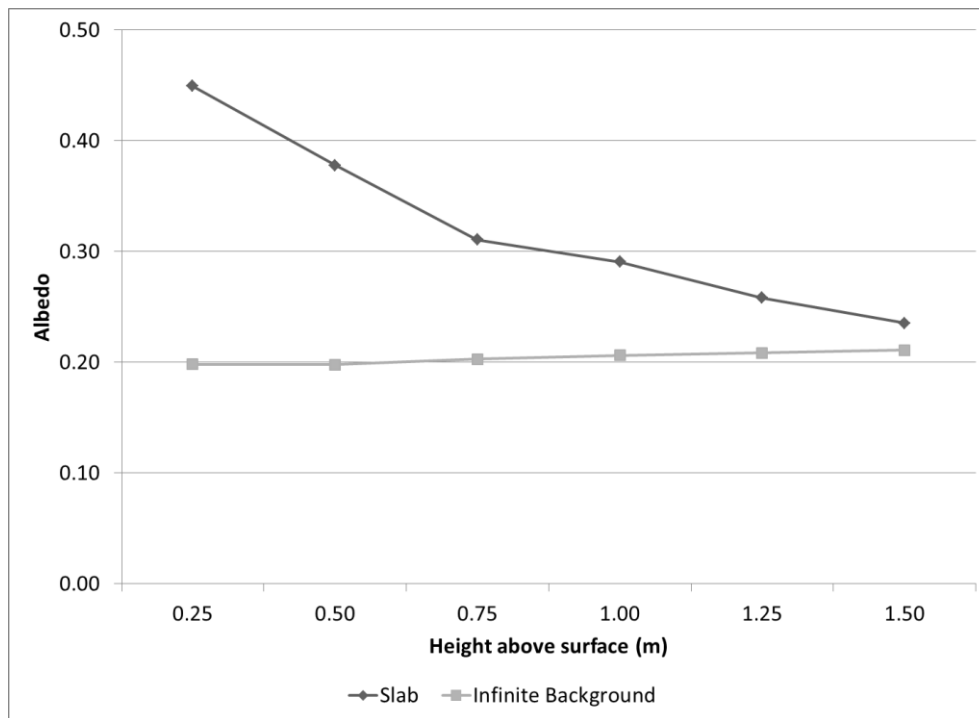


Figure 6-18: Variation of mean albedo with height of albedometer above slab surface

6.4.3 View Factors

As view factors depend only on geometric configuration and not the material, the view factors for the slab and the infinite background were the same as in Figure 6-15(a) (for 1.0 m exposed size) and Figure 6-15 (c), respectively. As in Stage I, the shadow from the albedometer was not considered in the calculation and the instrument was oriented to avoid any shadow falling on the slab. Because both the slab and the infinite background were much larger than the shadow, the error was negligible.

6.4.5 Albedo Calculation: Field Method

Similar to Section 3.5, the slab and infinite background albedo can be evaluated assuming they are unknown or one of them is known.

6.4.5.1 Albedo of the Slab is Unknown

In this case, the albedo of the infinite background is assumed to be its average value of 0.20 and the albedo of the slab at each height is evaluated using Equation 6.7 with $F_{dA \rightarrow bg-fin} = 0$. The average albedo was found to be 0.51 with a standard deviation of 0.04.

6.4.5.2 All Albedos are Unknown

This case was solved using Equations 6.8 and 6.9 with $F_{dA \rightarrow bg-fin} = 0$. The albedo of the slab and the infinite background were found to be 0.50 and 0.21, respectively. The RMSE was just 0.01. The albedo of the slab differs from the previous case by just 1.5% because of the negligible interference from other surfaces that were not explicitly considered in the calculations.

6.4.5.3 Summary

A summary of the cases from Stage II is given in Table 6-5. Based on the method proposed and validated in Section 3, the more conservative value of 0.50 for albedo is chosen as the most likely ‘true’ albedo of the TiO₂ concrete after weathering, which is less than the albedo of 0.54 before weathering that was determined using the same method. Thus, weathering appeared to reduce albedo by 8% in this case.

Table 6-5 Summary of albedo calculation for varying number of unknowns for stage II

| | TiO ₂ Concrete Slab | | Infinite Background | |
|--------|--------------------------------|------------|---------------------|------------|
| | Albedo | | Albedo | |
| Case 1 | 0.51 | Calculated | 0.20 | Known |
| Case 2 | 0.50 | Calculated | 0.21 | Calculated |

This weathering included dust and dirt accumulated on the surface as well as any chemical or physical changes that may have taken place. The slab was not trafficked by vehicles, which could bring in much more dirt and debris while also abrading the concrete surface. Thus, this reduction in albedo was on account of environmental factors and did not consider the possibility of in-service reduction.

6.4.6 Albedo Calculation: Lab Method

After field measurements, three spatially distributed cores were taken from the slab (Figure 6-19) and washed thoroughly so that any accumulated dust and dirt was removed. Thus, by comparing laboratory-measured albedo of these samples with those in Section 3.6, the effect of weathering excluding dirt and dust could be quantified.

Spectral reflectance of each of the three cores was determined using a Cary 5000 UV-Vis-NIR Spectrophotometer, as shown in Figure 6-20, which also shows the standard AM 1.5G solar spectrum from ASTM G173. The albedo of each core was determined using Equation 6.11 and then averaged.

The albedo was calculated to be 0.59, nearly the same as the albedo of 0.58 determined using the same method in Section 3.6 for the cubes cast with the same mix design. This finding suggests that there was no fundamental chemical or physical change in the concrete because of weathering, and only dust and dirt accumulation on the surface.



Figure 6-19 Spatially-distributed cores from the slab surface obtained by wet coring

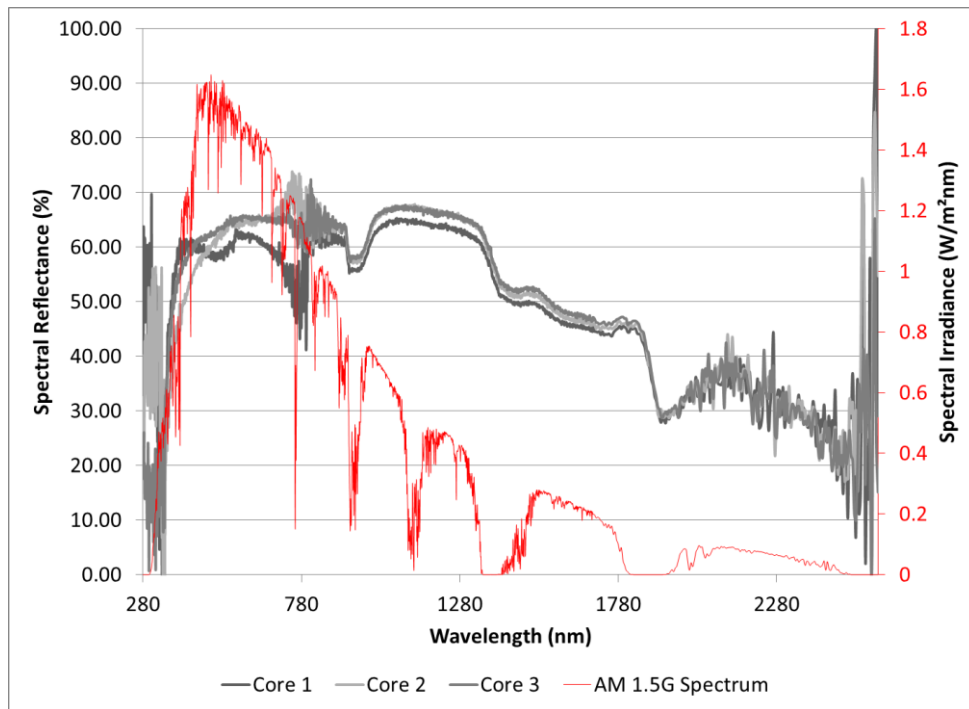


Figure 6-20 Spectral reflectance of cores and AM 1.5G standard solar spectrum with AM 1.5 G spectrum on the secondary axis

6.5 CONCLUSION

Albedo is an important component of a pavement LCA but, short of building a full-scale section, it is difficult to measure, particularly with sample sizes typical of civil engineering applications. Methods have been developed in the literature to measure albedo using a combination of geometric analysis and field measurements, which is a compromise between accuracy and convenience (Levinson, Akbari, & Berdahl, *Measuring solar reflectance—Part II: Review of practical methods*, 2010). The disadvantages of the previous methods were overcome by developing a new method that took into account background surfaces and site conditions that could be applied to finite sized concrete specimens.

Based on this new method, a conservative estimate of the albedo of a concrete specimen with TiO₂-containing Portland cement was found to be 0.54, which is higher than the albedo of 0.25-0.30 reported in literature for typical concrete mixes that use conventional (gray) Portland cement. After one winter cycle of uncontrolled weathering, this albedo decreased to 0.50 but, after being washed thoroughly, was restored to about the same value as before weathering. Therefore, the decrease in albedo due to weathering was concluded to be a result of dust and dirt accumulating on the surface rather than any chemical or physical changes in the concrete.

The major advantages of this new method over previous ones are the consideration, both implicitly and explicitly, of reflection from background surfaces; the applicability to specimens of many sizes; the ability to conduct the test at any convenient site (such as a parking lot); standard masks do not need to be maintained; the geometric analysis of view factors is relatively simple; and the measured albedo has been validated using an independent laboratory method. In addition, the proposed method with view factors is simpler and

relatively inexpensive compared to other methods in the literature. The major shortcomings of this method include human errors that may occur during field testing, such as erroneous centering of the albedometer over the sample or imprecise leveling; lack of consideration of the shadow cast by the instrument; and the need for clear skies and a limited testing window on a given day. Overall, this method is expected to be very useful for agencies and contractors to quickly measure albedo at a construction site for more accurate LCA analyses.

CHAPTER 7-CONCLUSIONS AND RECOMMENDATIONS

This research investigated the effects of pavement layers and their thermal properties on surface temperature, heat flux, and resultant Urban Heat Island. As compared to existing methods, which take a ‘top-down’ approach to UHI characterization using atmospheric models involving global-scale simulations, the ‘bottom-up’ approach was able to consider the entire pavement system including sub-surface layers. As a result of a top-down approach, existing UHI mitigation strategies have tended to focus on albedo as the sole determinant of pavement UHI. A consequence of this has been that pavements and roofs have been treated as equivalent surfaces, whereas pavements employ several sub-surface layers that can potentially contribute to UHI mitigation strategies. The bottom-up approach provided a way to overcome these shortcomings. Moreover, it made it possible to evaluate the Global Warming Potential of a pavement under a given climatic condition without having to average over the effect of the surrounding surfaces such as buildings, grass or water bodies, thus allowing for very specific pavement LCAs to be conducted and for agencies to correctly quantify the environmental effects of any given strategy. This was demonstrated by studying the effect of multi-functional concrete inlays on UHI.

7.1 FINDINGS

As opposed to parametric evaluation of pavement surface temperature and heat flux, a ground-based model was developed on the lines of the Enhanced Integrated Climatic Model (EICM) that uses historic weather data to perform a long-term thermal analysis of a complete pavement structure. An initial assessment found that UHI mitigation strategies are more effective in the warmer climate of Austin, TX than the colder climate of Chicago, IL, and more so in summer than in winter, with effectiveness ranging from 18% to over 90% for various strategies. While inclusion of a CTB under the concrete surface course (with or without steel fiber reinforcement) skewed the surface temperature lower in summer but higher in winter, each time with an effectiveness of over 50%, the use of a high albedo surface course as well as one made of lower density concrete skewed it lower in both seasons.

To understand the cause behind these effects as well as their impact on daytime and nighttime UHI, a heat-flux based approach was adopted using a newly-developed program, the Illinois Thermal Analysis Program (ILLI-THERM). This approach considered the average net ground heat flux over the design period to estimate the Radiative Forcing (RF) of the pavement, which the Global Warming Potential (GWP) could be evaluated and readily plugged into a full pavement LCA. It was found that on a long-term basis, only albedo had a significant effect on GWP of the pavement at a given location, lowering the GWP by 63 t CO₂-eq/lane-km for a five-year analysis period in Austin. However, as UHI is a diurnal phenomenon and is observed more prominently in the Canopy Layer at night, it is possible to redistribute the heat stored within a pavement so as to decrease the heat flux at night and increase it during the day, thus mitigating the intensity of the UHI. To prove this, the heat stored in and conducted through a variety of pavement designs was analyzed using the average season day metric. The thermal delay or time lag induced by the entire pavement structure was clearly observed by this approach and this delay, which was found to range from 2 to 7 hours, was shown to be key in delaying the heat flux from a pavement at night and thus lowering UHI intensity. A CTB below the concrete surface course was found to be effective in storing the heat, with an effectiveness of 76%, although a highly conductive surface course using steel-fiber reinforced concrete diminished those benefits to an effectiveness just 27% by allowing heat to conduct out faster at night. In contrast, the use of

a reflective surface course lowered the daytime heat flux but was found to have little effect during nighttime, with an effectiveness of just 2% in summer. Interestingly, the use of lightweight aggregates (LWA) in the surface course was able to achieve a similar result by emitting the heat stored in the surface course much faster and not allowing it to be conducted and stored too deep into the pavement structure.

To demonstrate an application of the consideration of the bottom-up approach to analysis, the potential role of multi-functional inlays for pavement preservation was considered. These inlays, made of a special type of white cement containing TiO₂ nanoparticles, created a reflective surface while also increasing the pavement's thermal inertia. This reflective surface decreased the Global Warming Potential of the pavement while also having a percentage of effectiveness of over 50%, with most of that being during the day, as compared to the asphalt pavement substrate. Therefore, these multi-functional inlays were found to be beneficial in mitigating surface UHI.

Considering the important role played by the thermal properties of the pavement materials, the second challenge in this study was to find ways to better characterize those properties. In this study, the focus was on albedo since it has the largest impact on reflecting shortwave radiation. Based on multiple albedo measurements of test sections in Rantoul, IL, using an albedometer, an aging albedo model for asphalt pavements was calibrated. This three-parameter power model indicated that a majority of weathering and subsequent increase in albedo takes place in the first 1-2 years, with very limited change beyond that. This aging model was implemented using ILLITHERM. By using this model to compare a static albedo model to an aging one, it was found that the current practice of using a static albedo overestimated the GWP by 25% over a ten-year design period. In addition, the albedo of a section of Flowable Fibrous Concrete (FFC) was also measured. The translucent polymer fibers were visible from the surface but were covered by the cement paste. However, it is possible that with abrasion, they would become exposed, in which case their albedo would have an effect on the overall pavement albedo. The albedo of a single (polymer) fiber was found to be 0.07 using a spectrophotometer, which is high enough to have a potential impact on the pavement if the fiber becomes exposed. However, the extent of this impact depends on the relative area of exposure.

Finally, a new method to evaluate the albedo of a concrete sample of any dimension using an albedometer was introduced. The existing specification ASTM E1918 requires an impractically large sample size of at least 4 m x 4 m. Yet, the method has several benefits against the alternative method, ASTM E903, which uses a spectrophotometer and a standard solar spectrum, which does not necessarily mimic site conditions. The proposed method combines measurement of the apparent specimen albedo at different heights with geometric analysis of the experimental conditions through site and sample geometry view factors. Through the measured composite albedo and least square analysis, the true albedo of the specimen and background surface could be estimated. An example, with white cement containing TiO₂ estimated the slab albedo to be 0.54 and was validated using a spectrophotometer. The proposed method depended on the number of unknown albedos in the problem, e.g., background albedo, slab albedo, black paper mask. The advantage of this method is that it can be used for lab-sized concrete specimens, such as beams and cylinders, which are typically 150-200 mm in their smallest dimension. Being a non-destructive method, the same specimens can be used for measuring albedo as well as strength, saving time and effort in casting new specimens. Moreover, the method explicitly considers the testing location and thus gives engineers more freedom to choose less than ideal sites. In addition, the albedo of the white cement concrete slab after one winter cycle of weathering

was evaluated and was found to decrease to 0.50. However, upon washing the surface thoroughly, the original albedo was restored. This suggests that for this particular mix, the weathering was largely on account of dust and dirt on the surface rather than any chemical reactions at the concrete surface. This may not be true for all concrete surfaces and a more focused, long-term investigation is required before any general conclusions may be drawn.

7.2 RECOMMENDATIONS FOR FUTURE WORK

While this study covered several aspects of pavements UHI characterization and thermal analysis of materials, much scope for future work exists that would extend the bottom-up approach presented here and also cover a wider array of concrete mixes for thermal characterization. These avenues are summarized below:

- (a) While GWP is certainly a metric for UHI, it is only an equivalent number that cannot be directly measured. An alternative metric has been the heating and cooling loads of buildings adjacent to pavements, which are affected by the heat flux from the pavement. A thorough analysis of this effect would involve enclosing these surroundings within the pavement LCA boundaries. Existing literature (Yang, Wang, & Kaloush, 2015; Yang, Wang, & Kaloush, 2013) suggests that this inclusion could dramatically change the inferences obtained by evaluating the GWP of a pavement. This aspect is worth considering and involves considerable thermal modeling using a Computational Fluid Dynamics (CFD)-based approach.
- (b) Even the existing approach to pavement UHI analysis does not truly take into account the complexities of the urban fabric. Shadow effects from adjacent buildings, increased wind speeds due to the urban canyon, cars covering pavements for most of the day over busy streets etc. are some of the complex effects that have a potentially important role to play but are not sufficiently characterized in the state of the art work in the area.
- (c) In the thermal characterization of concrete materials, thermal conductivity and heat capacity are important considerations, particularly in designing a pavement to mitigate UHI without relying exclusively on albedo. Clearly the measured albedos in this study varied much more dramatically than typically understood by pavement engineers. Differential scanning calorimetry (DSC) is a potential tool in evaluating heat capacity while hot-disk analysis is useful for thermal conductivity. While these values have been measured previously for conventional concrete and its constituents (Dawson, Dehdezi, Hall, Wang, & Isola, 2012; Dehdezi P. K., Hall, Dawson, & Casey, 2013), very little is known about how the corresponding values for specialized concrete and asphalt constituents including recycled and by-product materials, a gap that needs to be filled.
- (d) Specialized, unconventional materials specifically for UHI mitigation, such as phase change materials or insulation layers, seem to have potential. They also take advantage of the several layers that pavements have that can be manipulated. While some work on these aspects has been undertaken by other researchers, more can be done, especially in numerically modeling their effects and determining an optimum balance between strength requirements and UHI mitigation.
- (e) Finally, a growing area of pavement research involves the use of hydronic systems or pavement-coupled ground source heat pumps to carry heat stored in the pavement out and put it to use elsewhere. These systems consider a pavement as an active thermodynamic system that can be coupled with a heat exchanger to obtain useful energy from the system. A potential area of investigation is in the optimization of the

configuration of the system to derive maximum benefit while also considering various options of how best to use the heat thus obtained.

Urbanization is the defining feature of an ever-industrializing world and with it comes several engineering challenges. Urban areas must promote human well-being while enabling their growth and the pursuit of happiness. By designing pavements that can mitigate the UHI effect, pavement engineers can contribute to that effort and help build better, more sustainable cities of the future.

REFERENCES

- Aggarwal, R. M., Guhathakurta, S., Grossman-Clarke, S., & Lathey, V. (2012). How do variations in Urban Heat Islands in space and time influence household water use? The case of Phoenix, Arizona. *Water Resources Research*, 48, W06518.
- Akbari, H., & Konopacki, S. (2004). Energy effects of heat-island reduction strategies in Toronto, Canada. *Energy*, 29, 191-210.
- Akbari, H., & Konopacki, S. (2005). Calculating energy-saving potentials of heat-island reduction strategies. *Energy Policy*, 33, 721-756.
- Akbari, H., Levinson, R., & Stern, S. (2008). Procedure for measuring the solar reflectance of flat or curved roofing assemblies. *Solar Energy*, 82, 648-655.
- Akbari, H., Menon, S., & Rosenfeld, A. (2009). Global cooling: increasing world-wide urban albedos to offset CO₂. *Climatic Change*, 94, 275-286.
- al-Qadi, I. L., Abuawad, I. M., Dhasmana, H., Coenen, A. R., & Trepanier, J. S. (2014). *Effects of Various Asphalt Binder Additives/Modifiers on Moisture-Susceptible Asphaltic Mixtures*. Illinois Center for Transportation.
- al-Qadi, I. L., Carpenter, S. H., Leng, Z., Ozer, H., & Trepanier, J. S. (2009). *Tack Coat Optimization for HMA Overlays: Accelerated Pavement Test Report*. Rantoul, IL: Illinois Center for Transportation.
- American Concrete Pavement Association (ACPA). (2002). *R&T Update: Albedo: A Measure of Pavement Surface Reflectance, Report No. 3.05*. Skokie, IL: ACPA.
- ARA, Inc. (2004). *Guide for Mechanistic-Empirical Pavement Design of New and Rehabilitated Pavement Structures*. Washington, D.C.: National Cooperative Highway Research Program Report 1-37A.
- ASTM International. (2003). *ASTM Standard G173: Standard Tables for Reference Solar Spectral Irradiance: Direct Normal and Hemispherical on 37° Tilted Surface*. Standard, West Conshohocken, PA.
- ASTM International. (2012). *ASTM Standard E903: Standard Test Method for Solar Absorptance, Reflectance, and Transmittance of Materials Using Integrating Spheres*. West Conshohocken, PA: ASTM.
- ASTM Standard E1918. (2006). *Standard Test Method for Measuring Solar Reflectance of Horizontal and Low-Sloped Surfaces in the Field*. ASTM International, West Conshohocken, PA.
- Bacci, P., & Maugeri, M. (1992). The Urban Heat Island of Milan. *Il Nuovo Cimento C*, 15(4), 417-442.
- Balaguru, P. N., & Shah, S. P. (1992). *Fiber-reinforced cement composites*. New York: McGraw-Hill.
- Bentz, D. P., & Turpin, R. (2007). Potential applications of phase change materials in concrete technology. *Cement & Concrete Composites*, 29, 527-532.
- Bird, D. N., Kunda, M., Mayer, A., Schlamadinger, B., Canella, L., & Johnston, M. (2008). Incorporating changes in albedo in estimating the climate mitigation benefits of land use change projects. *Biogeosciences Discussions*, 5(2), 1511-1543.
- Bo Yeon, L. (2012). *Effect of titanium dioxide nanoparticles on early age and long term properties of cementitious materials*. PhD Dissertation, Georgia Institute of Technology, Atlanta.

- Boonen, E., & Beeldens, A. (2013). Photocatalytic roads: from lab tests to real scale applications. *European Transportation Review*, 5, 79-89.
- Bordelon, A. C., & Roesler, J. R. (2011). Flowable Fibrous Concrete for Thin Concrete Inlays. *Proceedings of the 1st Congress of the Transportation and Development Institute of ASCE* (pp. 874-883). American Society of Civil Engineers.
- Boriboonsomsin, K., & Reza, F. (2007). Mix Design and Benefit Evaluation of High Solar Reflectance Concrete for Pavements. *Transportation research record: journal of the transportation research board*, 2011(1), 11-20.
- Bretz, S., Akbari, H., & Rosenfeld, A. (1998). Practical Issues for using Solar-Reflective Materials to Mitigate Urban Heat Islands. *Atmospheric Environment*, 32(1), 95-101.
- Cackler, T., Alleman, J., Kevern, J. T., & Sikkema, J. (2012). *Technology demonstrations project: environmental impact benefits with "TX active" concrete pavement in Missouri DOT two-lift highway construction demonstration*. Report, National Concrete Pavement Technology Center (CP Tech Center), Ames, Iowa.
- Carnielo, E., & Zinzi, M. (2013). Optical and thermal characterisation of cool asphalts to mitigate urban temperatures and building cooling demand. *Building and Environment*, 60, 56-65.
- Cervantes, V., & Roesler, J. (2009). *Performance of Concrete Pavements with Optimized Slab Geometry*. Illinois Center for Transportation.
- Chiasson, A. D., Spilter, J. D., Rees, S. J., & Smith, M. D. (2000). A model for simulating the performance of a pavement heating system as a supplemental heat rejecter with closed-loop ground-source heat pump systems. *Journal of solar energy engineering*, 122(4), 183-191.
- Chow, W. T., Brennan, D., & Brazel, A. J. (2012). Urban heat island research in Phoenix, Arizona: Theoretical contributions and policy applications. *Bulletin of the American Meteorological Society*, 93(4), 517-530.
- Cotana, F., Rossi, F., Filippini, M., Coccia, V., Pisello, A. L., Bonamente, E., . . . Cavalaglio, G. (2014). Albedo control as an effective strategy to tackle Global Warming: A case study. *Applied Energy*, 130, 641-647.
- Dave, E. V., Ahmed, S., Buttlar, W. G., Bausano, J. P., & Lynn, T. (2010). Investigation of strain tolerant mixture reflective crack relief systems: an integrated approach. *Journal of the Association of Asphalt Paving Technologists*, 79.
- Dawson, A. R., Dehdezi, P. K., Hall, M. R., Wang, J., & Isola, R. (2012). Enhancing thermal properties of asphalt materials for heat storage and transfer applications. *Road Materials and Pavement Design*, 13(4), 784-803.
- Dehdezi, P. K., Hall, M. R., & Dawson, A. (2011). Thermophysical Optimization of Specialized Concrete Pavement Materials for Collection of Surface Heat Energy and Applications for Shallow Heat Storage. *Transportation Research Record: Journal of the Transportation Research Board*, 2240, 96-106.
- Dehdezi, P. K., Hall, M. R., Dawson, A. R., & Casey, S. P. (2013). Thermal, mechanical and microstructural analysis of concrete containing microencapsulated phase change materials. *International Journal of Pavement Engineering*, 14(5), 449-462.
- Dempsey, B. J. (1969). *A Heat-Transfer Model for Evaluating Frost Action and Temperature Related Effects in Multilayered Pavement Systems*. Urbana, IL: University of Illinois.

- Dempsey, B. J., & Elzeftawy, A. (1976). Mathematical Model for Predicting Moisture Movement in Pavement Systems. *Transportation Research Record*(612), 48-55.
- Dempsey, B. J., & Thompson, M. R. (1970). A heat transfer model for evaluating frost action and temperature related effects in multi-layered pavement systems. *Highway Research Record*, 342, 39-56.
- Fabrizi, R., Biondi, S., & Biondi, R. (2010). Satellite and ground-based sensors for the urban heat island analysis in the city of Rome. *Remote Sensing*, 2(5), 1400-1415.
- FHWA. (2015). *Towards Sustainable Pavement Systems: A Reference Document*. FHWA-HIF-15-002, US Department of Transportation.
- Gary, P. (2007). Geothermal heat pumps. *Journal of Energy Engineering*, 133(1), 32-38.
- Golden, J. S., & Kaloush, K. E. (2006). Mesoscale and microscale evaluation of surface pavement impacts on the urban heat island effects. *International Journal of Pavement Engineering*, 7(1), 37-52.
- Golden, J. S., Carlson, J., Kaloush, K., & Phelan, P. E. (2007). A comparative study of the thermal and radiative impacts of photovoltaic canopies on pavement surface temperatures. *Solar Energy*, 81, 872-883.
- Golden, J. S., Guthrie, P. M., Kaloush, K., & Britter, R. R. (2005). Summertime urban heat island hysteresis lag complexity. *Proceedings of the ICE-Engineering Sustainability*, (pp. 197-210).
- Goward, S. N. (1981). Thermal Behavior of Urban Landscapes and the Urban Heat Island. *Physical Geography*, 2(1), 19-33.
- Guan, B., Ma, B., & Qin, F. (2011). Application of asphalt pavement with phase change materials to mitigate urban heat island effect. *Proceedings of the International Symposium on Water Resource and Environmental Protection* (pp. 2389-2392). IEEE.
- Guangxi, W., & Yu, X. (2012). System design to harvest thermal energy across pavement structure. *Energytech*, 1-4.
- Guerrini, G. L., & Peccati, E. (2007). Photocatalytic Cementitious Roads for Depollution. *Proceedings of the International RILEM Symposium on Photocatalysis, Environment and Construction Materials*. Florence, Italy.
- Guhathakurta, S., & Gober, P. (2007). The Impact of the Phoenix Urban Heat Island on Residential Water Use. *Journal of the American Planning Association*, 73(3), 317-329.
- Gui, J., Carlson, J., Phelan, P. E., Kaloush, K., & Golden, J. S. (2002). Impact of pavement thickness on surface diurnal temperatures. *Journal of Green Building*, 2(2), 121-130.
- Gui, J., Phelan, P. E., Kaloush, K. E., & Golden, J. S. (2007). Impact of Pavement Thermophysical Properties on Surface Temperatures. *Journal of Materials in Civil Engineering*, 19(8), 683-690.
- Haselbach, L., Boyer, M., Kevern, J. T., & Schaefer, V. R. (2011). Cyclic heat island impacts on traditional versus pervious concrete pavement systems. *Transportation Research Record: Journal of the Transportation Research Board*, 2240, 107-115.
- Hunger, M., Entrop, A. G., Mandilaras, I., Brouwers, H. J., & Founti, M. (2009). The behavior of self-compacting concrete containing micro-encapsulated phase change materials. *Cement and Concrete Composites*, 31(10), 731-743.

- Intergovernmental Panel on Climate Change (IPCC). (2001). *Climate Change 2001: The Scientific Basis*. (J. T. Houghton, Y. D. Ding, D. J. Griggs, M. Noguer, P. J. van der Linden, X. Dai, . . . C. Johnson, Eds.) New York: Cambridge University Press.
- Jeanjean, A., Olives, R., & Py, X. (2013). Selection criteria of thermal mass materials for low-energy building construction applied to conventional and alternative materials. *Energy and Buildings*(63), 36-48.
- Jiachuan, Y., Wang, Z.-H., & Kaloush, K. E. (2015). Environmental impacts of reflective materials: Is high albedo a ‘silver bullet’ for mitigating urban heat island? *Renewable and Sustainable Energy Reviews*, 47, 830-843.
- Joos, F., Prentice, I. C., Sitch, S., Meyer, R. H., Plattner, G., Gerber, S., & Hasselmann, K. (2001). Global warming feedbacks on terrestrial carbon uptake under the Intergovernmental Panel on Climate Change (IPCC) emission scenarios. *Global Biogeochemical Cycles*, 15(4), 891-907.
- Kaloush, K. E., Carlson, J. D., Golden, J. S., & Phelan, P. E. (2008). *The thermal and radiative characteristics of concrete pavements in mitigating urban heat island effects*. Portland Cement Association (Report No. PCA R&D SN2969), Skokie, IL.
- Keeler, J. M., & Kristovich, D. A. (2012). Observations of urban heat island influence on lake-breeze frontal movement. *Journal of Applied Meteorology and Climatology*, 51(4), 702-710.
- King, D. (2015). *Surface and Microstructural Properties of Photocatalytic Cements*. Masters Thesis, University of Illinois at Urbana-Champaign, Urbana, IL.
- Kleerekopera, L., van Esch, M., & Salcedo, T. B. (2012). How to make a city climate-proof, addressing the urban heat island effect. *Resources, Conservation and Recycling*, 64, 30-38.
- Kodur, V., & Khaliq, W. (2011). Effect of temperature on thermal properties of different types of high-strength concrete. *Journal of Materials in Civil Engineering*, 23(6), 793-801.
- Kolokotronia, M., Gowreesunker, B. L., & Giridharan, R. (2013). Cool roof technology in London: An experimental and modelling study. *Energy and Buildings*, 67, 658-667.
- Kolokotsa, D., Santamouris, M., & Zerefos, S. C. (95). Green and cool roofs’ urban heat island mitigation potential in European climates for office buildings under free floating conditions. *Solar Energy*, 95, 118-130.
- Krimalis, S., & Karamanis, D. (2015). A novel approach to measuring the solar reflectance of conventional and innovative building components. *Energy and Buildings*, 97, 137-145.
- Kuennen, T. (2006). *Pavement Preservation Compendium II, Publication FHWA-IF-06-049*. FHWA, US Department of Transportation.
- Kusaka, H., Kondo, H., Kikegawa, Y., & Kimura, F. (2001). A simple single-layer urban canopy model for atmospheric models: comparisons with multi-layer and slab models. *Boundary-Layer Meteorology*(101), 329-358.
- Larson, G., & Dempsey, B. J. (1997). *Enhanced Integrated Climatic Model, Version 2.0, Final Report*. Contract DTFA MN/DOT 72114.
- Levinson, R., & Akbari, H. (2002). Effects of composition and exposure on the solar reflectance of portland cement concrete. *Cement and Concrete Research*, 32, 1679–1698.
- Levinson, R., Akbari, H., & Berdahl, P. (2010). Measuring solar reflectance—Part II: Review of practical methods. *Solar Energy*, 84, 1745-1759.

- Li, H., Harvey, J. T., & Jones, D. (2014). Development and Preliminary Validation of Integrated Local Microclimate Model for Numerical Evaluation of Cool Pavement Strategies. *Transportation Research Record: Journal of the Transportation Research Board*, 2444, 151-164.
- Li, H., Harvey, J. T., Holland, T. J., & Kayhanian, M. (2013). The use of reflective and permeable pavements as a potential practice for heat island mitigation and stormwater management. *Environmental Research Letters*, 8(1), 015023.
- Li, H., Harvey, J., & Kendall, A. (2013). Field measurement of albedo for different land cover materials and effects on thermal performance. *Building and Environment*, 59, 536-546.
- Lin, T.-P., Matzarakis, A., Hwang, R.-L., & Huang, Y.-C. (2010). Effect of pavements albedo on long-term outdoor thermal comfort. *Berichte des Meteorologischen Instituts der Albert-Ludwigs-Universität Freiburg*, 497-503.
- Liu, L., & Zhang, Y. (2011). Urban Heat Island Analysis Using the Landsat TM Data and ASTER Data: A Case Study in Hong Kong. *Remote Sensing*, 3(7), 1535-1552.
- Mackey, C. W., Lee, X., & Smith, R. B. (2012). Remotely sensing the cooling effects of city scale efforts to reduce urban heat island. *Building and Environment*, 49, 348-358.
- Matthias, A. D., Post, D. F., Accioly, L., Fimbres, A., Sano, E. E., & Batchily, A. K. (1999). Measurement of Albedos for Small Area of Soil. *Soil science*, 164(5), 293-301.
- Memon, R. A., Leung, D. Y., & Chunho, L. (2008). A review on the generation, determination and mitigation of Urban Heat Island. *Journal of Environmental Sciences*, 20, 120-128.
- Menon, S., Akbari, H., Mahanama, S., Sednev, I., & Levinson, R. (2010). Radiative forcing and temperature response to changes in urban albedos and associated CO₂ offsets. *Environmental Research Letters*, 5(1), 014005.
- Mingshi, L., Du, L., & Shen, W. (2012). Spatio-temporal variations in urban heat islands effects of Nanjing, China derived from the dense Landsat imagery (1992–2011). *Proceedings of the 5th International Congress on Image and Signal Processing (CISP)* (pp. 1104-1108). IEEE.
- Mirzaei, P., & Haghighat, F. (2010). Approaches to study Urban Heat Island - Abilities and Limitations. *Building and Environment*, 45(10), 2192-2201.
- Munoz, I., Campra, P., & Fernandez-Alba, A. R. (2010). Including CO₂-emission equivalence of changes in land surface albedo in life cycle assessment. Methodology and case study on greenhouse agriculture. *International Journal of Life Cycle Assessment*(15), 672–681.
- National Climatic Data Center. (n.d.). Retrieved September 5, 2014, from National Oceanic and Atmospheric Administration: <http://cdo.ncdc.noaa.gov/qclcd/QCLCD>
- National Climatic Data Center. (2014). Retrieved March 12, 2015, from <http://cdo.ncdc.noaa.gov/qclcd/QCLCD>
- National Climatic Data Center. (2014). *NCDC: Quality Controlled Local Climatological Data*. Retrieved December 10, 2014, from <http://www.ncdc.noaa.gov/qclcd/QCLCD>
- National Climatic Data Center. (2015). *NCDC: Quality Controlled Local Climatological Data*. Retrieved April 20, 2015, from <http://www.ncdc.noaa.gov/qclcd/QCLCD>
- National Concrete Pavement Technology Center. (2012). *Environmental Impact Benefits with “TX Active” Concrete Pavement in Missouri DOT Two-Lift Highway Construction Demonstration: Final Report I*. Iowa State University, Institute for Transportation.

- National Cooperative Highway Research Program Report 1-37A. (2004). *Guide for Mechanistic-Empirical Pavement Design of New and Rehabilitated Pavement Structures*. Transportation Research Board.
- Nguyen, L. H., Beaucour, A.-L., Ortola, S., & Noumowé, A. (2014). Influence of the volume fraction and the nature of fine lightweight aggregates on the thermal and mechanical properties of structural concrete. *Construction and Building Materials*, *51*, 121–132.
- Novo, A. V., Bayon, J. R., Castro-Fresno, D., & Rodriguez-Hernandez, J. (2012). Monitoring and Evaluation of the Thermal Behavior of Permeable Pavements for Energy Recovery Purposes in an Experimental Parking Lot: Preliminary Results. *Journal of Energy Engineering*, *139*(3), 230-237.
- Oke, T. R. (1982). The Energetic Basis of the Urban Heat Island. *Quarterly Journal of the Royal Meteorological Society*, *108*, 1-24.
- Osborn, D., Hassan, M. M., & Dylla, H. (2012). Quantification of Reduction of Nitrogen Oxides by Nitrate Accumulation on Titanium Dioxide Photocatalytic Concrete Pavement. *Transportation Research Record: Journal of the Transportation Research Board*, *2290*, 147-153.
- Pan, P., Wu, S., Xiao, Y., & Liu, G. (2015). A review on hydronic asphalt pavement for energy harvesting and snow melting. *Renewable and Sustainable Energy Reviews*, *48*, 624-634.
- Peshkin, D., Smith, K. L., Wolters, A., Krstulovich, J., Moulthrop, J., & Alvarado, C. (2011). *Preservation Approaches for High-Traffic-Volume Roadways, SHRP2 Report S2-R26-RR-1*. The Second Strategic Highway Research Program. Washington, D.C.: Transportation Research Board.
- Philip, J. R., & de Vries, D. A. (1957). Moisture movement in porous materials under temperature gradients. *Eos, Transactions American Geophysical Union*, *38*(2), 222-232.
- Pichierri, M., Bonafoni, S., & Biondi, R. (2012). Satellite air temperature estimation for monitoring the canopy layer heat island of Milan. *Remote Sensing of Environment*, *127*, 130-138.
- Pisello, A. L., Pignatta, G., Castaldo, V. L., & Cotana, F. (2014). Experimental Analysis of Natural Gravel Covering as Cool Roofing and Cool Pavement. *Sustainability*, *6*, 4706-4722.
- Qin, Y. (2015). Urban canyon albedo and its implication on the use of reflective cool pavements. *Energy and Buildings*, *96*, 86-94.
- Reifsnyder, W. E. (1967). Radiation geometry in the measurement and interpretation of radiation balance. *Agricultural Meteorology*, *4*(4), 255-265.
- Richard, C., Dore, G., Lemieux, C., Bilodeau, J.-P., & Haure-Touze, J. (2015). Albedo of Pavement Surfacing Materials: In Situ Measurements. *Cold Regions Engineering 2015* (pp. 181-192). ASCE.
- Rizwan, M. A., Dennis, Y. C., & Liu, C. (2008). A review on the generation, determination and mitigation of Urban Heat Island. *Journal of Environmental Sciences*, *20*(1), 120-128.
- Roma, Jr., L. C., Martello, L. S., & Savastano, Jr., H. (2008). Evaluation of mechanical, physical and thermal performance of cement-based tiles reinforced with vegetable fibers. *Construction and Building Materials*, *22*, 668-674.
- Sailor, D. J., Resh, K., & Segura, D. (2006). Field measurement of albedo for limited extent test surfaces. *Solar Energy*, *80*, 589-599.

- Santamouris, M. (2013). Using cool pavements as a mitigation strategy to fight urban heat island—a review of the actual developments. *Renewable and Sustainable Energy Reviews*, 26, 224-240.
- Santamouris, M. (2014). Cooling the cities – A review of reflective and green roof mitigation technologies to fight heat island and improve comfort in urban environments. *Solar Energy*, 103, 682-703.
- Santamouris, M., Synnefa, A., & Karlessi, T. (2011). Using advanced cool materials in the urban built environment to mitigate heat islands and improve thermal comfort conditions. *Solar Energy*, 85, 3085-3102.
- Santero, N. J., & Horvath, A. (2009). Global warming potential of pavements. *Environmental Research Letters*, 4, 034011.
- Santero, N. J., Masanet, E., & Horvath, A. (2011). Life-cycle assessment of pavements Part II: Filling the research gaps. *Resources, Conservation and Recycling*, 55, 810-818.
- Santero, N. J., Masanet, E., & Horvath, A. (2011). Life-cycle assessment of pavements. Part I: Critical review. *Resources, Conservation and Recycling*, 55, 801-809.
- Shahmohamadi, P., Che-Anil, A. I., Ramly, A., Maulud, K., & Mohd-Nor, M. (2010, June). Reducing urban heat island effects: A systematic review to achieve energy consumption balance. *International Journal of Physical Sciences*, 5(6), 626-636.
- Sharma, A., Tyagi, V. V., Chen, C. R., & Buddhi, D. (2009). Review on thermal energy storage with phase change materials and applications. *Renewable and Sustainable energy reviews*, 13(2), 318-345.
- Simpson, J. R., & McPherson, E. G. (1997). The effects of roof albedo modification on cooling loads of scale model residences in Tucson, Arizona. *Energy and Buildings*, 25, 127-137.
- Stempihar, J., Pourshams-Manzouri, T., Kaloush, K., & Rodezno, M. (2012). Porous asphalt pavement temperature effects for urban heat island analysis. *Transportation Research Record: Journal of the Transportation Research Board*, 2293, 123-130.
- Susca, T. (2012). Enhancement of life cycle assessment (LCA) methodology to include the effect of surface albedo on climate change: Comparing black and white roofs. *Environmental Pollution*, 163, 48-54.
- Swaid, H., & Hoffman, M. E. (1989). The Prediction of Impervious Ground Surface Temperature by the Surface Thermal Time Constant (STTC) Model. *Energy and Buildings*(13), 149-157.
- Synnefa, A., Karlessi, T., Gaitani, N., Santamouris, M., Assimakopoulos, D. N., & Papakatsikas, C. (2011). Experimental testing of cool colored thin layer asphalt and estimation of its potential to improve the urban microclimate. *Building and Environment*, 46, 38-44.
- Synnefa, A., Santamouris, M., & Apostolakis, K. (2007). On the development, optical properties and thermal performance of cool colored coatings for the urban environment. *Solar Energy*, 81, 488-497.
- Taha, H., Akbari, H., Rosenfeld, A., & Huang, J. (1988). Residential Cooling Loads and the Urban Heat Island - the Effects of Albedo. *Building and Environment*, 23(4), 271-283.
- Taha, H., Sailor, D., & Akbari, H. (1992). *High-albedo materials for reducing building cooling energy use*. Berkeley, CA: Lawrence Berkeley Lab (No. LBL-31721).

- Tran, H., Uchihama, D., Ochi, S., & Yasuoka, Y. (2006). Assessment with satellite data of the urban heat island effects in Asian mega cities. *International Journal of Applied Earth Observation and Geoinformation*, 8(1), 34-48.
- Tran, N., Powell, B., Marks, H., West, R., & Kvasnak, A. (2009). Strategies for design and construction of high-reflectance asphalt pavements. *Transportation Research Record: Journal of the Transportation Research Board*, 2098(1), 124-130.
- Tung-Chai, L., & Poon, C.-S. (2013). Use of phase change materials for thermal energy storage in concrete: An overview. *Construction and Building Materials*, 46, 55-62.
- Wei, J., & He, J. (2013). Numerical simulation for analyzing the thermal improving effect of evaporative cooling urban surfaces on the urban built environment. *Applied Thermal Engineering*, 51(1), 144-154.
- Wong, E., & Hogen, K. (2011). *Reducing Urban Heat Islands: Compendium of Strategies*. Environmental Protection Agency.
- Wong, E., Akbari, H., Bell, R., & Cole, D. (2011). *Reducing Urban Heat Islands: Compendium of Strategies*. Environmental Protection Agency.
- Wong, K. V., & Chaudhry, S. (2012). Use of Satellite Images for Observational and Quantitative Analysis of Urban Heat Islands Around the World. *Journal of Energy Resources Technology*, 134(4), 042101.
- Yaghoobian, N., & Kleissl, J. (2012). Effect of reflective pavements on building energy use. *Urban Climate*, 2, 25-42.
- Yang, J., Wang, Z., & Kaloush, K. E. (2013). *Unintended Consequences: A Research Synthesis Examining the Use of Reflective Pavements to Mitigate the Urban Heat Island Effect*. Arizona State University, National Center of Excellence for Smart Innovations, Tempe.
- Yang, J., Wang, Z.-H., & Kaloush, K. E. (2015). Environmental impacts of reflective materials: Is high albedo a 'silver bullet' for mitigating urban heat island? *Renewable and Sustainable Energy Reviews*, 47, 830-843.
- Yu, B., & Lu, Q. (2014). Estimation of albedo effect in pavement life cycle assessment. *Journal of Cleaner Production*, 64, 1-4.